UNIVERSITY OF MINES AND TECHNOLOGY
TARKWA

FACULTY OF ENGINEERING

DEPARTMENT OF ELECTRICAL AND ELECTRONIC ENGINEERING

A THESIS REPORT ENTITLED

EMPLOYING UNIFIED POWER FLOW CONTROLLER TO IMPROVE STABILITY OF THE NORTHERN SECTION OF GHANA'S ELECTRIC POWER TRANSMISSION SYSTEM

BY
WILLIAM DUODU ASIHENE

SUBMITTED IN PARTIAL FULFILLMENT OF THE REQUIREMENTS FOR THE AWARD OF THE DEGREE OF MASTER OF SCEINCE IN ELECTRICAL AND ELECTRONIC ENGINEERING

THESIS SUPERVISORS

……
DR FRANCIS B. EFFAH

…….……..
MR ERWIN NORMANYO

TARKWA, GHANA
APRIL 2019

DECLARATION

I declare that this thesis is my own work. It is being submitted for the degree of Master of Science in Electrical and Electronic Engineering in the University of Mines and Technology (UMaT), Tarkwa. It has not been submitted for any degree or examination in any other University.

……
(Signature of Candidate)

….. day of June, 2019

ABSTRACT

The demand for electricity in Ghana has been increasing for over a decade, with no corresponding increase in the transmission capacity. This led to the transmission network operating close to its stability limits. In addition, the system has inadequate transfer capability during peak periods resulting in decreased system voltages and increased transmission losses, which lead to voltage instability. This is evident on the major power outages experienced recently in the country. In this thesis, the major instability issue on Ghana's transmission system is investigated with a computer model of the network developed in MATLAB Simscape Power Systems. Load flow studies conducted on the modelled network revealed that voltage instability was predominant, where some buses experienced voltages outside the stability margin of $\pm 5\%$ p.u. Different techniques are used to solve stability related issues and the thesis employed the use of the UPFC, which is a current member of the FACTS family. The device is modelled as two sets of four GTO-based square wave inverters connected back to back with a common DC link capacitor. The controllers of these devices are designed to operate within the power capability of Ghana's 161 kV network. The performance of these controllers were effective on the system. The Tumu bus was identified as the weakest and a candidate for the UPFC placement using Fast Voltage Stability Index analysis. With the UPFC in circuit, the voltage across the buses improved significantly. The power transfer capability also increased leading to low system losses. The UPFC is therefore recommended to be incorporated into Ghana's transmission system for a stable and secure operation.

DEDICATION

To Jason

ACKNOWLEDGEMENTS

All praise and honour to the Almighty God for making it possible for me to complete this thesis work. I would also like to express my sincere gratitude to my supervisors, Dr Francis B. Effah, and Mr Erwin Normanyo for their continuous support on my thesis research, for their patience, motivation, enthusiasm, and immense knowledge. Their guidance helped me during the time of my research and writing of this thesis.

Besides my supervisors, I would like to thank all lecturers from the electrical and electronic engineering department who in diverse ways, helped me during the writing and analysis of my thesis work.

TABLE OF CONTENTS

LIST OF FIGURES

LIST OF TABLES

LIST OF ABBREVIATIONS

Abbreviation	Meaning
A3BSP	Accra 3rd Bulk Supply Point
ABB	Asea Brown Boveri
AC	Alternating Current
AI	Artificial Intelligence
AVR	Automatic Voltage Regulator
BSPs	Bulk Supply Points
CIE	Ivorian Electricity Company
D1	Delta Lagging Y by 30^{o}
DC	Direct Current
DSA	Dynamic Security Assessment
ENTSO-E	European Network of Transmission System Operators for Electricity
EPRI	Electrical Power Research Institute
FACTS	Flexible Alternating Current Transmission Systems
FVSI	Fast Voltage Stability Index
GA	Genetic Algorithm
GPS	Ghana's Power System
GRIDCo	Ghana Grid Company
GSA	Gravitational Search Algorithm
GTO	Gate Turn-off Thyristor
GUI	Graphic User Interface
IEEE	Institute of Electrical and Electronics Engineers
IGBT	Insulated Gate Bipolar Transistor
IGCT	Insulated Gate Commutated Thyristor
IPFC	Interline Power Flow Controller
KV	Kilo-Volts
LQP	Line Stability Factor

MATLAB	Matrix Laboratory
MLA	Maximum Loadability Assessment
MVA	Megavolt Ampere
MVAr	Megavolt Ampere Reactive
MW	Megawatt
NITS	National Interconnected Transmission System
NMS	Network Manager System
PLL	Phase Lock Loop
PSS	Power System Stabiliser
PSSE	Power System Simulator for Engineers
PURC	Public Utilities Regulatory Commission
PV	Active Power-Voltage
PWM	Pulse Width Modulator
PQ	Load Bus
QV	Reactive Power-Voltage
SCC	System Control Centre
SMES	Super Conducting Magnetic Energy Storage
SMIB	Single Machine Infinite Bus
SSSC	Static Synchronous Series Compensator
STATCOM	Static Synchronous Compensator
SVC	Static VAr Compensator
TDS	Time-Domain Simulations
TCPS	Thyristor Controlled Phase Shifter
TCR	Thyristor Controlled Reactor
TCSC	Thyristor Controlled Series Capacitor
TSSC	Thyristor Switched Series Capacitor
TTC	Total Transformer Capacity
UPFC	Unified Power Flow Controller
VCPI	Voltage Collapse Point Indicator
VSC	Voltage Source Converter

LIST OF SYMBOLS

Active Power	P
Active Power at i^{th} bus	P_i
Base Voltage	V_{base}
Capacitance	C
Capacitor Current	I_C
Current at Bus 1	I_1
Current at Bus 2	I_2
DC Current	I_{DC}
Degree of Series Compensation	k_{se}
DC Voltage	V_{DC}
Direct Axis Current	I_d
Energy Released by Capacitor	W_c
Energy Released by Series Converter	W_{se}
Energy Release Time	t_r
Frequency	F
Ground Capacitance	C_g
Hertz	Hz
Impedance	Z
Inductance	L
Injected Reactive Power	Q_i
Injected Voltage Amplitude	$V_{p\,q}$
Level of Reactive Power Compensation	Q_c
Load Angle	δ
Load Current	I_L
Maximum Active Power	P_{max}

Maximum Capacitor Current	I_{CMAX}
Maximum Load Angle	δ_{MAX}
Maximum Load Current	I_{LMAX}
Maximum Reactive Power	Q_{max}
Maximum Receiving End Active Power	$P_{r\,max}$
Maximum Receiving End Reactive Power	$Q_{r\,max}$
Measured Voltage	V_{meas}
Mutual Inductance	L_M
Mutual Resistance	R_M
Phase Angle of Bus 1	δ_1
Phase Angle of Bus 2	δ_2
Power Angle	θ
Power Angle of Bus 1	θ_1
Power Angle of Bus 1	θ_2
Phase Capacitance	C_p
Quadrature Axis Current	I_q
Reactance	X
Reactive Power at j^{th} Bus	Q_j
Receiving End Active Power	P_r
Receiving End Reactive Power	Q_r
Receiving End Voltage	V_R
Resistance	R
Series Converter Voltage	V_{se}
Series Inductance	L_s
Series Compensating Reactance	X_c
Series Resistance	R_s

Short Circuit Power	P_{sc}
Shunt Converter Voltage	V_{sh}
STATCOM Current	$I_{STATCOM}$
SVC Current	I_{SVC}
Voltage at Bus 1	V_1
Voltage at Bus 2	V_2

INTERNATIONAL SYSTEM OF UNITS (SI UNITS)

Quantity	Unit	Symbol
Electric capacitance	farad	F
Electric current	ampere	A
Electric charge	coulomb	C
Electric potential	volt	V
Electric resistance	ohm	Ω
Frequency	hertz	Hz
Inductance	henry	H
Length	kilometre	km
Power	kilowatt	kW
Time	seconds	s

CHAPTER 1

GENERAL INTRODUCTION

1.1 Background to the Research

Increase in demand for electricity is becoming inevitable and for that reason, new power plants will be required to keep up with its increase, as will the need for transmission facilities to move large amounts of power to the areas of electrical energy usage. Increase in generating capacity requires construction of new power plants or retrofitting existing power plants, whereas its corresponding increase in transmission capacity requirements can be achieved by either constructing new transmission lines or improving the transfer capability of existing transmission facilities (Bhesdadiya, 2014). Electric power systems consist of a complex interconnection of various essential components, which are expensive to establish to meet up with the increasing electrical energy demand. Electricity grid upgrade cannot keep pace with the growing power plant capacity and energy demand. In addition, finding suitable rights of way for new transmission systems is particularly difficult, and gaining the necessary approval is time consuming due to some environmental considerations (Larruskain *et al*., 2016).

The only alternative to these challenges is to devise means to optimise the use of existing transmission system facilities for the provision of stable, secure and high-quality electricity supply. An effective solution is to consider the use of transmission system controllers (e.g., power electronics-based transmission controllers). Flexible AC Transmission System (FACTS) devices aim at controlling the flow of transmission line parameters. Unified Power Flow Controller (UPFC) is one of the recent technologies of the FACTS devices and according to Narain and Srivastava (2015), the UPFC shows better results for power system stability improvement compared to the other FACTS devices.

1.2 Problem Statement

Due to the continuous increase in load on Ghana's power system, a lot of planning goes into keeping the entire system stable. The transmission system is responsible for wheeling the generated power to the load centres with minimum possible contingency. The system is however burdened with faults and other problems that limit its continuous functionality, and a lot of research is currently being conducted to limit the effects of these problems.

The 2012 electricity supply plan of Ghana, published by the Ghana Grid Company realised that the transmission capacity of Ghana was inadequate. This was due to the transmission line not being able to carry the electricity demand during peak periods causing overloading, and insufficient reactive power compensation causing low substation bus voltages. This led to high generator reactive power production, and transfer of such reactive power over long distances causes high transmission line loss and voltage drops. The solution to these problems included the commissioning of the 330 kV Aboadze-Tema transmission line, reconstruction of the Prestea-Bogoso transmission line, the construction and commissioning of the 4th Tema-Achimota transmission line and installation of reactive power compensating devices at Achimota, new Tema, Sunyani and Kumasi (Anon., 2012a).

The 2013 electricity supply plan indicated that the transmission network had the capacity to evacuate a maximum generation of 470 MW and 620 MW from the eastern and western sections of the network respectively. Voltage instability is observed in the north and a variation of about 0.6 kV is noted even with a 1 MW change in load. A minimum of 300 MW power should be operating at Aboadze to ensure voltage stability of the network. The instability caused by the system was to be curtailed by installing capacitor banks at various locations as shown in Table 1.1.

Table 1.1 Capacitor Banks Installed in 2013

SN	Name of Substation	Number of Banks	Voltage (kV)	Unit (MVAr)	Total (MVAr)	Completion Date (2013)
1.	A3BSP	1	34.5	10.8	21.6	January
2.	Kumasi	1	34.5	21.6	21.6	April
3.	KNUST	2	34.5	21.6	43.2	April
4.	Tamale	2	34.5	10.8	21.6	June
5.	Mallam	2	34.5	21.6	43.2	June

(Source: Anon., 2013)

In 2014, with new transmission lines commissioned, the transmission network had the capacity to evacuate a maximum generation of 670 MW and 620 MW from the eastern and western sections of the network, respectively. However, a high line loading condition is observed on the Volta A3BSP during peak periods. With the commissioning of static VAr compensators and capacitor banks in Tamale, the voltage profile in the northern part of the network improved. However, during peak loading conditions, a minimum of 300 MW power is still required to be operating at Takoradi thermal plant at Aboadze to ensure voltage stability of the network (Anon., 2014).

The electricity supply plan published between 2016 and 2018, also indicated that the transmission system had inadequate transfer capability to the major load centres during peak periods and the situation results in low voltages, overloading and increase in transmission system losses. The losses are low with maximum generation at the west as with maximum generation at the east. To keep the system stable, 300 MW of generation at Aboadze needs to be operated as required in the previous years (Anon., 2016a; Anon., 2017; Anon., 2018a). In spite of all the installations and commissioning of lines and reactive power compensating devices, the transmission system is still under stress and a number of total and partial blackouts have been recorded in recent times.

The entire power system collapsed on December 7th, 2011, when a breaker exploded in an attempt to synchronise Akosombo's unit 1G2 to the rest of the system. The explosion led to high line loadings and the inability to control the power flows led to the system collapse. On March 21st, 2012, the country experienced another total system collapse due to voltage instability on the transmission system. The problem started with a generation deficit of 2 MW, which resulted in an unscheduled import of 2 MW from Ivory Coast. This condition rendered the system unstable. With the overloading of the transmission lines, heavy voltage drops were experienced on the lines and the generating stations had to evacuate more reactive power to the load centres. Voltage drop on the lines increased further and Table 1.2 shows the voltages at major substations just before system collapse (Anon., 2012b).

Table 1.2 Voltages at Selected Substations before System Collapse on March 2012

SN	Name of Station	Voltage (kV)	Voltage (p.u.)
1.	Akosombo	163	1.012
2.	Aboadze	156	0.969
3.	Tafo	145	0.901
4.	Mallam	145	0.901
5.	New Tema	153	0.950
6.	Kumasi	135	0.838
7.	Tamale	131	0.814
8.	Bolgatanga	124	0.770

(Source: Anon., 2012b)

From Table 1.2, transmission voltages before the incident were well below the ± 5% deviation allowed in the normal stable state by the Grid Code. Even the sending end voltage at Akosombo, which is usually around 167 kV - 169 kV had reduced to 163 kV. A further reduction in voltage as picked by the recorder indicates 156 kV leading to a complete voltage collapse and hence, total system blackout (Anon., 2012b).

On the 21st and again the 25th of January, 2016, the Ghana power system experienced partial system collapse plunging major parts of the country into darkness. The two events occurred as a result of a sudden loss in the transmission system capability along the 330 kV Aboadze-Volta lines due to harsh atmospheric conditions resulting from the severe harmattan weather. The limited transfer capability occurred due to the inability of the Akosombo generating station to operate optimally to provide adequate reactive power compensation for the power system. The findings on the outage were finalised on the issue that the entire power system does not generate the required reactive power needed for stability (Anon., 2016b).

Other outages experienced in recent times are presented in Table 1.3.

Table 1.3 Major Outages Experienced on Ghana's Power System in Recent Times

SN	Type of Outage	Date
1.	Partial Collapse	20th October, 2018
2.	Partial Collapse	29th January, 2018
3.	Partial Collapse	16th July, 2017
4.	Total Collapse	4th May, 2017
5.	Partial Collapse	11th March, 2016
6.	Partial Collapse	8th June, 2016
7.	Total Collapse	26th February, 2012

(Source: Anon., 2016b; Anon., 2018b)

Voltage instability has been identified as one of the major issues with Ghana's transmission system and traditionally, utilities have used static VAr compensators and capacitor banks to support the reactive power demand of the system. This method of reactive power compensation is becoming less relevant in today's power system due to the dynamic nature of modern loads. A fast acting and variable source of reactive power compensation is therefore required. Hence, going by the above highlighted factors that limit the power transfer capability of the transmission lines, there is the need to employ the use of fast acting and less expensive technology such as the second-generation FACTS devices, which can improve the efficiency of transmission lines by enhancing the power flow to serve the increasing load demand in Ghana.

1.3 Purpose of the Research

The purpose of this research is to assess how the stability of the electric power system of Ghana can be improved by employing UPFC on the transmission lines.

1.4 Objectives of the Research

The main objective of the research is to improve the stability of the electric power transmission system of Ghana by employing the UPFC.

However, for the main objective to be met, the following specific objectives should be achieved:

i. Modelling of Ghana's transmission system using MATLAB Simscape Power Systems software;
ii. Performing load flow analysis on the modelled system;
iii. Modelling the UPFC and studying system performance on the modelled system; and
iv. Determining the most appropriate location for the UPFC and using it to solve the stability problem.

1.5 Research Questions and Hypothesis

The objectives of the research give rise to the following stated research questions:

i. What are the other ways of improving stability in electric power transmission systems?
ii. Why go in for UPFC and no other stability improving device?

The research hypothesis is stated thus: The use of UPFC provides better improvement on power system stability of electric power transmission lines.

1.6 Expected Outcomes

The expected outcomes of the research are as follows:

i. To improve the stability of Ghana's electrical transmission system; and
ii. To be able to optimise the control of transmission line parameters

1.7 Scope of the Research

The research focuses on using power electronic devices to control the transmission line parameters on Ghana's electric power transmission system, which is operated by the Ghana Grid Company (GRIDCo).

1.8 Research Methods Used

The research methods employed include:

i. Review of related literature;
ii. Field visits, data collection and analysis;
iii. Mathematical modelling of transmission system; and
iv. Computer simulations of the transmission system with UPFC optimally located based on Fast Voltage Stability Index (FVSI) using MATLAB Simscape Power System software.

1.9 Facilities Used for the Research

i. Library, Laboratory, Computer and Internet facilities at the University of Mines and Technology;
ii. Laptop Computer with MATLAB Simscape Power System software; and
iii. Electric Power Transmission System of Ghana.

1.10 Significance of the Research

This research is significant because Ghana's electric transmission network currently faces major challenges due to instability problems. Lack of compensation at some buses and inappropriate placement of compensating devices has led to this problem. A critical look into FACTS devices and consequently the most recent, which is the UPFC can help tackle the power instability issues in the country.

1.11 Definition of Terms and Key Concepts

Flexible alternating current transmission systems: They refer to a family of power electronics-based devices, which enhance AC system controllability and stability and increase power transfer capability.

Unified power flow controllers: They are a member of the FACTS family, which use a combination of a shunt controller (STATCOM) and a series controller (SSSC) interconnected through a common Direct Current (DC) bus.

Power transmission system stability: It is the ability of the power system, for a given initial operating condition, to regain a state of operating equilibrium after being subjected to a

physical disturbance with most system variables bounded so that practically the entire system remains intact.

1.12 Organisation of the Thesis

The thesis is organised into five main chapters. These chapters have sections, which explain the main chapters.

Chapter 1 is the general introduction to the research. It includes the background to the research, problem statement, purpose and objectives of the research. The chapter further discusses the research questions and hypothesis, expected outcomes and the scope of the research. The research methods and facilities used are also given in this chapter. Finally, the significance of the research, and definition of terms and key concepts are stated.

Chapter 2 is dedicated to the literature review. The chapter explains the power system stability problem. The branches of stability, which affect the transmission system are discussed. Ways in dealing with the identified category of instability are assessed and the most recent remedy is elaborated. FACTS devices as a modern strategy in dealing with power system stability related issues are expanded and narrowed down to the UPFC, which is one of its current members with wide control strategies. The fast voltage stability index as a method of optimal placement of FACTS devices into a power system is also discussed.

Chapter 3 entails the methods used in achieving the research objectives and finding answers to the research questions. The methods used in modelling the power system and the UPFC are addressed. The optimal placement of the UPFC on the power system to solve the stability problem is also discussed.

Chapter 4 is dedicated to the presentation of the simulation results and their discussions. The parameter status of the power system before and after placing the UPFC in the network is analysed. The outcome of the performance and placement of the device on the network are also discussed. The summary of findings is also presented in this chapter.

Finally, Chapter 5 presents the conclusions based on the findings, with recommendations and possible further works enumerated.

CHAPTER 2

LITERATURE REVIEW

2.1 Introduction

The chapter reviews related literature on power system stability and assesses improvement methods considered for the stability issue. The category of stability related to the transmission is addressed. A comprehensive review of FACTS devices is provided with emphasis made on the operation and characteristics of the UPFC. The optimal allocation of the device is discussed and a suitable method chosen for the implementation. A general overview of Ghana's transmission network is finally provided.

2.2 Definition and Classification of Power System Stability

The purpose of a power system is to provide electrical energy to load centres at a continuous and secure manner. However, the emergence of fault conditions hampers the continuity and security of the power supply to the load centres. Fault conditions like lightning, human errors, accidents as well as incremental changes in power system parameters cause the disturbance of either the generator, transformer or other sections of the system leading to unbalance between generator and load. The system is stable if it is able to recover from these disturbances with no loss of supply (Al – Shamli *et al.*, 2015). Power system stability is therefore defined as "the ability of an electric power system, for a given initial operating condition, to regain a state of operating equilibrium after being subjected to a disturbance, with most system variables bounded so that practically the entire system remains intact" (Gibbard *et al.*, 2015).

Grigsby (2016) realised that the stability of a power system during a fault normally depends on the initial operating condition and the nature of the fault. The system must be able to survive numerous faults of small nature like the continuous changing of loads as well as large faults like loss of a generator. Even though power system stability is a single problem, the different causes of instability necessitate its classification in order to find appropriate solutions to dealing with the issue. The problem may be due to the resulting mode of instability, the size of the disturbance and the devices, processes and time span used in assessing the stability problem. Power system stability is classified under rotor angle, voltage and frequency stabilities as shown in Figure 2.1 (Morval *et al.*, 2016).

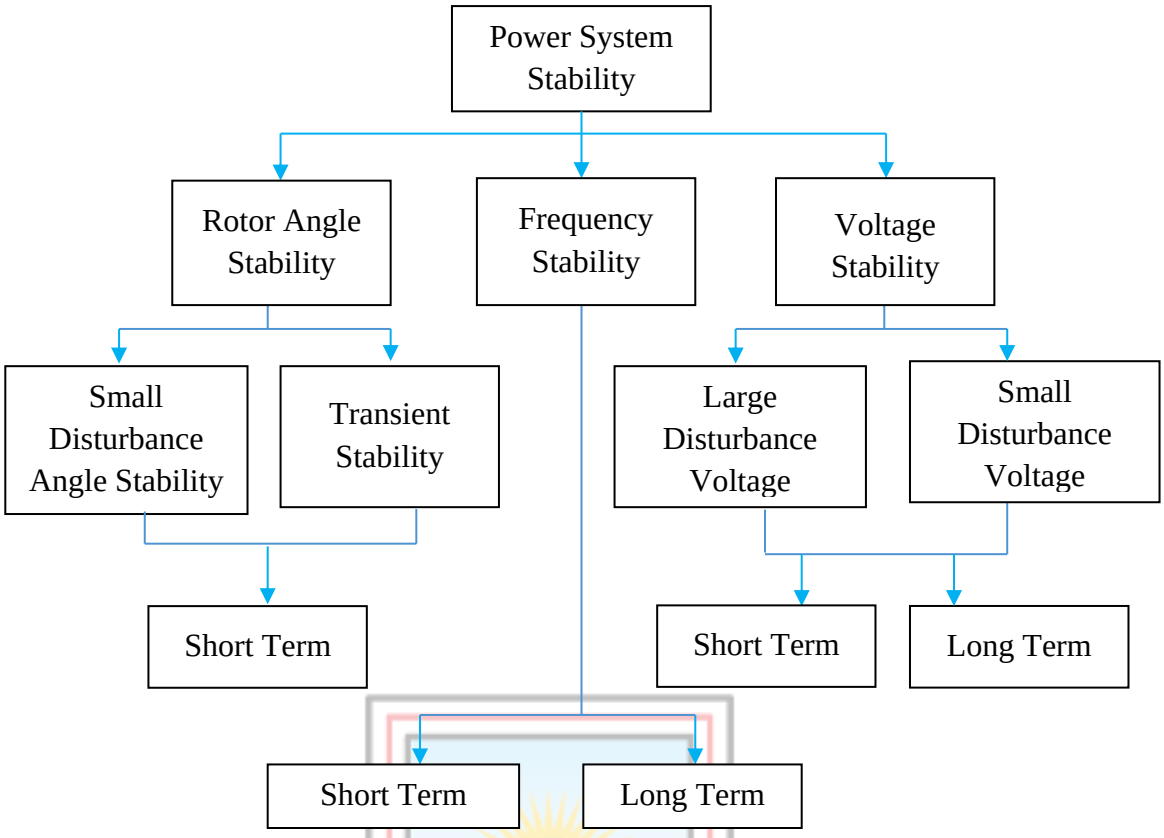

Figure 2.1 Classification of Power System Stability

Increased load demands and market economics are pushing transmission networks closer and closer to their operational limits. It is, therefore, necessary to perform in-depth studies into the different types of stability problems in order to check the system's reliability and its resilience to the various disturbances (Morval *et al.*, 2016).

2.2.1 Rotor Angle Stability

Rotor angle stability focuses on the ability of a synchronous machine, connected to a power system to remain in synchronism under normal operating conditions or after a disturbance (Songkin *et al.*, 2017). The instability occurs with a change in angular velocity of the synchronous machine, leading to loss of synchronism with other interconnected machines. The mechanical torque must be in equilibrium with the electrical torque under steady-state conditions to result in constant rotation and stable operating condition. Rotor angle stability is classified further into steady-state stability and transient stability (Songkin *et al.*, 2017).

Steady-state stability

Due to numerous generators connected in the power system to enhance reliability and increased capacity, oscillations occur. These oscillations are because of changes in kinetic

energy of various generator rotors as a result of inertia and synchronising torque. Control devices in a power system also contribute to rotor oscillations and if the disturbance is small (continuous changes in load) the oscillations should decay for a small-signal stable system else, the power system is unstable (Songkin *et al*., 2017).

Transient stability

Large disturbance causes excessive changes in the power system. These disturbances include faults on a transmission facility, loss of generation or loss of large load. The disturbances manifest in many ways like high excursions on generator rotor angle, intermittent power flows, irregular bus voltages and abnormal behaviour of other system components. If the system is able to restore normal operating conditions then the power system is transiently stable, otherwise, it is unstable (Songkin *et al*., 2017).

2.2.2 Voltage Stability

Voltage stability is the state where a power system is able to maintain steady voltages at all buses in service or after a disturbance, from an initial operating condition. Voltage instability may occur due to the progressive fall or rise of voltages on the system buses. This form of instability depends on the reactive and active power balance between generation and load and the system's ability to maintain this balance at all conditions. Two conditions contribute to the voltage instability problem in a system, and these are reactive power deficiency and high voltage drop on the transmission lines during the evacuation of power to load centres. A state of voltage instability occurs when a disturbance causes the reactive power demand in the system to increase beyond the capability of the reactive power sources in the power system, causing a progressive drop of bus voltages and consequently, voltage collapse. Voltage collapse occurs when a sequence of events from voltage instability causes blackouts or abnormally low voltage in a large portion of the power system. Another form of voltage instability can also occur due to overvoltages, when transmission lines are loaded below surge impedance and under-excitation limiters prevent generators and synchronous condensers from absorbing excess reactive power (Gibbard *et al.*, 2015).

Voltage stability can be classified in terms of the nature of the disturbance, under large and small disturbance. Large disturbance voltage stability is the ability to maintain steady voltages after a large disturbance such as system faults or heavy circuit contingencies. This form of instability can be investigated with the examination of the dynamic performance of the system over a time sufficient to capture the interaction of devices such as under load tap

changing transformers. Small disturbance voltage stability is being able to maintain steady system voltages after a small perturbation such as incremental changes in system loads. A criterion for small signal voltage stability is that, at a given operating condition for every bus, the voltage magnitude should increase as the reactive power injection increases (Danish, 2015).

Voltage stability is categorised under time, into short term and long-term. When there is a loss of heavily loaded transmission line, under high-stress conditions and reactive power at a minimum, there would be considerable reduction in voltages at adjacent buses, thereby reflecting into the distribution system. Tap changing transformers and feeder changing regulators can be used to restore the voltage to normal, the action of these devices are slow acting hence constitute long term voltage stability. Short-term voltage stability involves the dynamics of fast-acting devices such as induction motors and electronically controlled loads (Danish, 2015).

2.2.3 Frequency Stability

Frequency stability is the ability of a power system to maintain steady frequency after a disturbance that results in a substantial imbalance between load and generation. Losing a generator in a power system can cause an unbalance in generation and load leading to frequency instability. A frequency stable network should be able to restore the balance between generation and load with minimal loss of load. Severe system upsets generally result in large excursions of frequency, power flows, voltage, and other system variables, thereby invoking the actions of processes, controls, and protections that are not modelled in conventional transient stability or voltage stability studies. Automatic load shedding schemes are employed as last resort during frequency instability, where under-frequency relays shed the required amount of load needed to cause a generation-load balance (Gomez–Exposito *et al*., 2018).

2.3 Measures to Improve Power System Stability

The important variables that influence power system stability are the rotor angle, the nodal voltage and frequency. There are numerous methods used to enhance these variables in order to improve the stability of the system. Financial consideration, however, determines the extent to which these enhancements can be implemented and there must always be a trade-

off between a system operating near its stability limit and operating the system with excessive reserve generation and transmission capacity (Grigsby, 2016).

The methods used to improve the various forms of stability problems are discussed as follows (Grigsby, 2016):

2.3.1 Power System Stabilisers

Power System Stabilisers (PSS) provide additional control loops to the automatic voltage regulator system and the turbine governing system of a generating unit thereby causing damping of rotor oscillations. It is one of the most cost-effective methods of enhancing power system stability. The primary focus of stability is to realise that at steady state, when the change in speed is zero or near zero, the voltage controller has to be driven by only the voltage error. However, when there is a transient, rendering the generator speed not constant, the rotor swings and voltage change undergoes oscillation. The task of the PSS is then to add supplementary signals that compensate for change on voltage oscillations and provide a damping component that is in phase with the change in speed.

2.3.2 Fast Valving

Large disturbances close to generators cause a sudden drop in the power output and the mechanical power input needs to be reduced as fast as possible to maintain the stability of the system. Restoring the power to the pre-fault value needs to be done about half a swing period and this cannot be achieved with hydro turbines due to large changes in pressure and huge torque necessary to move the control gates. The steam turbine, on the other hand, can quickly respond to the fast changes in the mechanical output hence, termed fast valving.

2.3.3 Braking Resistors

A braking resistor can be connected at the generator or substation terminals to limit the rotor swings following a disturbance. The resistor may be switched using a circuit breaker or controlled using FACTS devices. In the case of the switched form of the braking resistance, the switching time should be based on detailed simulations. If the resistors remained connected too long, there is a possibility of instability on the “backswing”.

2.3.4 Excitation Systems

Improvements in transient stability are achieved by a rapid temporary increase in generator excitation. When a fault occurs on a transmission line leading to isolation of the faulted line the automatic voltage regulator increases the field voltage. This can lead to degrading the damping of local plant oscillation, hence control systems are used to check the problem.

2.3.5 Compensation using Flexible AC Transmission System Devices

FACTS devices have proven to be effective in dealing with power system stability. The reactive power needed by the network can be supplied by a series or shunt connected device. The generating station is relieved of producing and transmitting the needed reactive power over long distances. Control systems associated with these devices are capable of controlling the power flow parameters on the transmission system.

Many other techniques are used to reduce the stability of the power system including reactor switching, single pole switching and ultimately load shedding as the last resort.

2.4 Assessment of Power System Stability and Dynamic Security

Dynamic Security Assessment (DSA) is an evaluation of a power system being able to withstand specific contingencies and surviving the change to a new stable position (Grigsby, 2016). Contingencies such as loss of a transmission line, decaying voltage and other events push the power system towards an unsafe limit and when this limit is reached the operator has minimal or no time to remedy the situation. The system, therefore, needs to be assessed to verify when the power system is approaching such a limit where blackouts become inevitable (Savulescu, 2014).

The security of a power system is somewhat different from a stable network. This is because a disturbance may lead to loss of load (due to the action of protective devices) to stabilise the system, and such a power system is stable but not secured. A secured system must however be stable. The assessment of security of the power system is therefore paramount in dealing with a stable and secure network and must be performed for every new operating state. Mathematical analysis of these responses and determining the new equilibrium condition is called security assessment. Security assessment, now referred to as DSA, is defined by the Institute of Electrical and Electronics Engineers (IEEE), as “An evaluation of the ability of a certain power system to withstand a defined set of contingencies and to

survive the transition to an acceptable steady-state condition". Two types of DSA exist that is, off-line DSA and on-line DSA but recently on-line DSA has become more attractive due to advances in computation algorithm development, real-time data acquisition and analysis and computer technologies. Figure 2.2 (Grigsby, 2016) shows the functional model of an on-line DSA system.

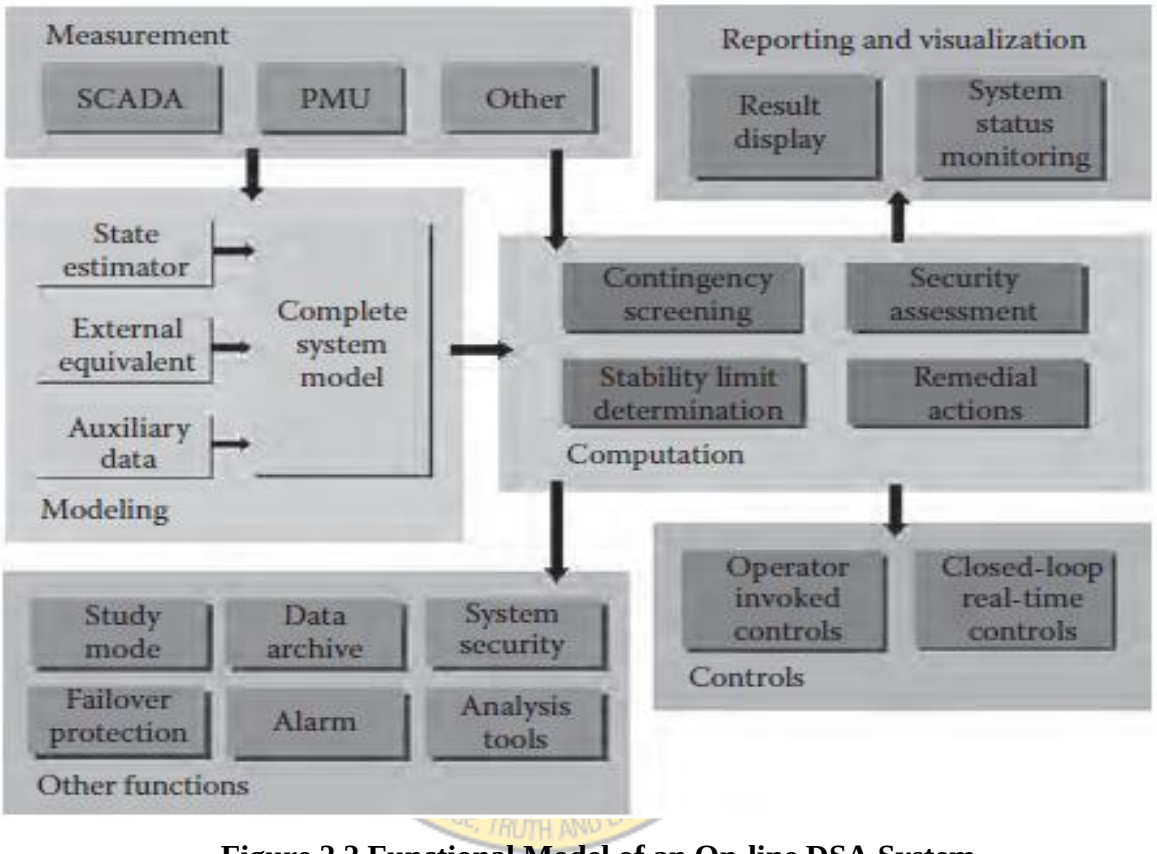

Figure 2.2 Functional Model of an On-line DSA System

Different analytical methods can be used for the DSA depending on the performance concerned and the criteria to be applied. A brief overview of these methods are provided as follows (Grigsby, 2016):

2.4.1 Power Flow Analysis

This refers to the determination of the steady-state operating condition of a power system for a given set of network configurations, control and known inputs. It can be used for tasks such as thermal loading and voltage analysis. The power flow analysis problem is deduced as a set of non linear algebraic equations and well-developed solutions like the Newton-Raphson and Gauss-Seidel methods are available (Grigsby, 2016).

2.4.2 P-V Analysis and Continuation Power Flow Methods

In system analysis such as the voltage stability analysis, the stability margin needs to be determined. An example is the maximum power that can be transferred from generation to load. This can be done by the power voltage angle analysis as shown in Figure 2.3 (Grigsby, 2016).

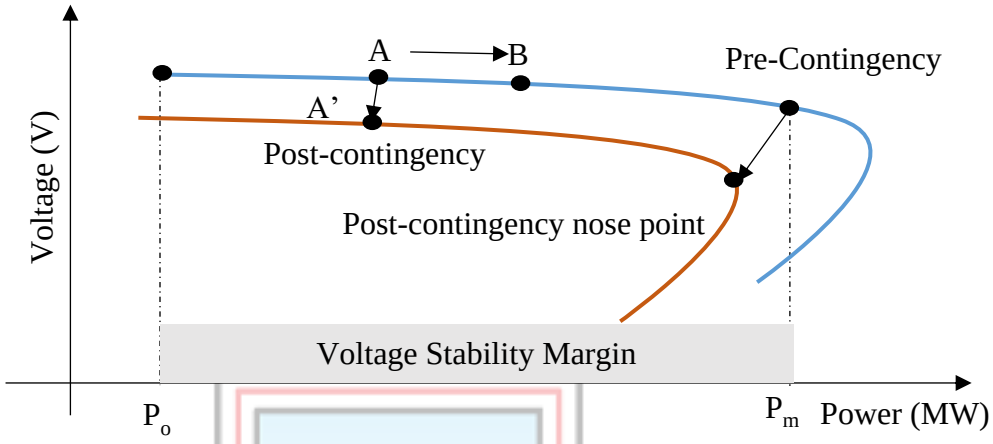

Figure 2.3 Power-Voltage (PV) Analysis Curve

The analysis is started by solving the power flow (A) at the pre-contingency condition for a specified transfer level. Contingencies are then applied and the power flow (A') solved. If all post-contingency power flows can be solved without security violations, the contingency analysis is repeated. If any of post-contingency power flows cannot be solved, or can be solved but with security violations (such as low voltages), the voltage stability limit is found (Grigsby, 2016).

2.4.3 Time-Domain Simulations

Transient stability and security performance are commonly solved by the so-called Time-Domain Simulations (TDS). Numerical integration algorithms are used to solve a set of non-linear differential equations that describe the dynamics of the model. The input data required by the simulations are: A solved power flow case, the network topology, parameter and initial operating condition of the system, a set of dynamic models that match the components in the power flow case and a set of contingencies to be applied as disturbances during simulations. The basic outputs from the simulations are the time-domain responses of various physical quantities in the system, such as generator rotor angles, speeds, bus voltages, flows in transmission lines and load powers (Grigsby, 2016).

2.4.4 Eigenvalue Analysis

Eigenvalue Analysis can be used to solve both frequency and voltage stability problems. For the frequency-domain method, the nonlinear differential equations describing the system dynamics are linearised around an operating condition and eigenvalues corresponding to electromechanical oscillations are computed from the linearised model. With the voltage stability method, the smallest eigenvalue of the power flow (Jacobian matrix) gives a good indication of how close the system is to its nose point (or stability limit). In addition, the eigenvector associated with this eigenvalue contains information on the mode of voltage instability. This is very useful in practice for the understanding of voltage stability problems and for deriving remedial controls (Grigsby, 2016).

2.5 Transmission System Stability

The increase in electricity consumption leads to the expansion of AC systems as well as higher voltage levels to permit transmission of large power over long distances. Combined operation and interconnecting adjoining grids have lots of technical and economic advantages but also pose a lot of stability problems (Savulescu, 2014).

The major issue of concern with the stability of the transmission system of Ghana is that of voltage instability where the regulatory body (Ghana Grid Company) still keeps finding solutions (Anon., 2018a). An outcome of voltage instability is tripping of transmission lines and other elements by their protective devices, leading to cascading outages and eventually loss of synchronism and total system collapse. Although low voltages can be associated with the processes of rotor angle going out of step, the type of voltage collapse associated with voltage instability can occur where angle stability is not an issue (Savulescu, 2014).

Gomez-Exposito *et al*. (2018) described the main factor causing voltage instability as a system not being able to meet the demand for reactive power. This occurs in heavily stressed systems, as experienced on Ghana's network on March 21st, 2012, where high demand for reactive power led to transmitting large amounts from generating stations, causing voltage drops on the transmission lines and eventually resulting in total voltage collapse (Anon., 2012b). Other factors contributing to voltage collapse include generator reactive power control limits, characteristics of reactive compensating devices and the action of voltage control devices such as under-load tap changers (Savulescu, 2014).

To understand the effect of voltage instability on transmission systems, the characteristics of the system are analysed. The major interest of the analysis is the relationship between the transmitted power, P_r receiving end voltage, V_r and the reactive power injection, Q_c. The simple radial diagram in Figure 2.4 (Hossain and Pota, 2014) is used to explain the voltage stability phenomenon.

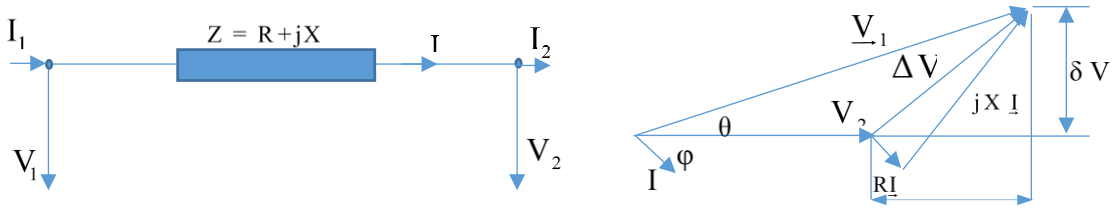

(a) Single Line Two Bus Illustration (b) Phasor Illustration

Figure 2.4 Illustration of Voltage Stability Phenomenon

From Figure 2.4, considering a line below 200 km, the absence of shunt admittance causes the line current to become $I = I_1 = I_2$ and it is constant throughout the entire transmission line. With the angle between the line current and receiving end voltage as φ, $I_a = I \cos \varphi$ and $I_r = I \sin \varphi$ for the respective active and reactive components of the current. Assuming a constant sending end voltage V_1 and the receiving end voltage taken as the phase origin, then the voltage drop becomes as expressed by Equation (2.1) (Eremia *et al.*, 2016).

$$\Delta \underline{V} = Z\underline{I} = \Delta V + j\delta V \qquad (2.1)$$

where, $\Delta V = RI_a + XI_r$ = longitudinal voltage drop component (V)

$\delta V = XI_a + RI_a$ = transversal voltage drop component (V)

Z = line impedance (Ω)

I = line current (A)

Equation (2.1) can be written in terms of single-phase apparent power, S_0 as given by Equation (2.2) (Eremia *et al.*, 2016).

$$S_0 = V_2 (I_a + jI_r) = P_{02} + jQ_{02} \qquad (2.2)$$

where, P_{02} = active power (MW)

Q_{02} = reactive power (MVAr)

S_0 = apparent power (MVA)

V_2 = receiving end voltage (V)

I_a = active current component (A)

I_r = reactive current component (A)

Then the change in voltage is expressed by Equations (2.3) and (2.4) (Eremia *et al*., 2016).

$$\Delta V = \frac{RP_{02} + XQ_{02}}{V_2} \tag{2.3}$$

$$\delta V = \frac{XP_{02} - RQ_{02}}{V_2} \tag{2.4}$$

where, R = line resistance (Ω)

X = line reactance (Ω)

Since $R << X$ for transmission lines, $\Delta V = XQ_{02}/V_2$ and $\delta V = XP_{02}/V_2$. It can be realised from the analysis that the change in voltage, ΔV between the sending end voltage and the receiving end voltage is primarily due to reactive power flows on the transmission line, whilst the active power flow depends on the phase difference. In order to limit the voltage drop, the transfer of reactive power should be avoided (Hossain and Pota, 2014). The voltage stability phenomenon is discussed by plotting the relationship between V_R and P_R for different values of load power factor with a constant source voltage as shown in Figure 2.5 (Grigsby, 2016).

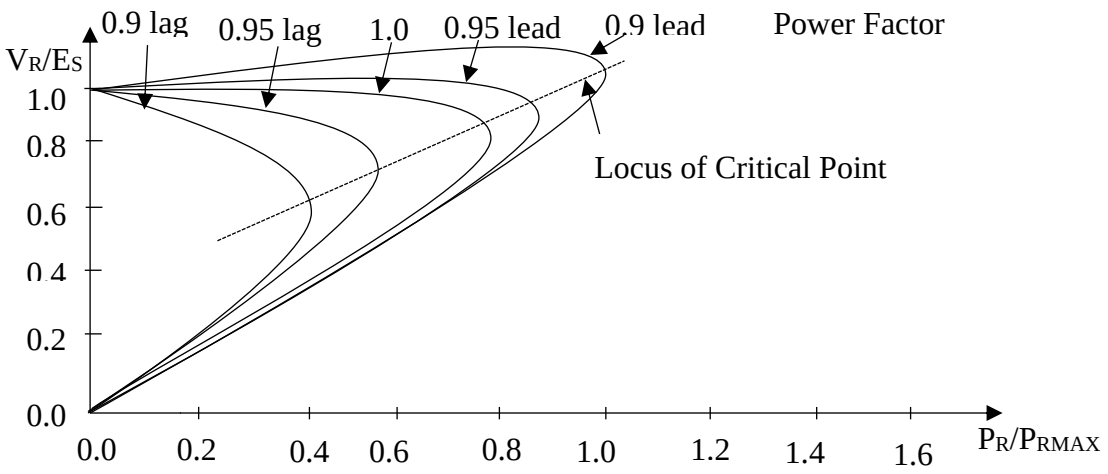

Figure 2.5 V_R – P_R Characteristics of the Transmission System

When the power is below maximum, either the voltage is high and current is low or vice versa. A high voltage means operating close to its generator voltage and represents a normal operating condition. The situation where current stays high for a long period might burden the system causing it to fail. The operating region above the critical point has a stable system condition and the region below the critical point exhibits instability conditions. A sudden increase in reactive load can cause the system to change from stable to unstable (Grigsby, 2016).

2.5.1 Improving Voltage Instability Associated with the Transmission System

The voltage in a transmission system can be controlled by generating, consuming or adjusting reactive power flow in the system. To maintain stability, it must be noted that the control of reactive power flow must yield a voltage magnitude as close to nominal as possible. Transmission systems primarily achieve this by accepting reactive power generation and control from the synchronous generators. The transfer of the reactive power together with its associated active power limits the total power transfer in the system. To increase the total power transfer, most of the reactive power needed by the system has to be produced and controlled locally. The use of FACTS devices at Bulk Supply Points (BSPs) offers fast and reliable generation and control of reactive power. These devices offer a flexible system operation in regards to their power flow capability and provide improvement options for transient and steady-state voltage stability (Hossain and Pota, 2014).

The best bargain for the improvement of the transmission system stability is by the use of these FACTS devices, which the next section seeks to address.

2.6 Flexible Alternating Current Transmission Systems and their Devices

2.6.1 Flexible Alternating Currents Transmission Systems

Recently, the rational on transmission development has enhanced the growth of competitive electric energy markets. The progression of new socio-economic and legislative issues have demanded a review of traditional power transmission theory, practice and the creation of new concepts to allow full utilisation of existing power transmission facilities, without compromising system availability and security. The Electric Power Research Institute (EPRI) in Palo Alto, California, USA in the late 1980's formulated the vision of FACTS in which various power electronics-based controllers enhance controllability and increase

power transfer capability while maintaining sufficient steady state and transient margins (Bhowmick, 2016; Patel and Paliwal, 2015). The enhanced controllability and power transfer capability are achieved by controlling the transmission flow parameters that are related to the operation of the system and these include current, voltage, phase angle and power (Eremia *et al.*, 2016). According to Grigsby (2016), the transmission line is utilised far below the limit set by its thermal capability, as depicted in Figure 2.6.

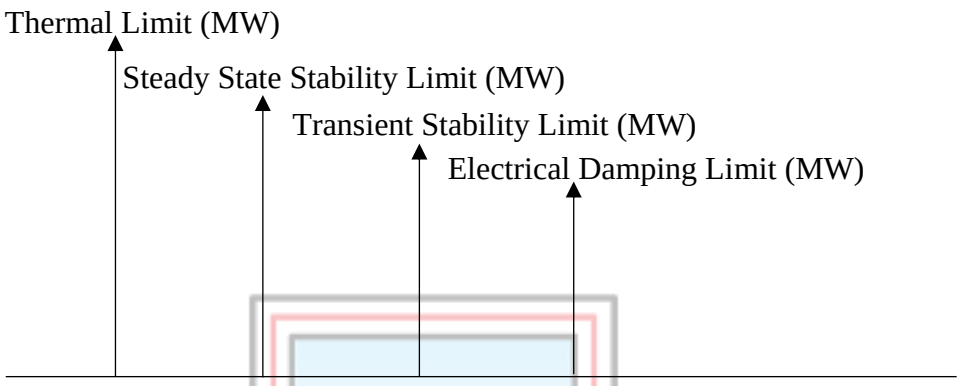

Figure 2.6 Limits of Power Transfer along a Transmission Line

FACTS devices can however, be used to enhance the power flow capabilities of the line close to its thermal limits, therefore avoiding or delaying the construction of a new power line. The power flow equation in Equation (2.5) (Padiyar and Kulkarni, 2019) is used to explain the control of power in the transmission line. Selecting δ_{max} between 30° and 40° based on the stability margin of the system and for line lengths exceeding a certain limit, P_{max} should be less than the thermal limit and the power transfer determined by the current carrying capacity of the conductors. As the line length increases, X increases in a linear fashion and P_{max} reduces as shown in Figure 2.7 (Padiyar and Kulkarni, 2019).

$$P_{max} = \frac{V_1 V_2 \sin \delta_{max}}{X} \qquad (2.5)$$

where, P_{max} = maximum transmittable power (MW)

δ_{max} = maximum power angle (degrees)

V_1 = sending end voltage (V)

The series compensation using series connected capacitors increases P_{max} as the compensated value of the series reactance X_c is given by Equation (2.6) (Padiyar and Kulkarni, 2019).

$$X_c = X (1 - K_{se}) \quad (2.6)$$

where k_{se} = degree of series compensation and typically does not exceed 0.7.

X_c = series compensating reactance (Ω)

P_{max} can also be increased by controlling the receiving end voltage of the line.

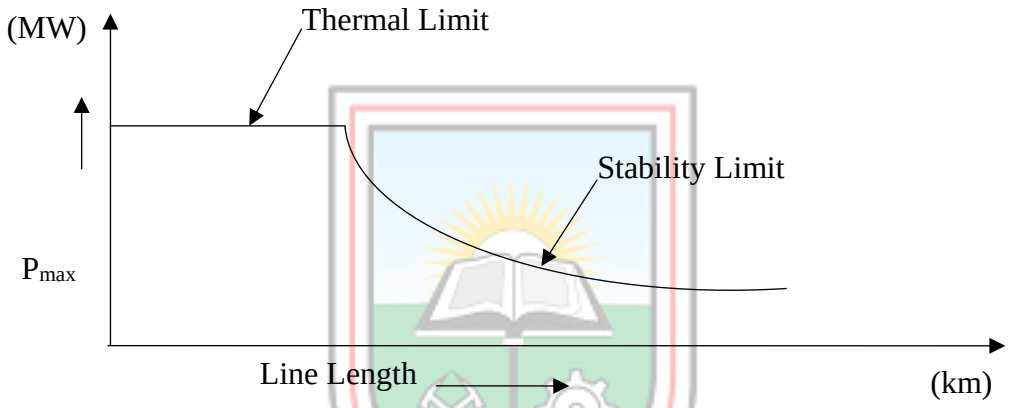

Figure 2.7 Power Transfer Capacity as a Function of Line Length

When a generator supplies a unity power-factor load, the maximum power occurs when the load resistance is equal to the line reactance. It is to be noted that the receiving end voltage V_2 varies with the load and can be expressed as in Equation (2.7) (Padiyar and Kulkarni, 2019).

$$V_2 = V_1 \cos (\theta_1 - \theta_2) \quad (2.7)$$

where, θ_1 = sending end phase angle (degrees)

θ_2 = receiving end phase angle (degrees)

P_{max} is then expressed by Equation (2.8) (Padiyar and Kulkarni, 2019).

$$P_{max} = \frac{V_1^2 \sin [2(\theta_1 - \theta_2)]}{2X} \quad (2.8)$$

According to Padiyar and Kulkarni (2019), providing dynamic reactive power support at the receiving bus makes it possible to regulate the bus voltage magnitude. Figure 2.8 (Padiyar and Kulkarni, 2019) shows the circuit of a transmission line compensated by a controllable reactive power source at the receiving end. The reactive power injected is given as in Equation (2.9) (Padiyar and Kulkarni, 2019).

$$Q_c = \frac{V_2^2 - V_1 V_2 \cos(\theta_1 - \theta_2)}{X} \qquad (2.9)$$

where, Q_c = level of reactive power compensation (MVAr)

The reactive power produced at the generating stations can therefore, be reduced to allow maximum capacity for the transfer of active power.

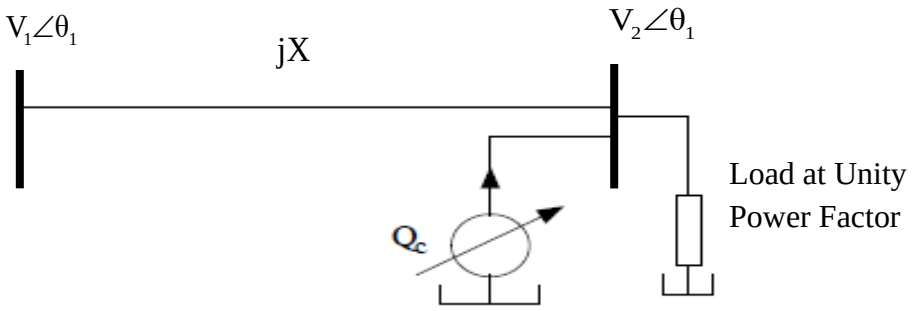

Figure 2.8 Transmission Line Compensated by Controllable Reactive Power Source at Receiving End

2.6.2 Flexible Alternating Current Transmission System Devices

Continuous progress in the development of power electronics has enabled a number of devices to be developed providing the same control action as the transformer tap changer but with much faster operation and with fewer technical problems. These electronic devices are referred to as FACTS devices. Depending on the connection of these devices to the power system, they can be classified under shunt and series devices (Eremia *et al*., 2016).

Bhowmick (2016) explained that the development of FACTS devices follows two generations both resulting in a comprehensive group of controllers able to address targeted transmission problems. The first group employs reactive impedances or a tap changing transformer with thyristor switches (that is having no intrinsic turn-off ability) as controlled elements, similar to breaker switched capacitors. They have a rather fast response but are

operated by a complex control circuit. Examples include the Static VAr Compensator (SVC), the Thyristor-Controlled Series Capacitor (TCSC), and the phase shifter. The second generation of FACTS devices uses self-commutated static converters as controlled voltage sources. Examples include the Static Synchronous Compensator (STATCOM), the Static Synchronous Series Compensator (SSSC), UPFC and the Interline Power Flow Controller (IPFC). Comparing both generations of FACTS devices, the voltage source converter based FACTS devices according to Bhowmick (2016), provides superior performance characteristics and uniform applicability for transmission voltage, effective line impedance, and angle control. They also have the potential to exchange real power directly with the AC system.

Zhang *et al*. (2012) made a comparison between the two generations of FACTS devices in Figure 2.9. The left is made up of first generation devices, which use thyristor valves having low power losses. The right side comprises second generation devices, which contains more advanced technology of Voltage Source Converter (VSC). These are based mainly on Insulated Gate Bipolar Transistor (IGBT), Insulated Gate Commutated Thyristor (IGCT) and Gate Turn-off Thyristor (GTO).

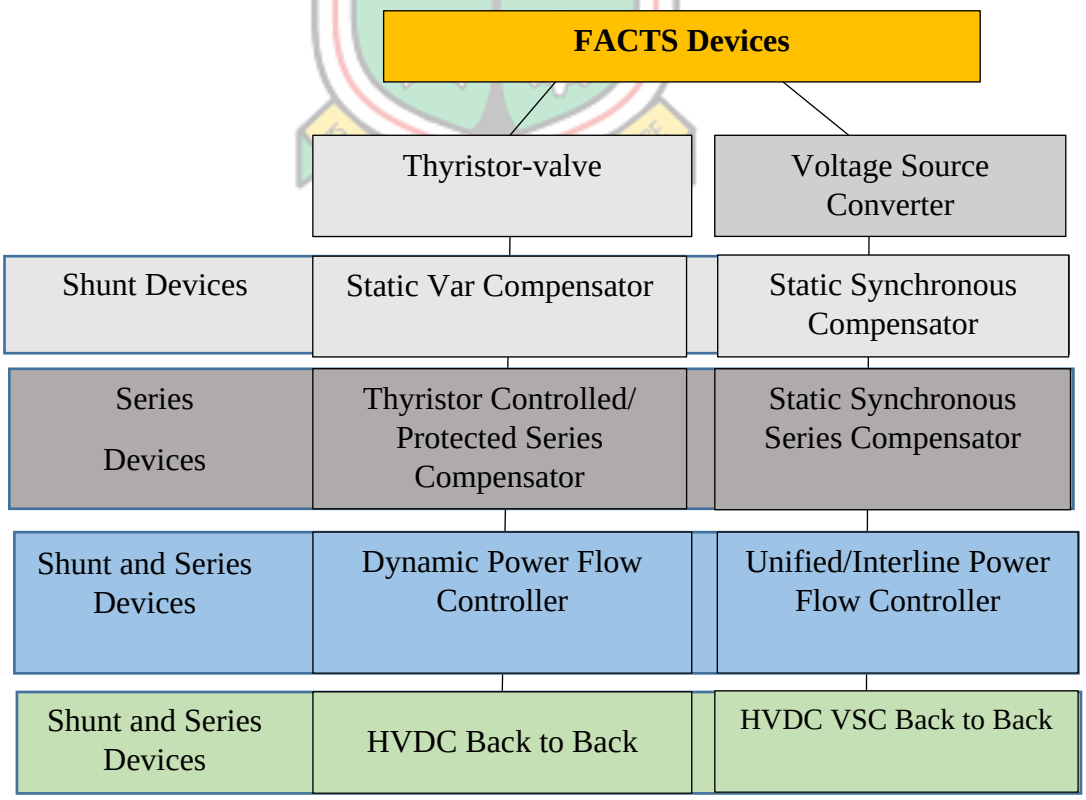

Figure 2.9 Comparison on the Generations of FACTS Devices

Static VAr compensator

SVC is a type of FACTS device employed in transmission systems to control voltage, enhance power oscillation damping, improve transient stability, increase transfer capability and reduce losses (Barot *et al*., 2014).

The major building blocks of the SVC is the thyristor valve made up of series connected anti-parallel thyristors. The reactive power elements consist of air core reactors, high voltage AC capacitors and a power transformer for step-up connection to the transmission lines (Zhang *et al.*, 2012). A single-phase Thyristor Controlled Reactor (TCR) shown in Figure 2.10 (Grigsby, 2016) consists of two anti-parallel connected thyristors in series with a fixed inductor.

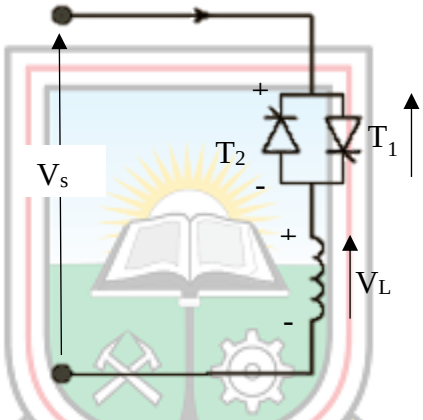

Figure 2.10 SVC as a Single-Phase Thyristor Controlled Reactor

To control the reactive power injected into the line, a thyristor-switched capacitor is connected in parallel to the TCR (Grigsby, 2016).

Voltage control of the SVC: Grigsby (2016) demonstrated voltage control on a transmission line using SVC, where the compensated bus voltage is given by Equation (2.10) (Grigsby, 2016).

$$V_c = V_s - I_{SVC} jX_s \qquad (2.10)$$

where, V_c = compensation bus voltage (V)

V_s = sending end bus voltage (V)

I_{svc} = SVC current (A)

X_s = short circuit impedance (Ω)

It is realised that the product $I_{SVC}X_s$ gives the contribution of the SVC for voltage control. This implies that the SVC is more effective for voltage control when:

i. I_{SVC} is large, that is, the reactive power capability of the SVC is high.

ii. X_s is large, that is, the system is weak and has a high short-circuit impedance.

In effect, the SVC can be seen to be only effective for a very weak system and tends not to strive well in a partially weak system.

Static synchronous compensator

The STATCOM is capable of providing continuous controlled reactive power generation and absorption by means of electronic processing of voltage and current waveforms in a VSC. The STATCOM does not require the physical capacitor banks and shunt reactors thereby making it have a more compact design. It also has low harmonic noise. Grigsby (2016) used a simple circuit as shown in Figure 2.11 to explain the operating principle of the STATCOM. It is basically made up of a VSC, a shunt coupling transformer and a capacitor connected at the DC side to provide a constant DC voltage.

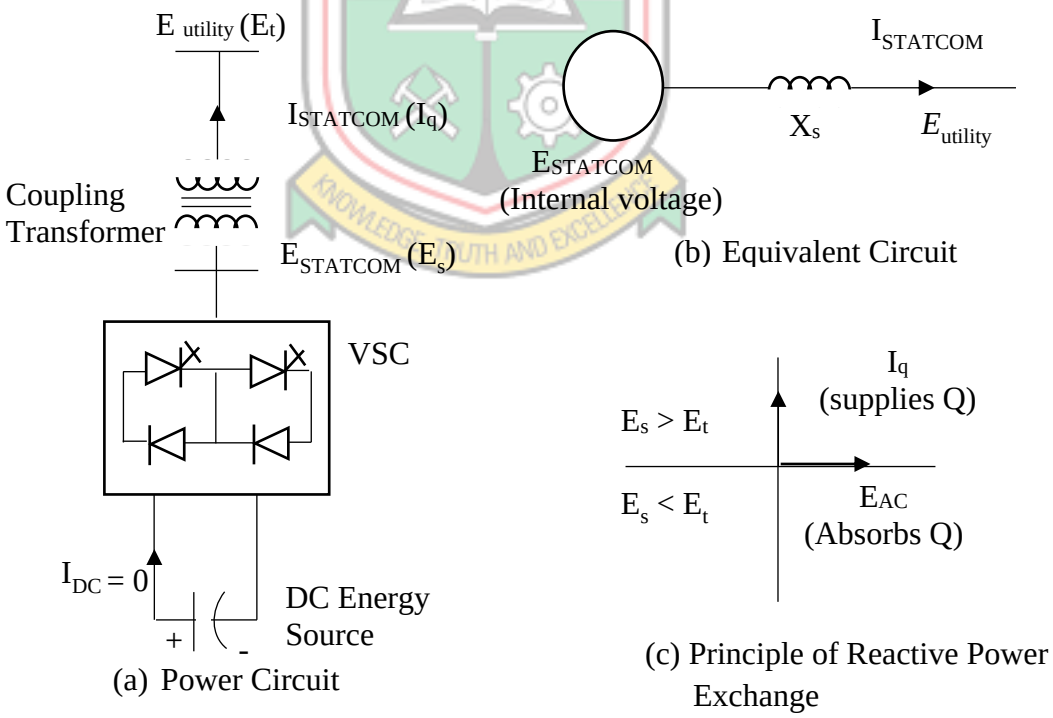

Figure 2.11 Power and Equivalent Circuits of the STATCOM

The STATCOM is connected to the AC system through the coupling transformer. Reactive power exchange between the converter and the AC system can be controlled by varying the

amplitude of the three-phase output voltage, of the converter. If the amplitude of the output voltage is increased above that of the utility bus voltage, then current flows through the reactance from the converter to the AC system and the converter generates capacitive reactive power for the AC system. If the amplitude of the output voltage is decreased below the utility bus voltage, then the current flows from the AC system to the converter, and the converter absorbs inductive reactive power from the AC system. If the output voltage equals the AC system voltage, the reactive power exchange becomes zero, and the STATCOM is said to be in a floating state.

A typical V–I characteristic of a STATCOM is depicted in Figure 2.12 (Ghosh and Ledwich, 2012). It can be observed that the STATCOM can supply both the capacitive and the inductive compensations and is able to independently control its output current over the rated maximum capacitive or inductive range irrespective of the amount of the AC system voltage (Ghosh and Ledwich, 2012).

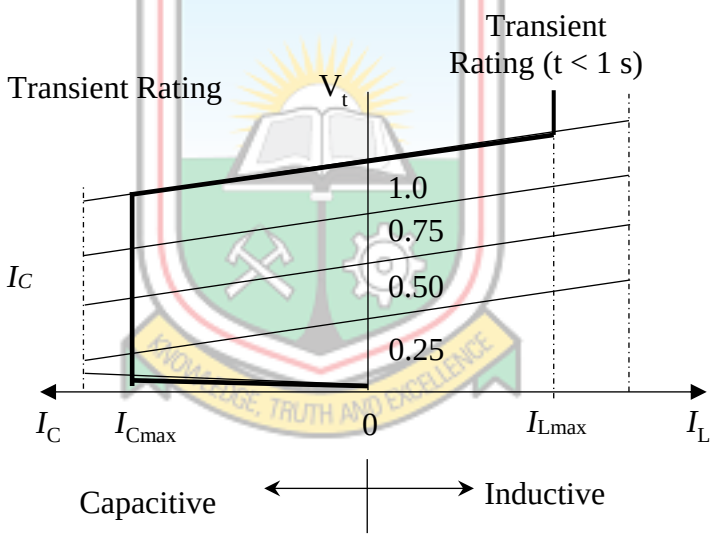

Figure 2.12 Typical V–I Characteristic of a STATCOM

The characteristics of the STATCOM reveal another strength of this technology: It is capable of yielding a full output of capacitive generation almost independently of the system voltage (constant current output at lower voltages). This is particularly useful in situations where the STATCOM is needed to support the system voltage during recovery after faults. The applications of the STATCOM are similar to those of SVC but with much faster and better results due to the turn-on and turn-off capability of its switching devices, as compared to the only turn-on capability of the thyristor in the SVC. Qatamin *et al*. (2017) made a comparison between SVC and STATCOM where an SVC was installed to enhance the

transmission capability of the line and solve the problem of the expected overload in 2020. The results were compared to installing a STATCOM at its optimum location. The comparison showed that, for the given power system, using STATCOM leads to a better voltage profile than using SVC.

Static synchronous series compensator

The SSSC is a voltage source converter, connected in series to the transmission line. It varies the effective impedance of the line by injecting a voltage with an appropriate phase angle in relation to the line current. SSSC mainly consists of a voltage source converter with some semiconductor devices having turn off capability for coupling with the transformer and a direct current capacitor. The DC capacitor operates as an energy storage element by providing a DC voltage support for the converter function as depicted in Figure 2.13 (Paul *et al.*, 2016).

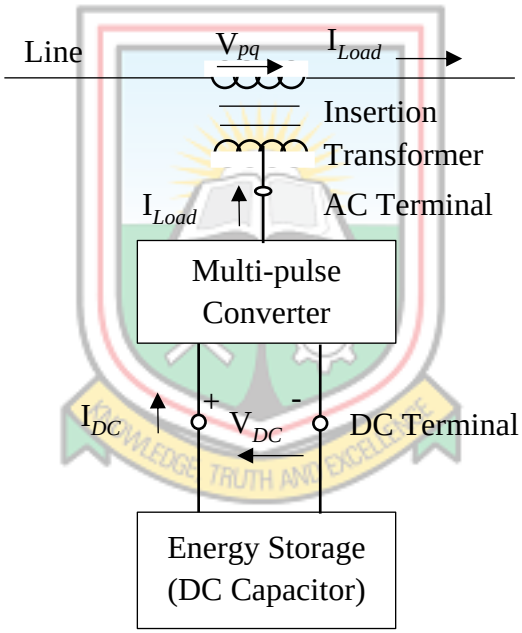

Figure 2.13 Static Synchronous Series Compensator

The valve-side voltage rating is higher than the line-side voltage rating of the coupling transformer to reduce the required current rating of the self-commutating valves. The valve-side winding is delta connected to provide a path for third harmonics to flow. Solid-state switches are provided on the valve side to bypass the VSC during situations of very large current flow in the transmission line or when the VSC is inoperative. The basic DC voltage for conversion to AC is provided by the capacitor (Paul *et al.*, 2016).

Adebayo *et al.* (2013) used SSSC to control voltage magnitude at low voltage buses in the Nigerian 330 kV grid. Simulations on the grid were done with and without the SSSC. The active and reactive power losses were reduced by 2.18% and 5.93%, respectively when SSSC was incorporated. The results from the analysis showed a considerable improvement in the voltage magnitude with the incorporation of SSSC and consequently, a significant reduction in the system losses.

Thyristor-controlled series compensator

TCSC is a series-controlled capacitive reactance controller that can provide continuous control of power on a transmission line. The basic TCSC module consists of a series capacitor, C in parallel with a TCR-L as shown in Figure 2.14 (Paul *et al.*, 2016).

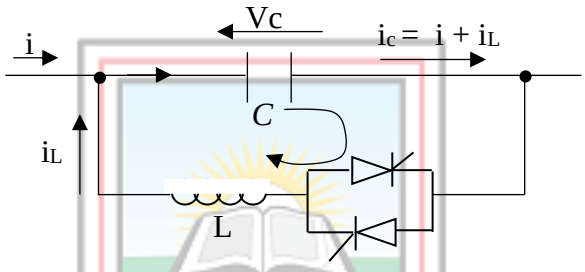

Figure 2.14 A Simple Circuit of a TCSC

The inductive reactance is controlled such that its current increases the effective voltage across the fixed series capacitor. This enhanced voltage changes the effective value of the series capacitive reactance with respect to the same line current. Depending on the amount of current drained in the inductive branch, the TCSC can increase or decrease the inductance of the transmission line on which it has been installed. TCSC was tested on a detailed representation of the Italian power grid and a part of the ENTSO-E network. After the incorporation of the TCSC, the security of the transmission system was enhanced and the voltage profile improved as compared to the system without the device (Bruno *et al.*, 2016). TCSC however, generates some amount of harmonics, therefore the need for including harmonic filters, which adds cost to its installation (Krishna and Sindhu, 2016).

2.6.3 The Unified Power Flow Controller

The UPFC is a second generation FACTS device, which has the capability of simultaneously controlling all the parameters that affect power flow on the transmission line (Bhowmick, 2016; Eremia *et al.*, 2016). It can be used for voltage regulation, series compensation and

phase shifting. This makes the UPFC the most powerful device for transmission system control.

Basic operation of the UPFC

Bhowmick (2016) used Figure 2.15 to Figure 2.19 to explain the action of the UPFC in controlling simultaneously or selectively, the line parameters that affect power flow on a transmission line.

Two primary conditions should be noted during the flow of active and reactive power on a transmission line.

i. Active power flow from a bus with a higher phase angle to a bus with a lower phase angle. From Equation (2.11) (Bhowmick, 2016), for power to flow from point 1 to point 2, $\theta_1 > \theta_2$.

$$P_{1,2} = \frac{V_1 V_2}{X} \sin(\theta_1 - \theta_2) \qquad (2.11)$$

ii. Reactive power flows from a bus of a higher magnitude voltage to a bus of a lower magnitude voltage.

On Figure 2.15 (Bhowmick, 2016), V_{se} is the series side voltage and V_{sh} is the shunt side voltage.

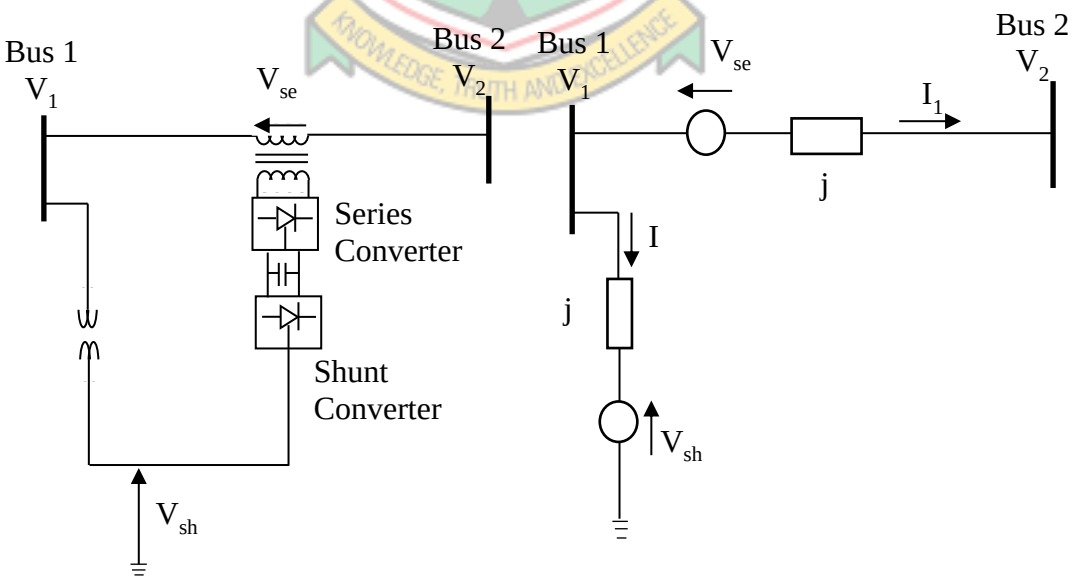

(a) Power Model (b) Equivalent Model

Figure 2.15 Power and Equivalent Circuits of an UPFC Connected in a Transmission Line

Assuming a non-zero active power flowing from sending end (1) to receiving end (2). When the series converter is not absorbing or delivering active power, then the series converter voltage either leads or lags the line current by 90^{o} as shown respectively with the phasor diagrams in Figure 2.16 (Bhowmick, 2016).

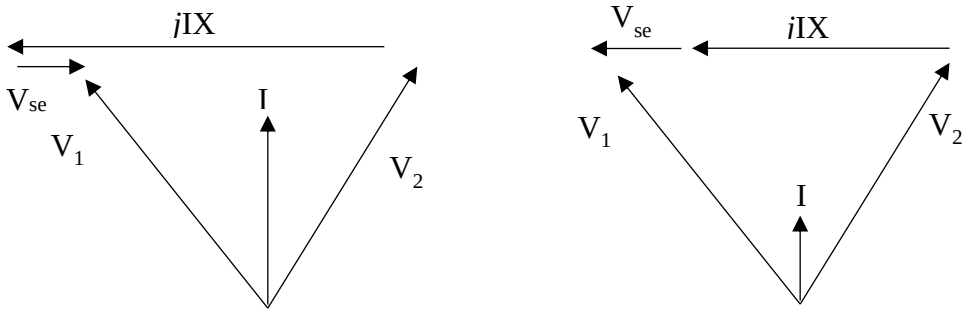

(a) Capacitive Mode (b) Inductive Mode

Figure 2.16 Phasor Diagram of Voltage in Capacitive and Inductive Modes

Since the series converter is not exchanging active power, the shunt converter can also not exchange power because the converter cannot consume or generate active power by itself so the phasor diagram would be as shown in Figure 2.17 (Bhowmick, 2016).

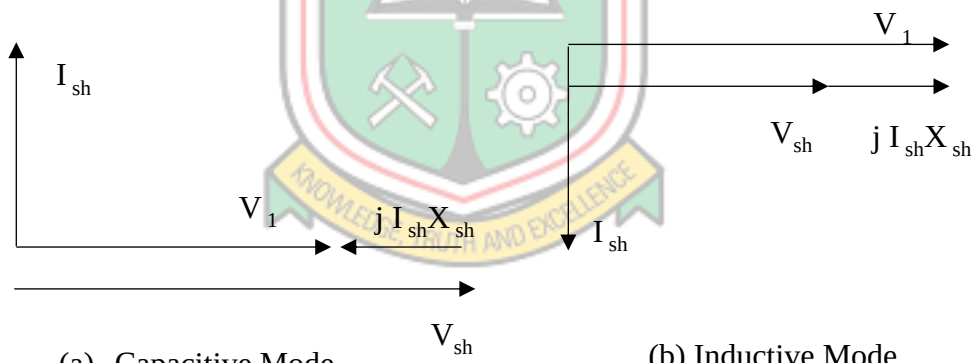

(a) Capacitive Mode (b) Inductive Mode

Figure 2.17 Phasor Diagram of Current in Capacitive and Inductive Modes

The action of the reactive power control is done independently of each other. When the magnitude of V_1 is higher than V_{sh}, reactive power will flow from the line to the shunt converter, hence the shunt converter will be absorbing reactive power. The reverse occurs when V_{sh} has a higher voltage magnitude than the line voltage, V_1, which causes the shunt converter to generate reactive power. The situation is the same for the series converter, which can also absorb or supply reactive power to the transmission line.

For active power flow and control, it is relevant to recall that $[V_{se}(-I^*) + V_{sh}(-I^*)] = 0$ where neither the series nor shunt converter can generate or absorb active power. Figure 2.18 (Bhowmick, 2016) is used to describe the phasor relationship between the components of the line, shunt and series converters.

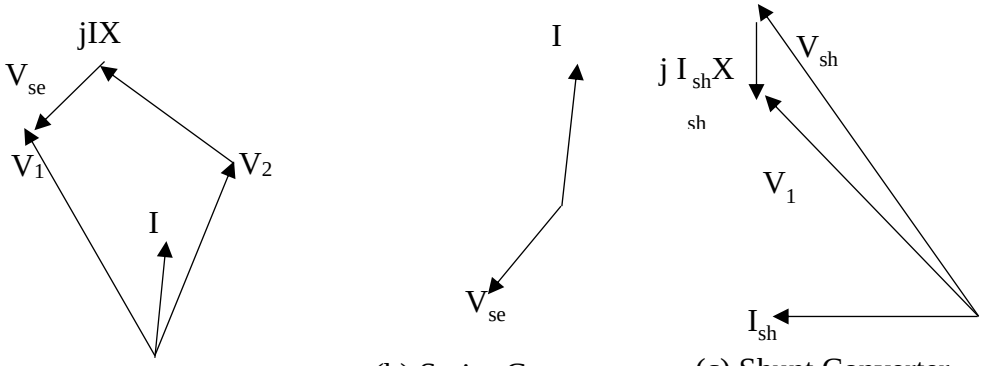

(a) Sending and Receiving End Voltages, Series Converter Voltage and Line Current Phasors

(b) Series Converter Voltage and Line Current Phasors

(c) Shunt Converter Voltage and Current Phasors

Figure 2.18 Phasor Diagram of UPFC Components with Series Converter Supplying Active Power and Absorbing Reactive Power

Figure 2.18 (a) shows the current and voltage at the receiving end, the line current, series voltage and line drop phasors. A separate comparison of the series voltage and line current in the second Figure 2.18 (b) reveals that the series voltage phasor is out of phase with the line current phasor, which implies that the series converter supplies active power to the line. The series converter is however not capable of generating its own active power, indicating that the active power supplied is coming from the shunt converter. Since the shunt converter can also not generate this active power, then the active power sent to the line is coming from the sending end side of the line, through the shunt converter and gets to the series converter with the help of the DC link. This scenario is evident in Figure 2.18(c), where the sending end voltage phasor leads the shunt converter voltage phasor. Considering the reactive power flow, it is realised from Figure 2.18 (b) that the line current, I has a quadrature component that lags the series converter voltage, V_{se} . This implies that the series converter is absorbing reactive power from the line. The Figure in 2.18 (c) confirms the supply of reactive power from the shunt converter to the sending end of the line, where phasor of the shunt converter voltage, V_{sh} has a higher magnitude as compared to the sending end voltage V_1. The control of both active and reactive power using the UPFC has given it an edge over the other FACTS devices, making it have numerous applications in today's power system.

Characteristics of the UPFC

From the active (P) and reactive (Q) power equation with parameters of bus voltage (V), line impedance (X) and transmission angle (δ), a simple power angle curve is achieved as explained earlier. When the transmission line is controlled by UPFC, the mathematical and graphical representations become complex because the UPFC can vary the parameters. Thus, the simple curves of the uncompensated transmission line become operating areas or regions, the boundaries of which are defined by the rating or control imposed on the UPFC. The mathematical representation of the UPFC is represented by Equation (2.12) and Equation (2.13) (Eremia *et al.*, 2016).

$$P = \frac{V^2}{X}\sin\delta + \frac{VV_{pq}}{X}\sin\left(\frac{\delta}{2}+\rho\right) \tag{2.12}$$

$$Q = -\frac{V^2}{X}(1-\cos\delta) + \frac{VV_{pq}}{X}\sin\left(\frac{\delta}{2}+\rho\right) \tag{2.13}$$

where, V_{pq} = amplitude of voltage injected by the UPFC (in series with the line) (V)

ρ = angle of bus 1 voltage (degrees)

The two equations contain an additional term, which is a function of the magnitude and angle of the injected voltage, V_{pq} . A plot showing the expansion of the single P versus δ curve into an operating band (the upper and lower boundary of which is determined by the magnitude V_{pq}) can be constructed for both P and Q as shown in Figure 2.19. It can be realised that at any transmission angle, the active or reactive power can be increased or decreased by VV_{pq}/X (that is 0.5 p. u. MW or MVAr as used for the illustration). Noting that the maximum increase in power is a fixed amount, independent of the operating point defined by the transmission angle.

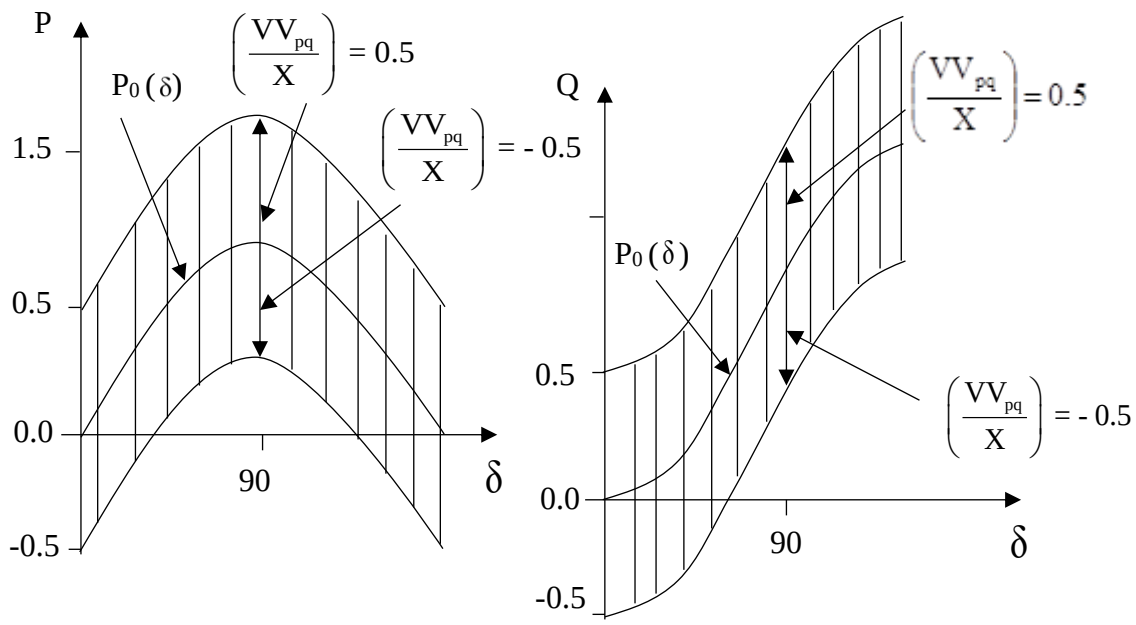

Figure 2.19 Range of Transmittable Active and Reactive Power versus Phase Angle

As the angle is reduced from 90^0, the percentage capability of the UPFC to increase the transmitted power is continuously increasing. Thus, at small transmission angles, a UPFC with relatively low MVA rating can provide highly efficient power control. This particular characteristic of the UPFC is due to its inherent capability to inject and maintain a fixed series compensating voltage in-phase with variable line current. This makes the device well desired for the condition discussed in this work.

2.7 Voltage Stability Index Analysis for Weak Bus Identification

The major condition responsible for voltage instability is related to reactive power imbalance. Increase in generator reactive power on a transmission line reduces the available transfer capability of the line, and these reactive powers evident on load buses affect the voltage levels on these buses. When the reactive power reaches its limit, the system tends to approach its voltage collapse point and at this stage, the power system is considered to be unstable. QV curves can be used to determine the maximum reactive power required by a system before reaching the maximum voltage limit. It is produced by adjusting the reactive power at the load bus and keeping the reactive power constant, the corresponding voltages can then be recorded (Sauer *et al.*, 2018).

The QV curve is used as an index for voltage instability and hence can be used to determine the critical bus for voltage compensation. There are basically two types of voltage stability

index known globally. The Jacobean matrix based VSI and the system variable based VSI. The difference between the two is that the former determines the voltage collapse point and establish the voltage stability margin, resulting in a high computational time, hence used as an offline measure. Meanwhile, the system variable based VSI is used to determine the weak bus or lines in the network, presenting a mechanism to determine the critical voltage level of the network elements. This type of index is fast, convenient and can be used online. It is suitable for determining the conditions of the system and contingency ranking, and in knowing the loadability of the power system, the element with the critical condition can be assessed. The system variable based voltage stability index can also be sub-divided into nodal voltage stability indices and line stability indices (Saadati and Mirzaei, 2016).

Modarresi *et al*. (2016) gives an in-depth analysis of the various types of voltage stability index. A few of such indices have been discussed below.

2.7.1 Line Stability Index

Considering a transmission line connecting two buses, and the parameters of both buses and line are specified, the Line Stability Index (LSI), L_{mn} can be used to find the voltage stability level of each line from Equation (2.14) (Modarresi *et al*., 2016).

$$L_{mn} = \frac{4Q_r X}{\left[V_s \sin(\theta - \delta)\right]^2} \tag{2.14}$$

where, L_{mn} = line stability index

Q_r = receiving end reactive power (MVAr)

V_s = sending end voltage (V)

When the value of L_{mn} is less than 1 in any line, then that line is said to be voltage stable else, unstable.

2.7.2 Line Stability Factor

Similar to the L_{mn}, when the power and voltage at say bus i and the reactive power at bus j are known, the proposed Line Stability Factor (LQP) index can be computed as in Equation (2.15) (Modarresi *et al*., 2016).

$$LQP = 4\left(\frac{X}{V^2}\right)\left(\frac{X}{V^2}P_i^2 + Q_j\right) \quad (2.15)$$

where, LQP = line stability factor

X = line reactance (Ω)

P_i = i^{th} bus active power (MW)

Q_j = j^{th} bus reactive power (MVAr)

V = line voltage (V)

2.7.3 Voltage Collapse Point Indicator

Using the maximum power transfer through a transmission line, the Voltage Collapse Point Indicator (VCPI) can be evaluated. Where the numerator denotes the active or reactive power transferred to the receiving end, whereas the denominator represents the maximum power that can be transferred to the receiving end at any given time, the VCPI is given by Equation (2.16) (Modarresi *et al*., 2016).

$$VCPI = \frac{P_r}{P_{r\,max}} = \frac{Q_r}{Q_{r\,max}} \quad (2.16)$$

where, VCPI = voltage collapse point indicator

P_r = receiving end active power (MW)

Q_r = receiving end reactive power (MVAr)

$P_{r\,max}$ = maximum receiving end active power (MW)

$Q_{r\,max}$ = maximum receiving end reactive power (MVAr)

Saadati and Mirzaei (2016) acknowledged the existence of a number of voltage stability indices and suggested that in selecting any of the indices for voltage stability analysis, factors such as time, convenience and accuracy of the index should be considered.

2.8 The National Interconnected Transmission System of Ghana

The transmission of the generated power from the various generating stations is predominantly through a 161 kV network together with a 69 kV network in the Volta region and two 330 kV circuits. There is a 225 kV tie line which connects the Ghana grid with that

of Cote d'Ivoire and two 161 kV tie lines that interconnect with Togo. The National Interconnected Transmission System (NITS) consists of approximately 5,207.7 circuit kilometres (km) of high voltage transmission lines, which connect generating plants at Akosombo, Kpong, Tema, Bui and Takoradi Thermal Plants at Aboadze to sixty-four (64) Bulk Supply Points (BSPs) across the nation. The transmission lines consist of 364 km of 330 kV line, 4,636.6 km of 161 kV and 132.8 km of 69 kV lines. In addition, there is a single circuit 225 kV tie-line of 74.3 km linking GRIDCO network with CIE of Cote d'Ivoire. The network has 123 transformers installed at various load centres across the country with a Total Transformer Capacity (TTC) of 4,598.86 MVA (Anon., 2016a).

The NITS has 636 MVAr of static capacitor banks installed in various substations such as Achimota, Mallam, Smelter, Winneba, Takoradi, Kumasi, etc. and a 40 MVAr Static VAr Compensator (SVC) installed at the Tamale substation. The capacitor banks and the SVC provide reactive power compensation on the NITS, which are installed to maintain good voltages and minimise transmission losses on the Ghana Power System (GPS). The System Control Centre (SCC) is responsible for the real-time dispatch (monitoring, coordination and control) of power system operations in Ghana, as well as cross-border power exchanges with neighbouring countries. The SCC is equipped with an Asea Brown Boveri (ABB) Network Manager System (NMS), which is the main tool used to monitor and control dispatch operations on the GPS (Anon., 2016a).

2.9 Review of Related Works on Employing Unified Power Flow Controller to Improve Stability of Electric Power Transmission System of Ghana

2.9.1 Stability Improvement on Ghana's Electric Power Transmission System

Mensah (2009) investigated the stability of Ghana's transmission system by activating the Power System Stabilisers (PSSs) on the excitation system of some generating units. Power System Stability Software for Engineers (PSSE) was used to model the power system of Ghana. After the modelling, steady-state stability analysis was performed to identify the weaknesses of the power system. The study revealed that the power system was likely to experience collapse and it was recommended that the PSSs at Akosombo be activated for a positive impact on the network. However, the power factor and voltage levels at BSPs were to be improved using other improvement techniques for a stable network.

Essilfie *et al.* (2013) modelled the power system of Ghana using Power System Analysis Toolbox (PSAT) and incorporated the SVC to improve voltage stability on the network. Small-signal voltage stability analysis indicated that voltages in Bolga and other regions still experienced instability even with the SVC in circuit. The work proposed further research in dealing with the instability that occurred in Bolga and beyond.

Essilfie *et al.* (2014) conducted further research with the installation of STATCOM in Tamale. The installation of the device saw an improvement in voltage level on the bus where the STATCOM was placed. The research realised that the STATCOM could not provide the needed voltage stability on interconnecting buses. Further research was proposed in dealing with stabilising voltages on the interconnected lines.

2.9.2 Comparison of Different FACTS Devices

FACTS devices can be used to minimise transmission loss and simultaneously reduce the operating cost of a transmission system. It can also improve stability and increase transmitted power flow on a line. Various FACTS devices perform different functionalities on a power system (Bhattacharyya *et al*., 2014).

Sundaram *et al.* (2018) investigated the small-signal stability on an IEEE 14-bus system, comparing the action of an AVR, PSS, SVC and UPFC. The results indicated a better performance with the UPFC as compared to the other devices. The UPFC provided a better stability margin, increased power transfer and improved the system's reactive power deficiency.

Ghahremani and Kamwa (2014) analysed the effect of an UPFC and STATCOM on the steady-state performance of the Hydro-Quebec network of Canada. These devices were modelled on a 735 kV power system using MAT-Power software. From the simulation results, the total power loss reduction with UPFC was 37 MW as compared to 13 MW for the STATCOM. The UPFC also provided a better voltage improvement of 1.05 p.u. as to 0.88 p.u. provided by the STATCOM.

Sode-Yome *et al.* (2013) presented a comprehensive comparison of five well-known FACTS devices (including the UPFC and STATCOM) for loadability enhancement. The detailed results showed that the UPFC gives the best loadability margin as compared to the rest of the FACTS devices for both normal and contingency cases. The UPFC also produced

lower real and reactive power losses and provided a better voltage profile at different loading conditions.

Verma and Vandana (2014) made a comparative study on major FACTS devices considering how these devices respond to different power system control attributes and problems. Table 2.1 depicts the outcome of the analysis. In conclusion, it was realised that the UPFC renders more controllability to the power system as compared to other FACTS devices.

Table 2.1 Comparison on Control Attributes for Different FACTS Devices

SN	Control Attribute	FACTS Controller					
		TCSC	SSSC	TSSC	STATCOM	SVC	UPFC
1.	Power Flow Control	●	●	●			●
2.	Voltage Profile Improvement				●	●	●
3.	Line Commutated	●		●		●	●
4.	Forced Commutated		●		●		●
5.	Voltage Source Converter		●		●		●
6.	Current Source Converter	●	●	●	●	●	
7.	Transient and Dynamic Converter	●	●	●		●	●
8.	Damping Oscillation	●	●	●	●	●	●
9.	Fault Current Limiting	●		●			●
10.	Voltage Stability	●	●	●	●	●	●

(Source: Verma and Vandana, 2014)

Sharma and Vadhera (2016) used a phasor model of an UPFC to maximise the real power transfer from one power system to another through interconnections for a 500 kV IEEE test system of 20-buses. However, the phasor model uses IGBTs with Pulse Width Modulator (PWM), which has high switching frequency accompanied by high converter losses (Farooq, 2018).

Hongmei *et al*. (2017) used a single back-to-back GTO inverter with a common DC link to control active power flow on a 500 kV power network. However, using a back-to-back inverter allows harmonics generated by the converter into the system, which tends to distort the final waveform (Kwon *et al.*, 2017).

The performance of the UPFC was tested on an IEEE 14 bus system, the system was tested with and without contingencies and the results indicated that the UPFC maintains voltage stability and improves the active power flow on transmission lines. However, for the UPFC

to perform as required, its parameters (power and voltage levels) must be determined for the network under study (Ray and Chandle, 2015).

2.9.3 Optimum Location of FACTS Devices

The placement of power electronic devices in a transmission system to control power flow and stability should not be done arbitrarily. Random placement of these devices may lead to high cost of incorporating the devices in the power system and might render the entire project unfeasible. For the maximum positive impact of the FACTS device on the transmission system, an optimum location for the device must be determined (Gawande and Jadhao, 2018). There are three broad categories with the placement of FACTS devices (like the UPFC) in a power system. These are the sensitivity-based, conventional optimisation-based and Artificial Intelligence (AI)-based methods (Lavanya and Rani, 2016). A number of papers suggest simple and reliable methods for the placement of FACTS devices for enhancing the stability of a power system over different topologies (Benaissa *et al.*, 2017).

Sarker and Goswami (2014) used the Gravitational Search Algorithm (GSA) to find the optimal location of multiple FACTS devices. The complex computational approach of the GSA enabled the handling of the large network and the multiple devices placed in the network. With three FACTS devices in the circuit, the network operated with low power loss and improved loadability.

Verma *et al.* (2017) found the optimal location of three FACTS devices using Genetic Algorithm (GA). The three devices were placed on an IEEE 40-bus network to increase loadability and minimise transmission losses. The simulations showed that the GA is very sensitive and may not converge if the initial population is not well selected.

Ray and Chandle (2015) in their work proposed an UPFC for controlling power flow in a transmission line and improving system voltages. Voltage stability index for each line was calculated and the line with the highest value determined as the weakest line for the optimal location of the UPFC. The results indicated that the UPFC controlled both active and reactive power flow across the transmission line, hence prevented outages during excess load demand and made system network voltage stable.

Singh *et al.* (2018) used the sensitivity-based method for the optimal placement of the UPFC in a 500 kV IEEE 14 bus network. With the UPFC in the circuit, stability of the power

system was improved as compared to when the device was not in circuit. The method was effective for the placement of a single device.

Gupta and Sharma (2013) used computational power flow and line stability index to identify the optimal placement of the UPFC. The paper concluded that the effective location of the device improved the static and transient stability of the system when subjected to disturbances.

The three techniques used for optimal placement of FACTS devices have their merits and demerits. The sensitivity-based method requires solving a large system of equations, hence not conducive for multi-device placement into a large network. The conventional optimisation-based method has a lot of penalty algorithms and may not work for some types of variables. The AI-based method is very expensive to implement and highly dependent on machines (Kannan and Miah, 2019).

In conclusion, for a multi-FACTS placement strategy, the use of an evolutionary algorithm and AI for the optimal location of the devices proved superior to the sensitivity-based methods. However, it is difficult and sometimes impossible to reach the optimal solution required by the objective function (Singh *et al.*, 2018). According to Albatsh *et al*. (2015), it is efficient and convenient to find the optimal location of a single FACTS device on a relatively smaller network (less than fifty buses) using the sensitivity-based method. In this research, voltage stability index analysis was used for the optimal placement of the UPFC in the proposed system.

2.10 Summary

The chapter presented a complete review of the literature on power system stability. The definition and types of stability (rotor angle, voltage and frequency stability) were discussed. An assessment of stability and dynamic security were addressed, where power flow analysis was found to be an effective tool in assessing the stability of a power network. The chapter also discussed the measures used in improving system stability, where techniques like power system stabilisers, fast valving, excitation system and FACTS devices are employed for improvement. The use of FACTS devices proved an edge in recent times over other methods of solving the stability issue.

The major issue of concern with the transmission system stability was found to be voltage related and occurs when system voltages fall below a predefined range. A comprehensive

review on FACTS devices was carried out and it was realised that different applications require different kinds and topologies of the various FACTS devices. The UPFC performed very well in most of the applications and was established as the most versatile device in the FACTS family for stability improvement. Comparing the UPFC to the STATCOM, SVC and PSS, which were previously used in the stability improvement of Ghana's power system, the UPFC promises better voltage stability.

It is certain that the random placement of the UPFC leads to a high cost of incorporating the device into the power system, which might render the entire project unfeasible. An optimum location of the device is hence required. The placement of the device can be done using sensitivity, conventional optimisation or AI-based methods. Since a single device is to be installed to solve the voltage stability problem of the northern section of Ghana's transmission system, which is made up of eleven buses and eleven transmission lines, a sensitivity-based technique using voltage stability index and maximum loadability assessment is proposed. This approach identifies the weakest bus in the system for the UPFC location.

It is evident from the literature that the UPFC has not yet been used on a 161 kV network. Since voltage levels affect the operating region and the entire design of the FACTS device, employing the UPFC to control power flow, reduce system losses and improve voltage levels on Ghana's power network can provide a new area of research. This research therefore, focuses on using four GTO-based square wave inverters at each side of a common DC-link capacitor, to enable the steady-state control of high power on a transmission system whilst providing an undistorted waveform.

CHAPTER 3

METHODS USED

3.1 Introduction

This chapter describes the methods used in achieving the proposed solution. Research has shown that the Ghanaian power system like any other power system can be modelled using different software for the analysis and improvement of the system. The implementation of the proposed framework is illustrated in MATLAB Simscape Power Systems software. The load flow analysis using Newton Raphson's approach is carried out on the existing network. The power system of Ghana comprising generators, transformers, bus bars, transmission lines and loads are modelled using Simscape Power Systems' blocks.

3.2 Overview of the MATLAB Simscape Power Systems Software

MATLAB is a programming language designed for solving complex technical problems in the science and engineering community. The advantage MATLAB has over other software is its ability to incorporate extensions with add-on toolboxes that are oriented towards a particular field of study.

The graphical programming language Simulink is an extension of MATLAB, which is intended for dynamic system investigation. Presumably, the system under study is reorganised as functional diagrams, which consist of equivalent blocks by their functions, to the program blocks that are included in the Simulink library. The blocks in Simulink use click and drag to make a model of the actual system. Simscape Power Systems is a sub-section of Simulink and it is made up of blocks whose field of application ranges from generation, transmission, transformation and utilisation of electrical power (Perelmuter, 2013).

Modelling of the various components of the entire power system is done using Simscape Power Systems. The various blocks depicting the actual system devices are picked from the Simulink library and the parameters of these blocks are changed to correspond to the parameters given by the data of the actual power system. The methods used for modelling the various power system components and the conducting of load flow studies are further explained.

3.3 Overview of the Methods Used

Figure 3.1 presents a summary of the methodology used to improve stability on Ghana's transmission system. The power system is modelled with the required blocks derived from the Simulink library, the parameters taken from the power utility company are used to configure the respective blocks. These parameters can be found in Table A1 and Table A2 of Appendix A.

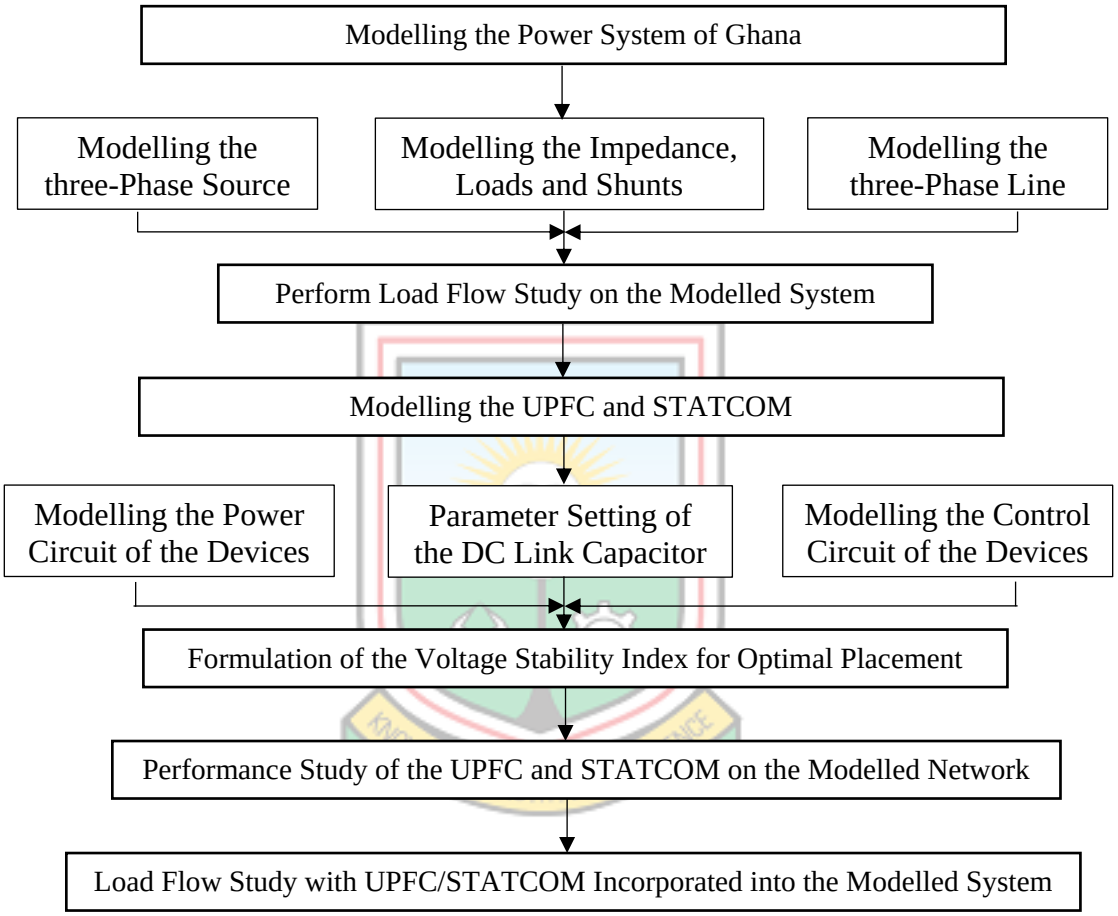

Figure 3.1 Summary of the Methodology

After modelling the power system, a load flow study is performed to determine the initial state of the network before compensation. The results are saved for further analysis later in the work. The next step models the different components of the UPFC. Formulation of the voltage stability index is carried out to determine the optimal position of the modelled UPFC. The performance of the UPFC on the modelled power system is assessed. The shunt portion of the UPFC, which consists primarily of a STATCOM is used to determine the effect of STATCOM on the modelled system. Load flow studies are performed initially with

the UPFC and then with the STATCOM. The results are compared to the load flow results obtained when the network had no FACTS device in circuit. Their effects are later discussed.

3.4 Modelling the Three Phase Source in Simscape Power Systems

The two power sources included in the test system need to be modelled in Simscape Power Systems. In order not to delve into the complex mechanical modelling of the synchronous machine, and since only frequency, voltage and power are needed from the power source for simulations, both electrical sources are represented by the three-phase source. In both cases, the voltage and frequency are derived from the primary substation at the transmission voltage level.

The block implements a symmetrically Y-connected three-phase voltage with an internal impedance and internally grounded neutral. The source resistance and inductance are specified based on the characteristics of the busbar from which the other parameters are obtained. The frequency is specified at 50 Hz at a voltage of 161 kV and the inductance of 0.825 H is derived from Equation (3.1) (Anon., 2016c). The short circuit power (P_{sc}) of the system is 100 MW.

$$L = \frac{1}{2\pi f}\frac{(V_{base})^2}{P_{sc}} \tag{3.1}$$

where, L = line inductance (H)

f = frequency (Hz)

V_{base} = base voltage (V)

P_{sc} = short circuit power (MW)

Figure 3.2 shows the block model of the three-phase source. To be able to perform the load flow analysis on this block, the load flow tab found on its dialogue box is utilised and the respective parameters entered.

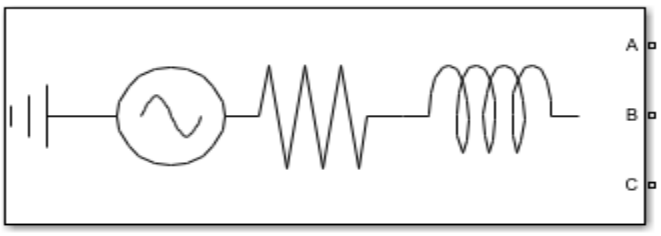

Figure 3.2 Block Diagram of the Three-phase Source with Internal Impedance

The option for generator type can be a swing bus, PV bus or PQ bus. The swing bus is selected to implement a generator controlling voltage magnitude and phase angle. The PV bus is selected to control active power and voltage magnitude, whilst the PQ bus is selected to control active and reactive power. With either generator type selected, the active and reactive power at the busbar and the voltage at that same bus can be specified. In order to specify the active and reactive power generated by the source, the voltage source block labelled Bui generation is selected as the PQ bus and Generation 2 is selected as the swing bus for the model.

3.5 Modelling the Impedances and Loads in Simscape Power Systems

Many factors are considered when modelling the load in a transmission system. The parameters required for the load in the system should be the active (W) and capacitive/inductive reactive (+Var or -Var) powers. The three-phase series RLC load is preferred over the three-phase RLC branch since the latter requires *R* (Ω), *L* (H), and *C* (F), which cannot be easily computed due to the dynamism of the various loads. The voltages across each component of the load are defined for the three-phase series RLC load and the convenience of using impedance makes the load block more attractive. Figure (3.3) depicts the model of the three-phase RLC load.

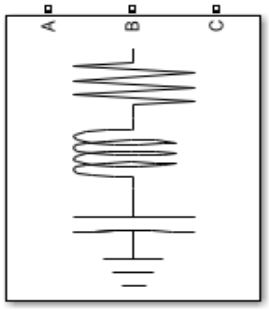

Figure 3.3 Block Diagram of the Three-Phase Series RLC Load

The block implements a three-phase balanced load as a series combination of RLC elements and at the specified frequency, the load exhibits a constant impedance.

To perform the load flow studies, the load type is indicated as a constant Z in order to determine the load impedance from the parameters specified by the actual system. The impedance is kept constant during the load flow solution and the effective P and Q varies proportionally to the square of the bus voltage.

3.6 Modelling the Shunt Devices in Simscape Power Systems

The shunt devices are modelled as a three-phase series RLC load and their values determined at the parameter tab as either an inductive component or a capacitive component. For the shunt devices, the load type is selected as constant PQ to keep the active and reactive power constant (as defined by the parameter tab). The description of the three-phase series RLC load has been discussed in Section 3.5.

3.7 Modelling the Transmission Line in Simscape Power Systems

The description of a transmission line by the wave propagation approach is not always suitable for computation and simulation on stability issues, hence the distributed parameter line is not considered when choosing transmission line block for stability studies. The three-phase Π section line and the three-phase series RLC branch is a suitable choice for the transmission line modelling. For shorter transmission lines (line section < 50 km), the three-phase series RLC branch is used, where the resistance and inductance of the line are specified and the line capacitance is ignored. For lines longer than 50 km, the three-phase Π section line is used. The specified model implements a balanced three-phase transmission line model with parameters lumped in a Π section as illustrated in Figure 3.4a with the block diagram represented in Figure 3.4b.

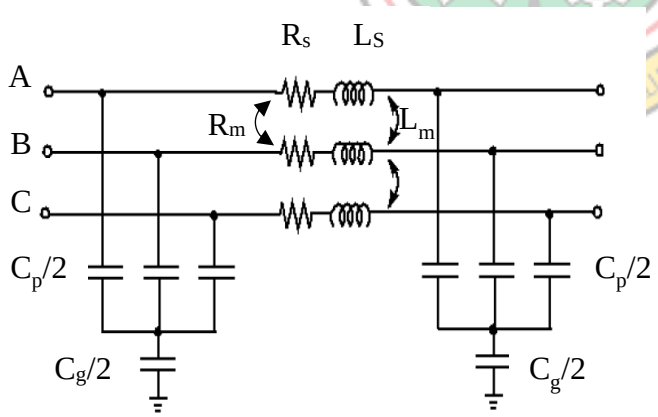

(a) Π Section Model of a Transmission Line

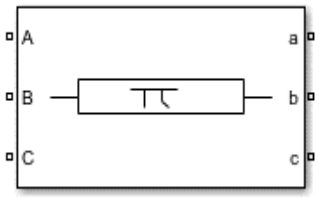

(b) Block Diagram of the Π Section Line

Figure 3.4 Model of the Three-Phase Π Section Line

The line parameters R, L, and C are specified under positive and zero-sequence parameters, taking into account the inductive and capacitive couplings between the three-phase conductors, as well as the ground parameters specifying a three phase balanced system. The parameters derived for the block were based on data taken from the actual system.

3.8 Modelling the UPFC in Simscape Power Systems

The UPFC used in this thesis is modelled to effect changes in the parameters of a 161 kV transmission line. It consists of two sets of VSCs, with one set connected in shunt and the other in series to the transmission system using a set of specialised transformers. The shunt inverter operates as a STATCOM and the series inverter operates as an SSSC, which are both coupled to a common DC link capacitor. A switch is connected between both sets of capacitors to enable the UPFC to operate in several modes. The opening and closing of the switch cause the device to either assume operation in the STATCOM, SSSC or UPFC mode. With both converters able to transfer active and reactive power through the common DC link capacitor, the injected voltage generated by the SSSC is not limited to stay in quadrature with the line current but can rather assume any angle with respect to the current, making it possible to transfer or absorb active and reactive power on the line. A breaker is connected between the two output terminals of the transformers linking the series side of the device. To operate the device in only STATCOM mode, the capacitor switch and the breaker are operated. Voltage control can now be achieved with the STATCOM by generating or absorbing reactive power. The succeeding section describes the modelling of the power and control circuits of the UPFC used for the analysis.

3.8.1 Modelling the Power Circuit of the UPFC

In order to control the high power on the transmission system whiles reducing the harmonic content to a bare minimum, a particular scheme of the power inverter circuit is adopted. The shunt and series converters employed in the work utilise a GTO-based VSC rated at 100 MVA. This is made up of four, three-phase, three-level neutral point clamped converters, which generate a 48-step voltage waveform. The DC link capacitor serves as the DC source voltage, which is proportional to the generated voltage of the converter. The voltage produced by each converter is applied to the secondary of four phase-shifting transformers that are connected either in star or in delta to produce a phase shift of 30 degrees. The secondary of the first and the third transformers are connected in star (Yn) whilst that of the second and fourth are connected in delta (D1). This yields a phase shift of 30 degrees between the star and delta connections cancelling 5^{th} and 7^{th} harmonics. With the primaries of the first two transformers having a phase shift of +7.5 degrees and the other two having a phase shift of -7.5 degrees, a total phase shift of 15 degrees is established between the two sets of transformers and this results in the cancellation of 11^{th} and 13^{th} harmonics.

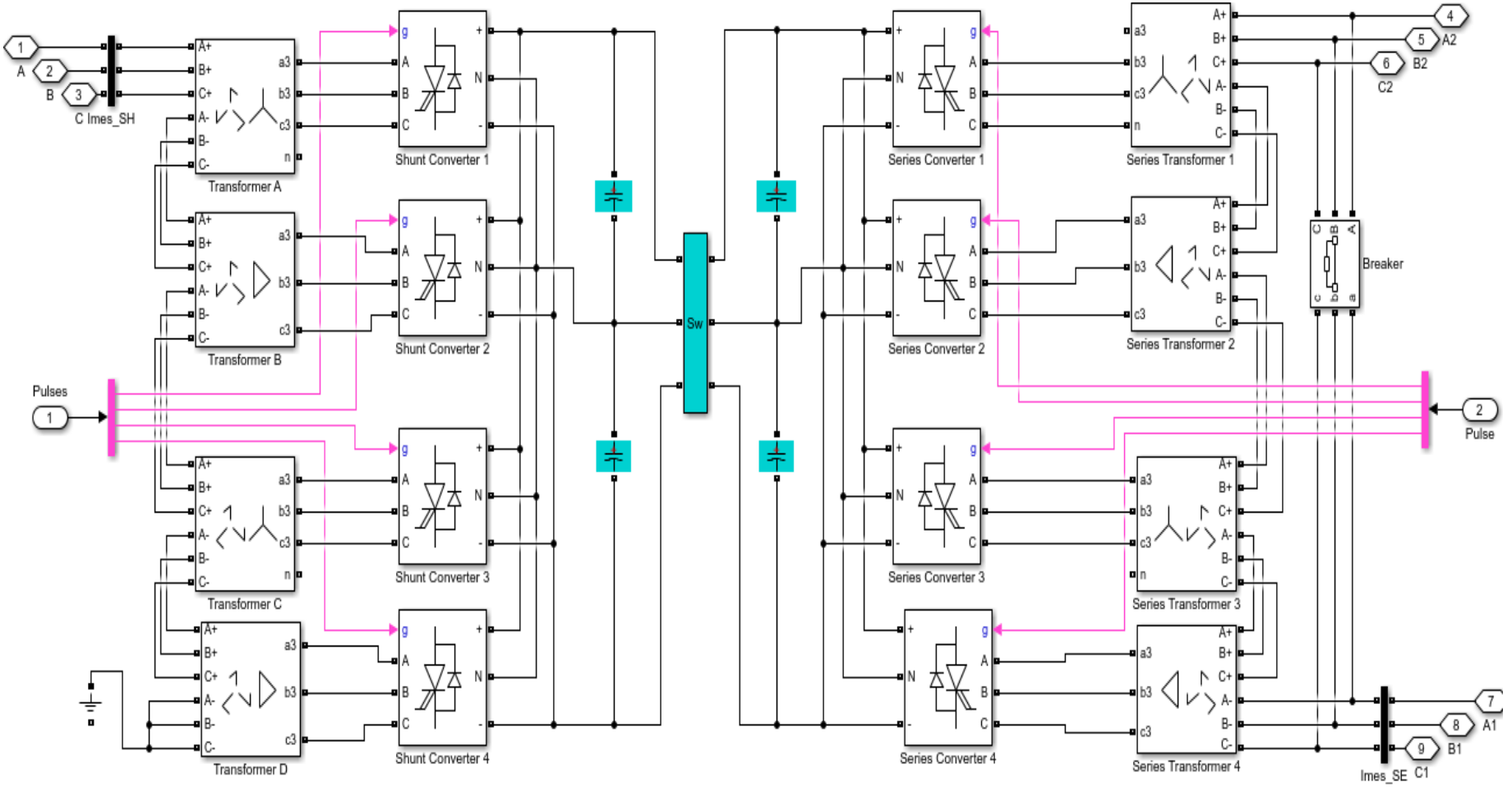

Figure 3.5 Power Circuit Model of the UPFC in Simscape Power Systems

The 23rd and 25th harmonics are also cancelled by choosing a conducting angle of 172.5 degrees. The serial connection of the output terminals sums up the primary voltage to produce the 161 kV required by the transmission line. Figure 3.5 indicates the configuration of the UPFC in Simscape Power Systems. The implementation of the proposed scheme for both the series and shunt inverters helps to neutralise harmonics up to the 45th level resulting in an almost sinusoidal waveform of 48 steps.

The Zigzag phase shifting transformer is selected from the Simulink library and the required parameters entered by selecting the parameter tab. The nominal power on each transformer is selected at 25 MVA and a frequency of 50 Hz. The transformer primary voltage is 40.25 kV on either side of the UPFC with a turns ratio of 9.5. The maximum injected voltage that is accepted to be produced by the series inverter is 10% the nominal value, since exceeding this value will cause a voltage swell and this violates the grid code for emergency conditions. A voltage of 4.237 kV is required on the secondary side of either end of the UPFC.

3.8.2 Determining the Size of the DC Link Capacitor

The DC link capacitor provides the voltage required by the two inverters for their operation. It also provides a medium for the supply of active and reactive power from the shunt to the series converter and vice versa. It also charges and discharges to supply real power needed by the series inverter during transients, when the shunt inverter is not able to operate on time. The charge and discharge lead to a reduction in capacitor voltage and therefore influence the design of the DC capacitor.

The initial voltage of the UPFC bus is 1.0 p.u. hence the shunt inverter is assumed to be controlling the voltage at the said value. Since the voltage on the line side is not supposed to exceed 1.1 p. u., the injected voltage required to be in phase with the line current is 0.1 p. u. With a Surge Impedance Loading (SIL) of 100 MVA at a voltage of 161 kV, the phase current is 358.6 A. The three-phase power that can be transferred by each inverter is given by Equation (3.2) (Ametani *et al.*, 2016).

$$P_{ph} = 3 \times V_{ph} \times I_{ph} \tag{3.2}$$

where, P_{ph} = three phase power (MW)

V_{ph} = phase voltage (V)

I_{ph} = phase current (A)

$$P_{ph} = 3 \times 92.95 \times 358.6 = 10 \text{ MW}$$

With maximum discharge at ¼ cycle, the rating of the DC capacitor is achieved using Equation (3.3) (Perelmuter, 2013).

$$W_c = \frac{1}{2} C V_{dc}^2 \tag{3.3}$$

where, W_c = energy released by the capacitor (Ws)

C = capacitance of the DC link capacitor (F)

V_{dc} = DC voltage across the capacitor (V)

With every power released there is a corresponding energy given by Equation (3.4) (Ametani *et al*., 2016).

$$W_{se} = P_{se} \times t_r \tag{3.4}$$

where, W_{se} = energy released by the series inverter (Ws)

P_{se} = real power generated by the series inverter (MW)

t_r = time taken for the energy to be released (s)

Hence, the energy released by the series inverter is:

$$w_{se} = 10 \times (\frac{1}{4} \times 50 \times \frac{1}{3600}) \times 10^6 = 34722 \text{ Ws}$$

The energy released by the series inverter is the same as the energy needed to discharge the capacitor. Considering the voltage across the capacitor to be equal to the voltage on the secondary side of the transformer, the energy discharged by the capacitor is given as

$$W_c = \frac{1}{2} C V_{dc}^2 = 0.5 \times C \times 4237^2$$

$$C = 3868 \ \mu F$$

The DC capacitor rating was hence chosen as $4000 \mu F$, which is the nearest available capacitor rating (Anon., 2015).

3.8.3 Modelling the UPFC Controller

The main function of the UPFC is to control the bus voltage, the reactive power and the real power on the transmission line. The controllers of both the shunt converter and the series

converter are modelled separately. When a voltage is injected using the series converter, the real and reactive powers of the line are controlled independently whilst the shunt converter varies the shunt voltage to inject a controlled reactive current. The methods used in modelling the shunt and series controllers are explained in the following sections.

Shunt controller design

The shunt converter is used to absorb or supply the reactive power needed by the system in which the UPFC is connected. A control system needs to be designed for the converter to be able to control the absorption or supply of the reactive power and maintain a constant DC link capacitor voltage. The control of the reactive power is done by adjusting the magnitude of the generated voltage whilst the DC link capacitor voltage is maintained by adjusting the phase angle of the generated voltage. The DC link capacitor voltage needs to be constant in order to provide the series inverter with the required voltage and supply its active power demand. To simultaneously control the reactive power and the DC voltage, the de-coupled control system is used. It makes use of an inner current control loop and an outer loop that regulates the AC and DC voltage. A simplified block diagram of the designed shunt controller is shown in Figure 3.6 (Modified after Perelmuter, 2013).

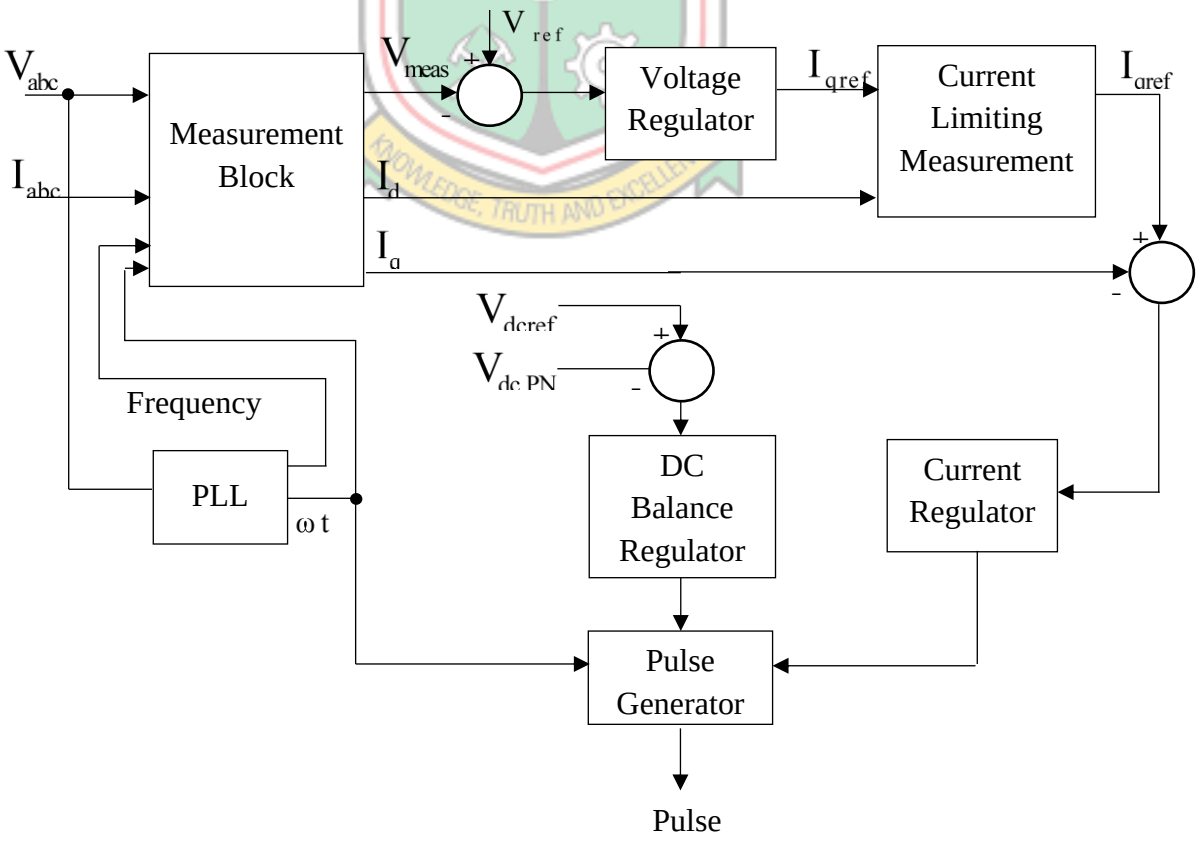

Figure 3.6 Simplified Block Diagram of the Shunt Controller

The control system consists of a PLL, which synchronises on the positive sequence of the input voltage. It splits the component into its frequency and reference angle (ωt). These outputs, together with the primary voltage and current form the input of the measuring system. Series of computations are done using the measurement block. Park's transformation is done for the current component to yield I_q and I_d. The voltage magnitude, V_{meas}, the real power, P and the reactive power, Q are also computed. The outer loop is made up of the AC and DC voltage regulators. This regulator accepts the measured voltage and reference voltage as input and in return, produces a quadrature reference current that forms the input of the current regulator, which makes up the inner control loop. With the reference current and the quadrature component of the primary current, the current regulator produces an angle that is the phase shift of the converter voltage with respect to the system voltage. With parameters from the PLL, the DC voltage regulator and current regulator, the pulse generator produces the required pulses needed to control the shunt converter.

Series controller design

The SSSC present in the UPFC assumes a different scheme as compared to the stand-alone type used for series compensation. The series controller in the UPFC configuration is used to control the active and reactive powers enabling the converter to operate either in manual voltage injection mode or in automatic power flow control mode. To be able to operate the UPFC in automatic power flow control or manual voltage injection mode, the configuration in Figure 3.7 (Perelmuter, 2013) is used. The PLL synchronises the positive sequence of the converter voltage. Both the voltage and current measurement blocks, with the help of the Park's transformation block, computes the active and reactive components of the voltage (V_d, V_q) and current (I_d, I_q). With these results taken as inputs to the PQ measurement block, the active and reactive powers of the system are computed using Equations (3.5) and (3.6) (Perelmuter, 2013).

$$P = V_d I_d + V_q I_q \tag{3.5}$$

$$Q = V_q I_d + V_d I_q \tag{3.6}$$

where, V_d = active component of voltage (V)

V_q = reactive component of voltage (V)

I_d = active component of current (A)

I_q = reactive component of current (A)

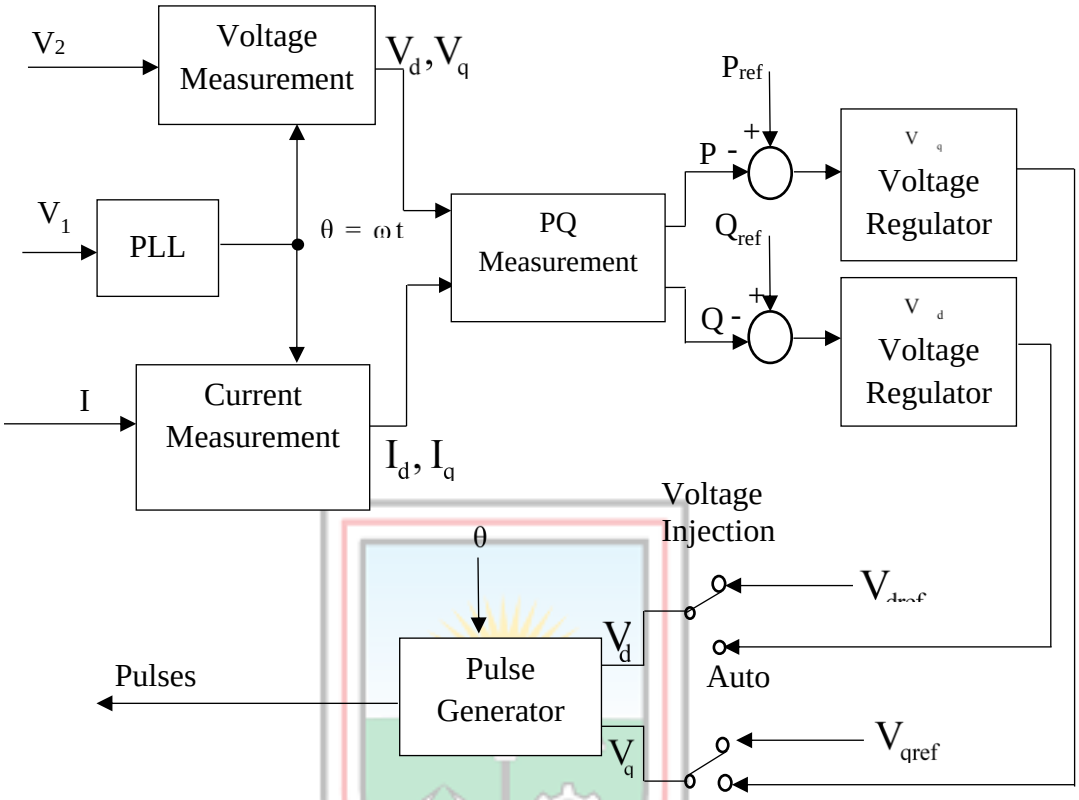

Figure 3.7 Simplified Block Diagram of the Series Controller

These power values are compared to their reference values and two PI regulators use the error to compute V_q and V_d components of the voltage to be synthesised by the VSC. Where V_q at a phase displacement of 90 degrees with the line voltage controls reactive power and V_d in-phase with the line voltage controls the active power. To operate the device in manual voltage injection mode, the PI regulators are made inactive and the reference values of the injected voltage V_{qref} and V_{dref} are used to synthesise the voltage of the VSC.

3.9 Formulation of Fast Voltage Stability Index

The ability of the system variable voltage stability index to determine and rank critical lines and buses makes it appropriate for the optimal location of FACTS devices (Aung *et al*., 2017; Ismail *et al*., 2017; Taleb *et al*., 2017).

The Fast Voltage Stability Index (FVSI) is a system variable based index that is formulated based on a single line two-bus criterion as shown in Figure 3.7 (Taleb *et al*., 2017).

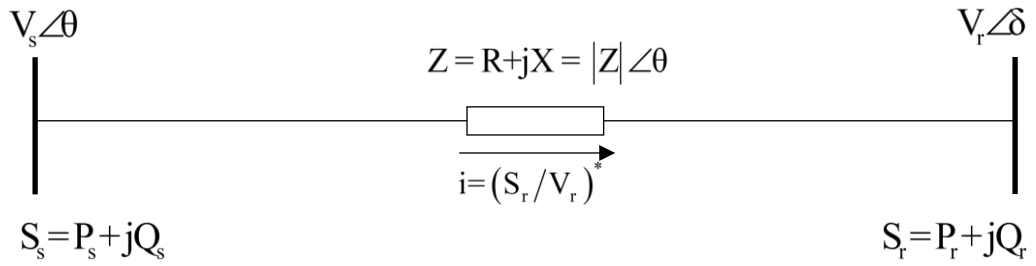

Figure 3.8 Typical Single - Line Two-Bus Diagram of a Transmission System

The power flow equation of the single diagram above is written as in equation (3.7) and Equation (3.8) (Taleb *et al*., 2017).

$$i = \frac{V_s\angle 0 - V_r\angle\delta}{R + jX} \tag{3.7}$$

$$P_r = \left(\frac{-V_s \times V_r\angle\delta}{R+jX}\right) \tag{3.8}$$

Considering the apparent power at the receiving end and the current through the line, Equations (3.9) and (3.10) (Taleb *et al*., 2017) hold valid.

$$V_s V_r X\cos\delta - V_r R\sin\delta + Q_r(R^2+X^2) \tag{3.9}$$

$$V_r^2 - \left(\frac{R}{X}\sin\delta + \cos\delta\right)V_s V_r + Q_r\left(\frac{R^2}{X}+X\right) = 0 \tag{3.10}$$

Solving for V_r yields Equation (3.11).

$$V_r = \frac{\left(\frac{R}{X}\sin\delta + \cos\delta\right)V_s \pm \sqrt{\left[\left(\frac{R}{X}\sin\delta + \cos\delta\right)V_s\right]^2 - 4Q_r\left(\frac{R^2}{X}+X\right)}}{2} \tag{3.11}$$

To determine the real solution of Equation (3.11), the determinant in Equation (3.11) should be greater than or equal to zero, giving Equation (3.12) (Taleb *et al*., 2017).

$$\left[\text{Rsin}\,\delta+\text{Xcos}\,\delta)V_s\right]^2 - 4Q_r(R^2+X^2) \geq 0 \quad (3.12)$$

Also, since δ is very small, $\delta \approx 0$, $\text{Rsin}\,\delta \approx 0$ and $\text{Xcos}\,\delta \approx 1$

$$V_s^2 X - 4Q_r Z^2 \geq 0 \quad (3.13)$$

Hence, the stability index is defined as given by Equation (3.14) (Taleb *et al*., 2017).

$$\frac{4Q_r Z^2}{V_s^2 X} \leq 1 \quad (3.14)$$

Equation (3.14) is used in the MATLAB environment to generate each index value for all bus bars that represent the bulk supply point. The connecting line that exhibits an index close to 1 or which has the highest value is termed as the weakest in the system and the modelled UPFC is placed on the bus connecting that line.

3.10 Load Flow Studies

Load flow studies is a method used in determining whether voltages remain within specified limits under normal and emergency operating conditions and whether equipment such as transformers and conductors are overloaded. The non linear algebraic equations derived from a power system network can be solved using iterative methods. The load flow tool in the Matlab Simulink (Simpower Systems) environment uses the Newton-Raphson method to provide a robust and fast convergence solution. The tool provides most of the functionality of other load flow software currently available.

The Graphical User Interface (GUI) "Powergui" from the Simulink blocks, helps in the tuning and correct operation of the model. It is used for the storage of the equivalent model scheme (Perelmuter, 2013). The load flow tab of the Powergui allows the execution of the simulation from steady state. With this tab, the voltage magnitude, angle, real and reactive power of the test system are determined. Two power sources are present in the model, with the first power source indicating the northern generation, whilst the second represents the power source that is transmitted from the southern section of the power system. The parameters of the transmission lines, loads and existing compensating devices are specified with the data taken from the utility provider (GRIDCO). The initialisation is done using the initial state tab of the Powergui block, which is then forced to represent the system's steady state. To be able to solve the load flow, a load flow bus block is inserted at each bulk supply

point. The simulation type adopted from the Powergui to solve the circuit under study is the discrete solver, which enabled the system for a solution at fixed time steps.

The procedure used in performing the load flow studies on the system is stated as follows:

i. The simulation type is selected as discrete;
ii. The load flow tool is selected and the fixed base value determined as 100 MVA; and
iii. Finally, the load flow is performed to determine the values of the block parameters.

3.11 Description of the Complete Modelled System

As indicated in the problem statement, voltage instability occurs predominately at the northern sector of Ghana's transmission network. The test system is hence, modelled as the power system present at the northern section of Ghana's transmission network, covering parts of the Brong-Ahafo, Northern, Upper East and Upper West Regions. The system consists of a generating station present at Bui, and a three-phase source depicting the power source coming from the southern generating stations. The test system also contains 1090.4 circuit kilometres of 161 kV transmission lines interconnecting 11 BSPs (Anon., 2016a). 17 MVAr static capacitor banks are located at four different BSPs on the system to verify the effectiveness of these devices on the improvement of voltage on the actual system. Figure 3.9 indicates the model of the actual system.

3.12 Simulations on the Test System

Series of simulations are performed under various conditions to determine the capability of the transmission system and the effect of the compensating device.

3.12.1 Performance Study of the FACTS Devices

MATLAB simulations were carried out to determine the performance of the UPFC on the test system. Scopes are connected at respective outputs of various UPFC blocks to determine the behaviour of individual line parameters (current, voltage, active and reactive powers) on the shunt converter, series converter and DC link capacitor. After the performance analysis, the initial state of the blocks forming the UPFC together with the modelled transmission system is calculated using the power GUI block. The result of the initial state is saved to enable the load flow study to output the desired results.

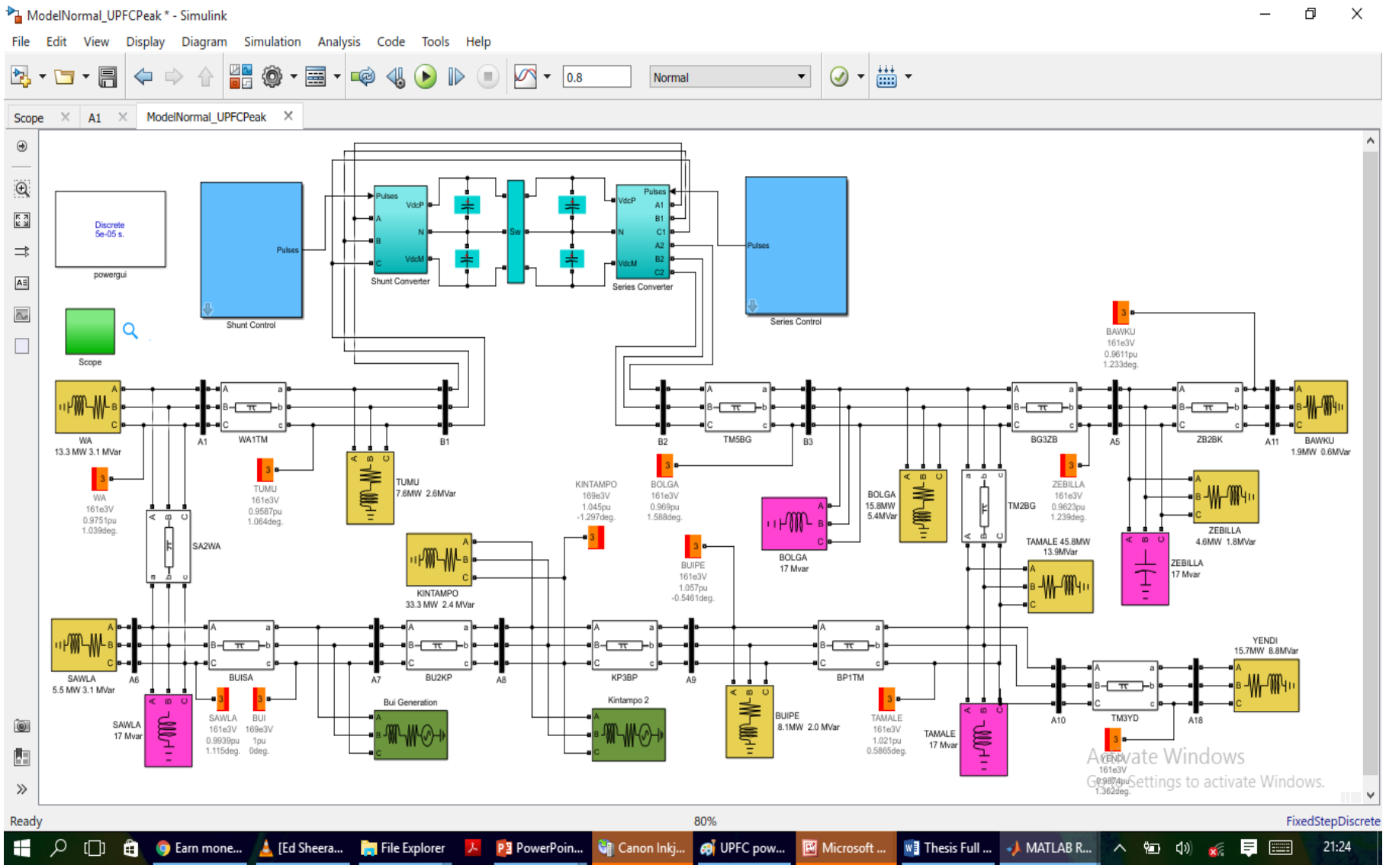

Figure 3.9 Model of the Northern Transmission System in Simscape Power Systems

3.12.2 Load Flow Simulations

The load flow studies realised changes in voltage, active and reactive powers from the different scenarios considered for the simulations. The study was performed with the field data collected and the loads realised during peak periods. Three sets of load flow simulations are performed. These are:

i. Load flow studies with no compensating device in circuit;
ii. Load flow studies with UPFC; and
iii. Load flow studies with STATCOM.

The first load flow simulation is conducted on the modelled power system without the FACTS devices. The simulations verify the current state of Ghana's power system, where the initial values of the various network parameters are determined and recorded. The next simulation is done with the UPFC connected to the critical bus in the power system. The simulation determines the level of improvement offered by the UPFC when connected in the circuit. The final load flow simulation is conducted to verify the level of improvement offered by the STATCOM. This helps us to assess the effects of the STATCOM on Ghana's power system. The simulations also assess why the STATCOM could not provide the best improvement when employed in the studies carried out by Essilfie *et al*. (2014).

3.12.3 Optimal Placement of UPFC Using Fast Voltage Stability Index

The optimal location of the UPFC is done by finding the weakest bus and the critical lines in the network. The weakest bus is identified using the maximum loadability criteria, with the adjoining critical line determined using the FVSI. The maximum loadability of each bus is assessed by increasing the value of its reactive power to its maximum, that is before the load flow program fails to converge, whilst keeping the reactive power of other buses at base value. The FVSI for each maximum loadability is calculated using Equation (3.14) and the line with the value closest to one (1) is rated the critical line. The maximum reactive power computed for the various buses is sorted in ascending order and the bus with the least value is classified as the weakest. The desired result must verify that the critical line connects the weakest bus. The optimal location is the point between the critical line and the weakest bus. A flowchart of the algorithm used to achieve the proposed solution is summarised in Figure 3.10.

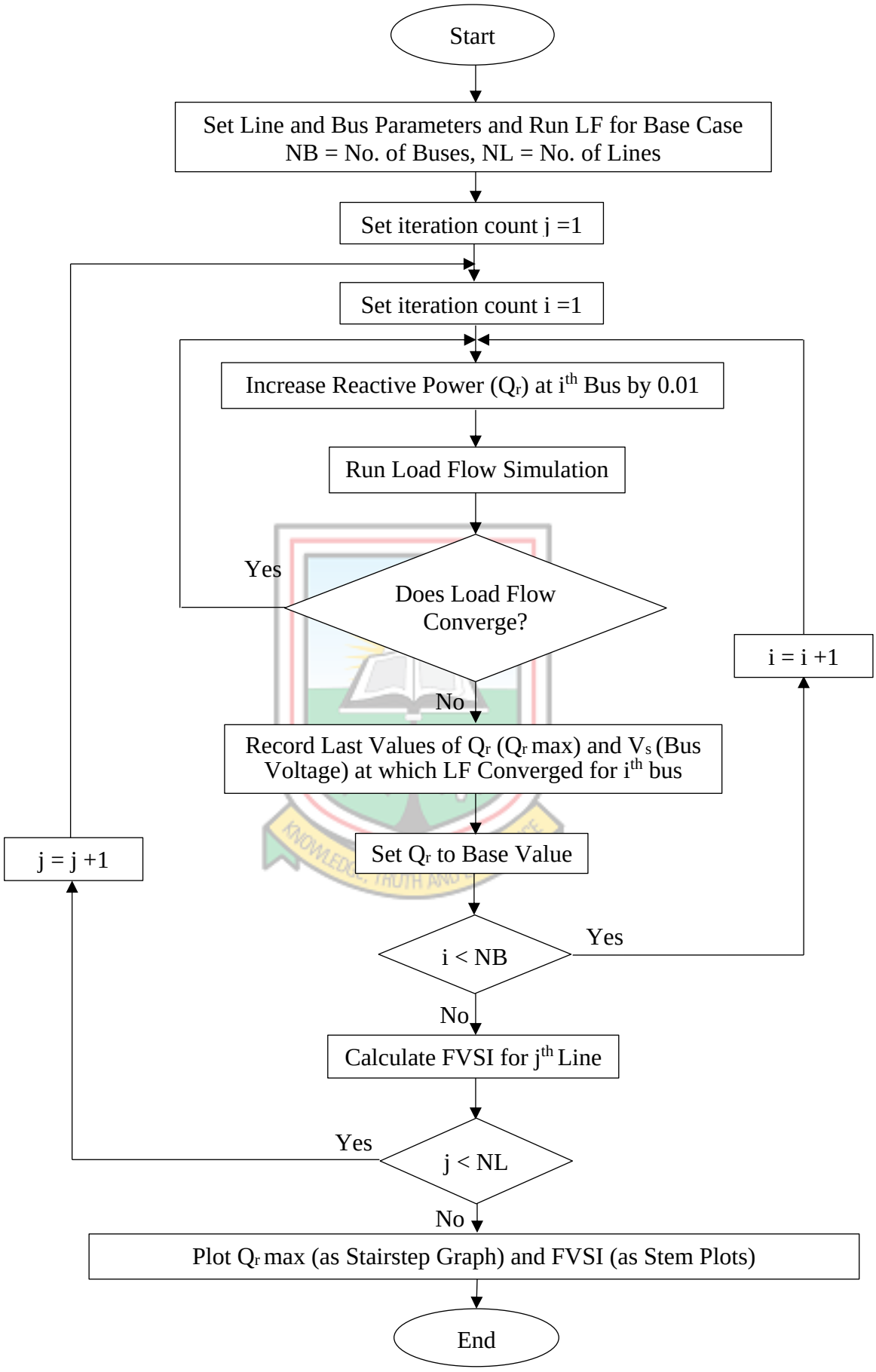

Figure 3.10 Algorithm for Maximum Loadability and FVSI Calculation

The steps of the flowchart are as follows:

i. Load system data and perform initial load flow studies for base case.
ii. Select one bus and progressively increase its reactive power by 0.01 MVAr.
iii. Perform load flow studies for each increment until load flow solution fails to converge
iv. Record the last value of reactive power increment (Q_r) and its corresponding adjoining bus voltage, (V_s) at which load flow converges. This indicates the maximum reactive power (maximum loadability), above which voltage collapse may occur on the said bus.
v. Repeat steps (ii) to (iv) until all buses have been selected.
vi. Insert Q_r and V_s into Equation (3.14) and determine the FVSI for each line
vii. Sort the maximum loadability, Q_r in ascending order. The bus with the least value is ranked the weakest bus.
viii. The line with the highest value of FVSI is the most critical line, which is capable of causing voltage collapse.

CHAPTER 4

SIMULATION RESULTS AND ANALYSIS

4.1 Introduction

This chapter discusses the simulation results on voltage stability. The simulations were carried out on Ghana's transmission system using MATLAB Simpower Systems. Load flow results of the system without UPFC are initially analysed, to give an idea on the status of the network before improvement. The results obtained using FVSI and the Maximum Loadability Assessment (MLA) helped in determining the optimal placement of the UPFC. Furthermore, the performance of the UPFC and STATCOM is presented and the dynamic responses of their controllers on the modelled network are analysed. A final load flow result is presented, this time with the UPFC in the circuit. The STATCOM is also connected in place of the UPFC to compare the behaviour of the line when either FACTS device is connected.

4.2 Weak Bus Identification Using Fast Voltage Stability Index and Maximum Loadability Assessment

The placement of the UPFC is done on the weakest bus in the network. The FVSI employed different network parameters for its computation, where dynamic parameters such as the receiving end reactive power and sending end voltage are derived from the load flow study. Figure 4.1 shows the results obtained from computing the FVSI for each transmission line with respect to the various buses in the network.

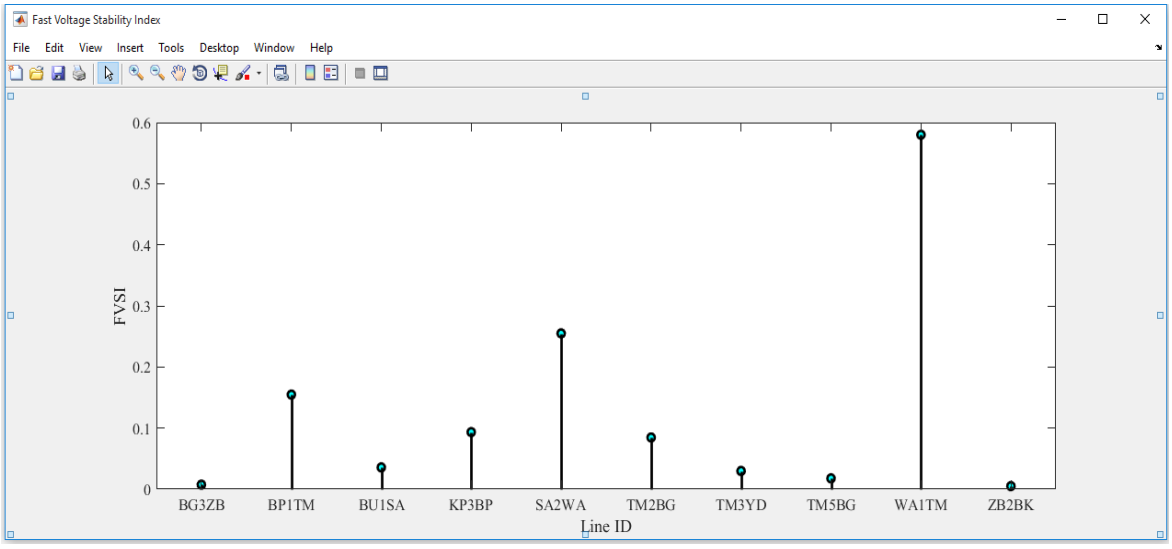

Figure 4.1 Fast Voltage Stability Index Results

The results indicate that the Wa – Tumu (WA1TM) transmission line is the most critical line with the highest index of 0.580. The line forms the weakest link in the network and requires maximum attention to prevent voltage collapse.

Since the critical line has been determined, the side of the line where the FACTS device needs to be placed is also identified. Figure 4.2 shows the results obtained from the MLA on each bus, which is arranged in ascending order.

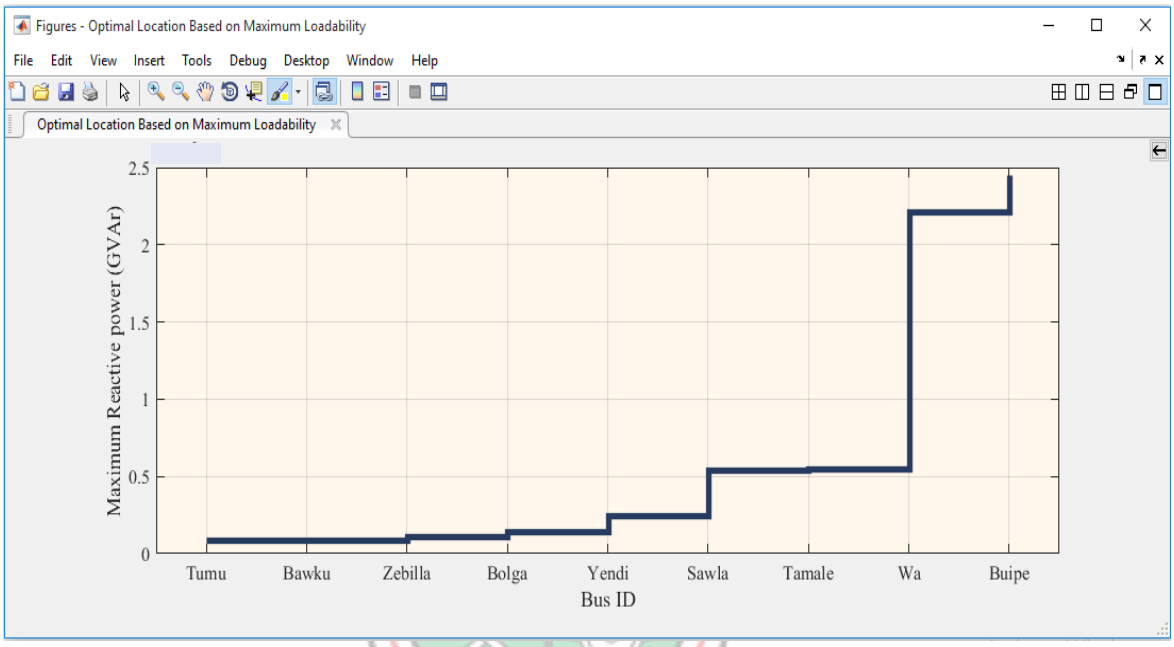

Figure 4.2 Results on Maximum Loadability Assessment of Each Bus

From Figure 4.2, the value of load that can be subjected to the respective buses increases upward away from Tumu. This is an indication that the Tumu bus, which has the least value, will collapse at a low reactive power loading hence determined as the weakest bus, whilst the Buipe bus is the strongest bus in the network. Since the Tumu bus connects the critical line, the optimal location of the UPFC is the Tumu BSP.

4.3 Load Flow Study of the Power System before Improvement

The voltage profile of the test system was recorded before insertion of the UPFC. The Newton-Raphson load flow method was used in generating the results as presented in Table 4.1. According to the Grid Code, a system is said to be stable on voltage, when the voltage deviation is ±5 % of the nominal (Anon., 2018c). Hence, for per unit analysis, the buses with a stable voltage should possess voltages between 0.95 and 1.05 p.u.

Table 4.1 Load Flow Study of System without FACTS Devices

SN	Bus ID	Bus Type	Vbase (kV)	Vref (pu)	Vangle (deg)	V_LF (pu)	Vangle LF(deg)
1.	Wa	PQ	161.00	1	0.00	1.0010	-0.31
2.	Bui	Swing	169.00	1	0.00	1.0000	0.00
3.	Sawla	PQ	161.00	1	0.00	1.0130	-0.30
4.	Kintampo	PQ	161.00	1	0.00	0.9960	0.00
5.	Buipe	PQ	161.00	1	0.00	0.9810	0.17
6.	Tamale	PQ	161.00	1	0.00	0.9248	0.85
7.	Tumu	PQ	161.00	1	0.00	0.8843	1.84
8.	Yendi	PQ	161.00	1	0.00	0.9122	1.15
9.	Bolga	PQ	161.00	1	0.00	0.8989	1.11
10.	Zebilla	PQ	161.00	1	0.00	0.8953	0.77
11.	Bawku	PQ	161.00	1	0.00	0.8945	0.77
12.	Kintampo	Swing	169.00	1	0.00	1.0000	0.00

Eleven BSPs (buses) were assessed in the network. Out of these, five buses had voltages in the range for a stable network, whilst the remaining 6 had voltage levels out of range, indicating instability at these buses. The most affected was the Tumu bus, with a voltage of 0.8843 p.u. The Zebilla and Bawku buses had p.u. voltages of 0.8989 and 0.8945, respectively. The bus at the end of the Tamale - Yendi line also recorded a low voltage.

4.4 Load Flow Study of the Power System after Optimal Placement of the UPFC

In this section, the load flow results obtained after the installation of the UPFC is presented. The STATCOM is also considered on the network to ascertain its performance with respect to the UPFC. Table 4.2 presents the results obtained after placing these FACTS devices on the Tumu bus which was identified as the optimum location.

As evident from Table 4.2, the UPFC produced voltage levels within the stability limit for all buses in the network. The bus voltage at Tumu improved significantly from 0.8843 p.u. to 0.9756 p.u. The lowest bus p.u. voltage of 0.9504 recorded in the network is found at Yendi. The lowest value at Yendi was as a result of the radial line connecting the Yendi Bus, and more importantly, this bus is most distant from the Tumu bulk supply point. When the STATCOM was connected to the same bus, four of its buses had voltages below the stability limit. However, the effect of the STATCOM produced voltage values that were better than when the system had no FACTS device in the circuit.

Table 4.2 Load Flow Study of System with UPFC and STATCOM placed at Tumu Bus

SN	Bus ID	Bus Type	Vbase (kV)	UPFC		STATCOM	
				V_LF (pu)	Vangle LF (deg)	V_LF (pu)	Vangle LF (deg)
1.	Wa	PQ	161	0.9557	0.28	0.9695	-0.26
2.	Bui	Swing	169	1.0390	-0.54	1.0390	-0.43
3.	Sawla	PQ	161	0.9886	-0.05	0.9967	-0.27
4.	Kintampo	PQ	161	1.0170	0.00	1.0130	0.00
5.	Buipe	PQ	161	1.0060	0.12	1.0000	0.17
6.	Tamale	PQ	161	0.9635	0.56	0.9539	0.83
7.	Tumu	PQ	161	0.9756	0.62	0.9514	1.77
8.	Yendi	PQ	161	0.9504	0.86	0.9410	1.14
9.	Bolga	PQ	161	0.9594	0.44	0.9431	1.07
10.	Zebilla	PQ	161	0.9562	0.11	0.9392	0.73
11.	Bawku	PQ	161	0.9554	0.10	0.9383	0.73
12.	Kintampo	Swing	169	1.0170	0.00	1.0130	0.00

In order to verify the results on the optimal location, the FACTS devices are placed on different buses in the network. The buses that have voltage sources connected to them (Bui and Kintampo) are not considered for the placement as well as the immediate connecting buses (Sawla and Buipe). The buses on the radial lines (Yendi, Zebilla and Bawku) are also not considered since the effect of a compensating device in a ring network is better than a radial one (Cano *et al*., 2015). The buses left to be considered are the Wa, Bolga and Tamale.

4.4.1 Load Flow Results with the FACTS Devices Placed at Wa Bus

When the UPFC was placed on the Wa bus, the voltage profile for all buses was within range except the Yendi bus that had a voltage of 0.9494 p.u., which is below the stability limit. The voltage values for STATCOM showed four buses having levels below the stability limit. Again, the results obtained for the network with the FACTS devices are an improvement of the values obtained with no FACTS device. The UPFC connected to the system produced better results compared to the STATCOM. These results are presented in Table 4.3.

Table 4.3 Load Flow Study of System with UPFC and STATCOM placed at Wa Bus

SN	Bus ID	Bus Type	Vbase (kV)	UPFC		STATCOM	
				V_LF (pu)	Vangle LF (deg)	V_LF (pu)	Vangle LF (deg)
1.	Wa	PQ	161	0.9780	0.28	0.9518	1.26
2.	Bui	Swing	169	1.0360	-0.54	1.0380	-0.43
3.	Sawla	PQ	161	0.9862	-0.05	0.9957	-0.14
4.	Kintampo	PQ	161	1.0150	0.00	1.0120	0.00
5.	Buipe	PQ	161	1.0040	0.12	0.9995	0.15
6.	Tamale	PQ	161	0.9625	0.56	0.9534	0.73
7.	Tumu	PQ	161	1.0020	0.61	0.9687	1.35
8.	Yendi	PQ	161	0.9494	0.86	0.9405	1.03
9.	Bolga	PQ	161	0.9592	0.44	0.9431	0.84
10.	Zebilla	PQ	161	0.9555	0.10	0.9393	0.50
11.	Bawku	PQ	161	0.9500	0.10	0.9384	0.49
12.	Kintampo	Swing	169	1.0150	0.00	1.0120	0.00

4.4.2 Load Flow Results with the FACTS Devices Placed at Bolga Bus

Table 4.4 shows the results obtained when the FACTS devices were placed at Bolga bus. With the UPFC on the Bolga BSP, voltages on most buses were improved except two (Tamale and Yendi), which had voltages below 0.95 p.u. This is because the UPFC was placed too far away from the power source at Bui (312.2 km apart), so not enough power flow control is achieved. The STATCOM also had the voltage level of four buses below the voltage stability limit. The UPFC performed better than the STATCOM because apart from the reactive power control, the active power flow control of the UPFC prevents overloading and hence minimum voltage drop, which accounts for a better voltage improvement.

Table 4.4 Load Flow Study of System with UPFC and STATCOM placed at Bolga Bus

SN	Bus ID	Bus Type	Vbase (kV)	UPFC		STATCOM	
				V_LF (pu)	Vangle LF (deg)	V_LF (pu)	Vangle LF (deg)
1.	Wa	PQ	161	0.9543	0.27	0.9701	0.42
2.	Bui	Swing	169	1.0260	-0.54	1.0390	-0.49
3.	Sawla	PQ	161	0.9821	-0.05	0.9969	0.05
4.	Kintampo	PQ	161	0.9966	0.00	1.0130	0.00
5.	Buipe	PQ	161	0.9837	0.12	1.0000	0.11
6.	Tamale	PQ	161	0.9365	0.56	0.9536	0.52
7.	Tumu	PQ	161	1.0220	0.61	0.9424	0.81
8.	Yendi	PQ	161	0.9235	0.86	0.9407	0.82
9.	Bolga	PQ	161	0.9555	0.45	0.9523	0.36
10.	Zebilla	PQ	161	1.0170	0.11	0.9385	0.03
11.	Bawku	PQ	161	1.0170	0.10	0.9377	0.02
12.	Kintampo	Swing	169	0.9966	0.00	1.0130	0.00

4.4.3 Load Flow Results with the FACTS Devices Placed at Tamale Bus

The load flow results obtained considering the Tamale bus is shown in Table 4.5. Two buses namely, Wa and Yendi violated the voltage stability limit with the UPFC in the circuit. The results from the network with the STATCOM also had three bus voltages below the set limit.

Table 4.5 Load Flow Study of System With UPFC and STATCOM placed at Tamale Bus

SN	Bus ID	Bus Type	Vbase (kV)	UPFC		STATCOM	
				V_LF (pu)	Vangle LF (deg)	V_LF (pu)	Vangle LF (deg)
1.	Wa	PQ	161	0.9402	0.27	0.9702	-0.12
2.	Bui	Swing	169	1.0300	-0.54	1.0390	-0.58
3.	Sawla	PQ	161	0.9981	-0.06	0.9968	-0.28
4.	Kintampo	PQ	161	0.9893	0.00	1.0390	0.00
5.	Buipe	PQ	161	0.9747	0.12	0.9998	0.15
6.	Tamale	PQ	161	0.9507	0.56	0.9632	0.75
7.	Tumu	PQ	161	0.9991	0.60	0.9532	0.01
8.	Yendi	PQ	161	0.9075	0.87	0.9404	1.05
9.	Bolga	PQ	161	0.9730	0.44	0.9528	-0.46
10.	Zebilla	PQ	161	0.9737	0.10	0.939	-0.79
11.	Bawku	PQ	161	0.9728	0.10	0.9381	-0.80
12.	Kintampo	Swing	169	0.9893	0.00	1.0390	0.00

4.5 Comparison of Voltage Profile and Active Power on Different Network Buses

It is realised from the results and analysis that the optimal placement of the devices using FVSI and maximum loadability criterion was predicted correctly.

The graph of Figure 4.3 is used to provide a summary on the comparison of the three scenarios presented in the system. That is the network without FACTS devices as well as with the UPFC and STATCOM located at the Tumu Bus.

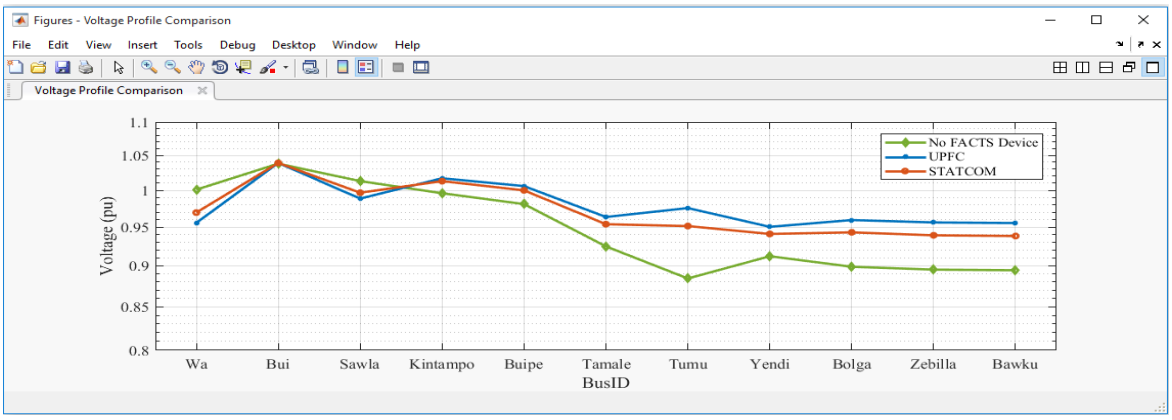

Figure 4.3 Comparison of Voltage Profile on System Buses with Emphasis on Tumu Bus

The presence of the STATCOM provided voltage improvement in eight of the eleven buses. However, the improvement made on four out of the eight buses did not meet the stability requirement. The improvement made by the STATCOM is due to its ability to generate reactive power to the line. A limit is however set on the amount of reactive power generated in order not to further increase the line loadings. In view of this, the Yendi, Bolga, Zebilla and Bawku buses had voltages below 0.95 p.u.

The installation of the UPFC provided better results, where all buses had voltages within range. This is possible due to the combined effect of the STATCOM and the SSSC. These devices provided different adjustments in order to meet the requirements of the transmission system. Connecting the two devices back-to-back provided the added advantage of real power flow control, which causes an increase in the available capacity and hence, a better voltage profile for the entire system.

Further analysis is done on the transfer of power on the modelled system. The results on generated power, received power and the corresponding power losses experienced in the network for Tumu, Wa, Bolga and Tamale are presented in Table 4.6.

Table 4.6 Load Flow Results on Power Flow in the Network for the Three Scenarios

Scenario	Device	Generation (MW)	Received (MW)	Power Loss (MW)
Tumu	No Device	134.57	121.17	13.40
	UPFC	131.75	121.36	10.39
	STATCOM	133.55	121.39	12.16
Wa	No Device	134.57	121.17	13.40
	UPFC	131.95	121.37	10.58
	STATCOM	133.61	121.39	12.23
Bolga	No Device	134.57	121.17	13.40
	UPFC	131.95	121.36	10.59
	STATCOM	133.85	121.38	12.48
Tamale	No Device	134.57	121.17	13.40
	UPFC	131.94	121.37	10.57
	STATCOM	133.74	121.35	12.39

From the Table 4.6, dynamics of power flow in the network with or without the FACTS devices on the various buses are presented. Since the load was selected as a constant PQ bus, the received power for all four cases was almost the same. The amount of power generated however differs for each scenario. The power losses recorded for each scenario indicated that Tumu recorded low values for both the STATCOM and the UPFC.

Figure 4.4 presents a comparison of results on power losses when the devices were connected to the Tumu bus.

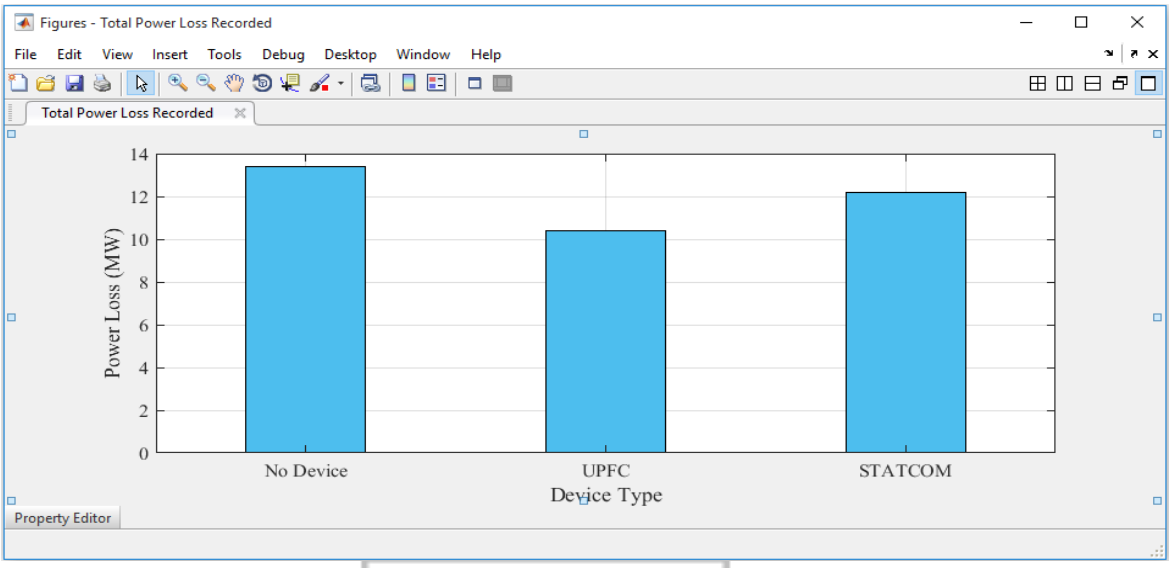

Figure 4.4 Total Power Loss Recorded in the Network for all Three Scenarios on Tumu Bus

When no FACTS device was connected to the Tumu bus, the total power loss recorded was 13.40 MW. When the STATCOM was connected, the power loss reduced to 12.16 MW due to the control of voltage by the device. The UPFC further reduced the power loss to 10.39 MW due to the device's ability to control both the active and reactive power flows in the network.

The complete load flow results for the system with and without the FACTS devices can be found in Appendix B.

4.6 Performance of the UPFC on the Power Transmission System

The operating characteristics of the UPFC are analysed in this section in order to access the performance of the device on the transmission network. To start the simulations, the UPFC together with other blocks in the model are initialised using the power GUI block. The simulation time is set at 1.2 s at which time the effect of every input has been achieved. The modelled device can run in several modes, but in analysing its effects on voltage and power flows, the simulation considers the power flow control and voltage injection mode. To determine the dynamism of the control system, step changes are included in the reference values of the parameters to be controlled, whilst scopes are used to read the waveforms produced from the simulations.

At the start of the power flow simulation, the natural active power flow on the network bus linking the UPFC bus is realised to be 5.4 MW. At time 0.025 s, when the UPFC is brought into circuit, the power capability of the connecting line increased to 32.50 MW as can be seen in the first trace of Figure 4.5.

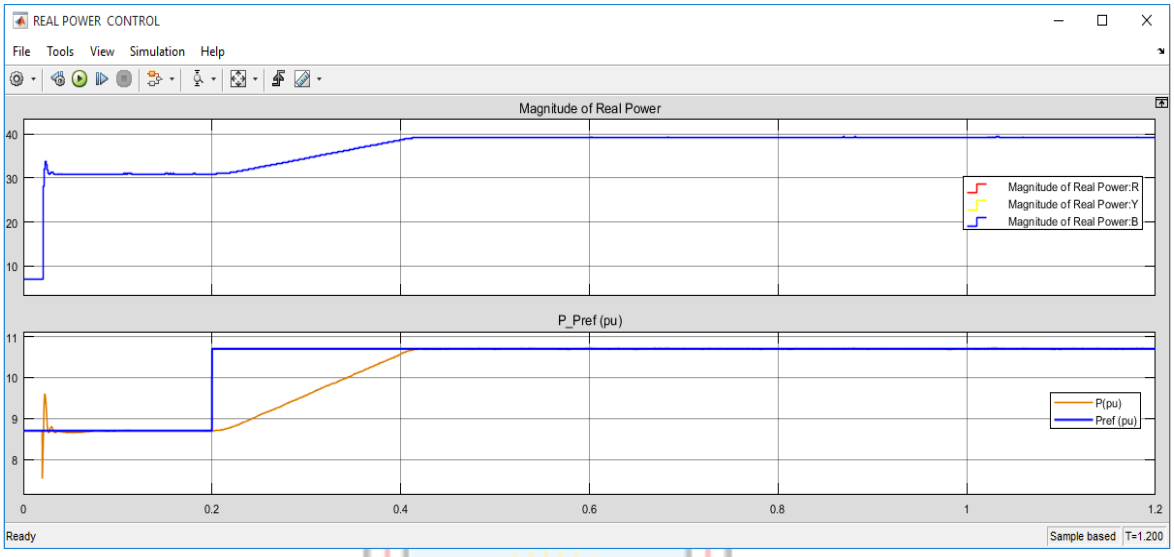

Figure 4.5 Simulation Results on Active Power Flow Control of the UPFC

From the active power flow control scope, a step is introduced into the reference power at time 0.2 s from 8.7 p.u to 10.7 p.u. The controller sensed the change and raised the measured p.u. power to trace the new value. The UPFC responded to the change and increased the line's capability of active power transfer from the initial 32.50 MW to a value of 40 MW.

The action of the reactive power controller is similar to the active power controller. From Figure 4.6, the UPFC initially produced a reactive power control of 3.4 MVAr.

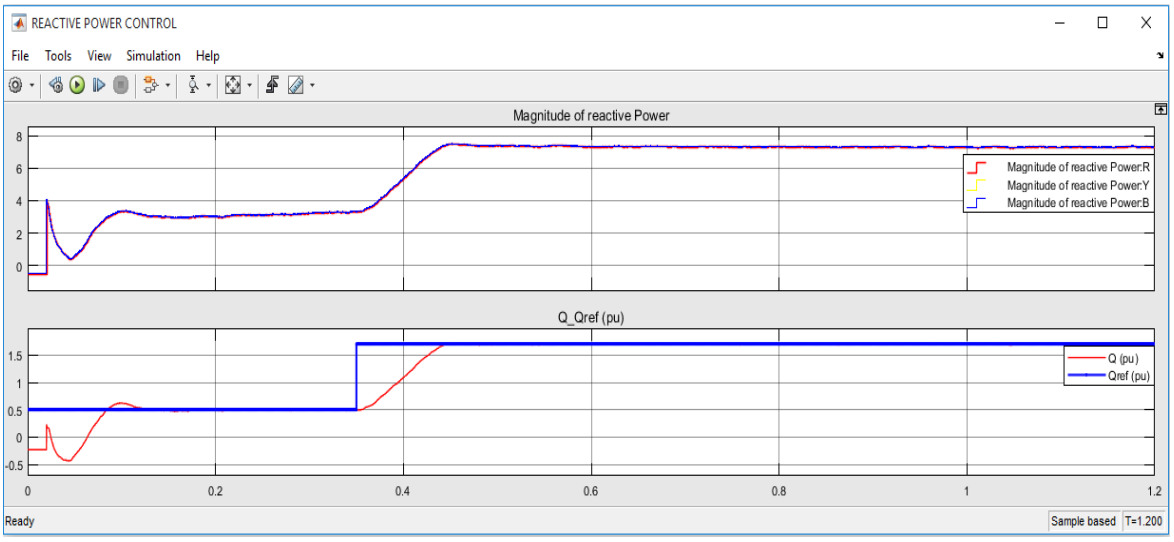

Figure 4.6 Simulation Results on Reactive Power Flow Control of the UPFC

A step input is introduced to the reference reactive power at 0.35 s, which is realised by the measured p.u. component and increased its value to cancel the error created by the step change. The UPFC realised the change and increased the reactive power transfer in the line to 7.8 MVAr.

As the UPFC controls power on the network, the voltage level on the connecting bus is monitored. Figure 4.7 shows the voltage profile on the busbar and the shunt side capacitor.

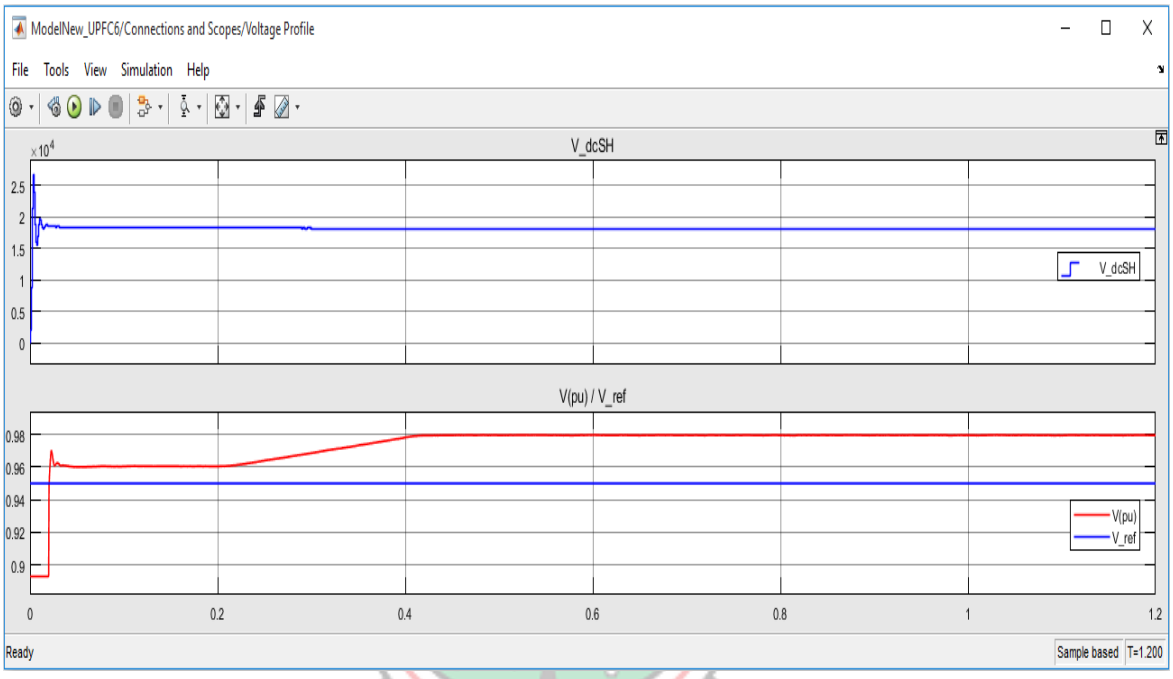

Figure 4.7 Simulation Results on Bus Voltage and Shunt Side DC Voltage

At the start of the simulations, the voltage realised on the connecting bus was 0.89 p.u. and the initial action of the UPFC increased the bus voltage to 0.96 p.u. When the active power flow on the line was increased, the voltage level on the connecting bus also increased to a new value of 0.98 p.u. It is evident from the results that an increase in active power transfer on a transmission line has a positive effect on bus voltage. The DC capacitor voltage on the shunt side remained constant throughout the entire simulations.

Further analysis of the UPFC was carried out in the voltage injection mode, where the characteristics of the series converter were assessed. In this mode, the magnitude of the injected voltage was chosen not to exceed 10% to prevent swelling on the line. Figure 4.8 depicts the waveforms generated by the SSSC scope.

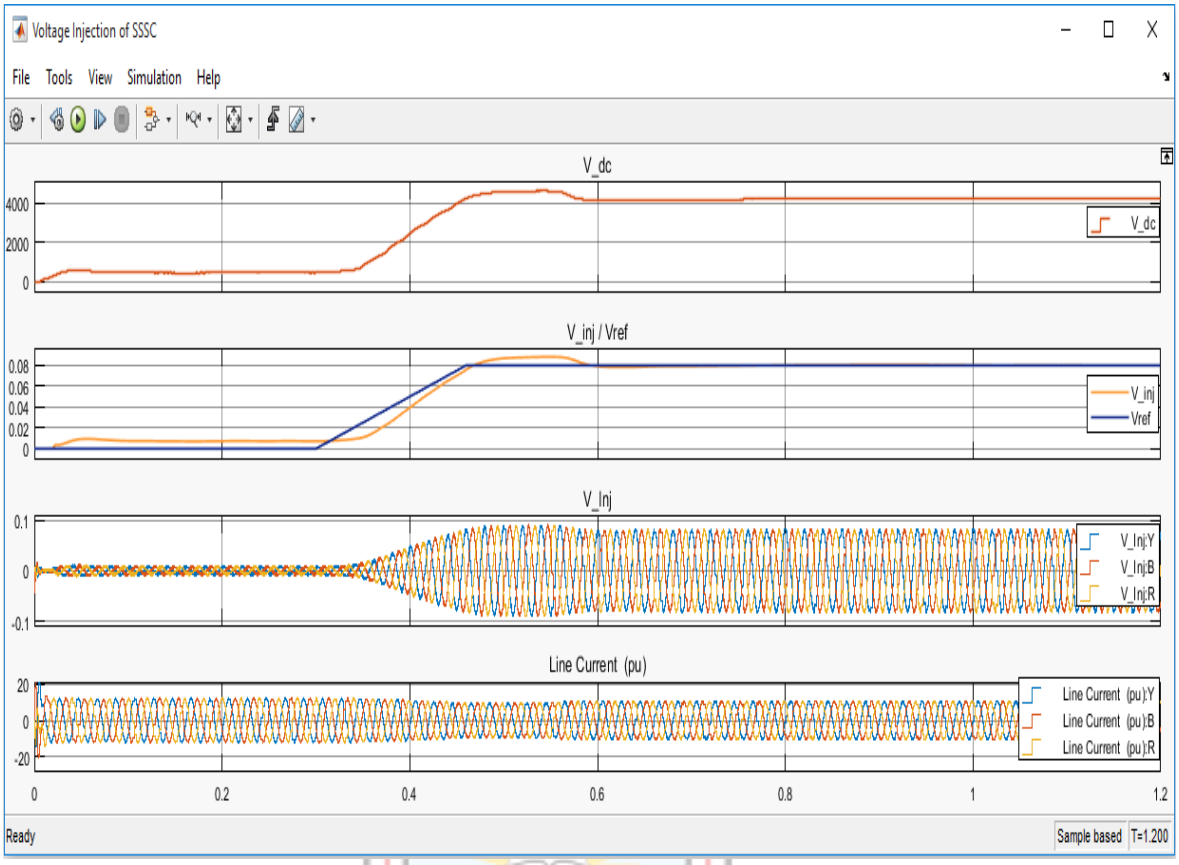

Figure 4.8 Simulation Results on the Performance of the Series Controller

The magnitude of the injected voltage is derived by the action of the DC controller, which determines the amount of voltage injected into the line at a given time. At the start of the simulations, the DC voltage waveform (V_dc) rose from zero to 500 V, which triggered the SSSC. The voltage became steady until 0.3 s when a step input was applied to the reference voltage (V_{ref}). The step change of 0.08 p.u. caused the DC voltage controller to respond by increasing the voltage to 4000 V. This action was realised by the series controller, which also responded by injecting voltage into the transmission line as shown by the voltage injection scope (V_Inj).

Figure 4.9 is a zoom in on the injected voltage and line current, which elaborates the waveform of the injected voltage (V_Inj) to be 90^{o} out of phase with the line current waveform. This indicates that the UPFC can either supply or generate reactive power to the line. The injected voltage phasor leads the line current phasor implying the transfer of active power from the UPFC to the line through the series inverter.

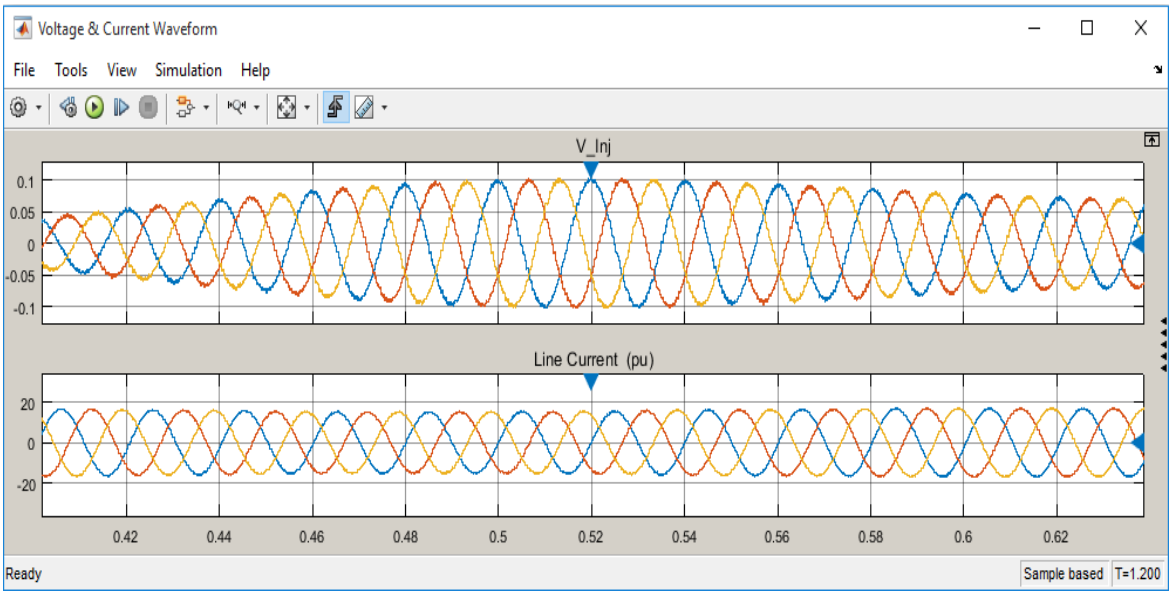

Figure 4.9 Simulation Diagram Explaining the Injected Voltage Phasor in Quadrature with the Line Current

The model of the STATCOM used in the comparative analysis is similar to the one used for the UPFC model. Figure 4.10 shows the simulation results obtained from the STATCOM controller. From the Figure 4.10, the STATCOM operated as a reactive power compensator, which can generate or absorb reactive power in order to vary the voltage. The bus voltage was initially ramped to 0.95 p.u.

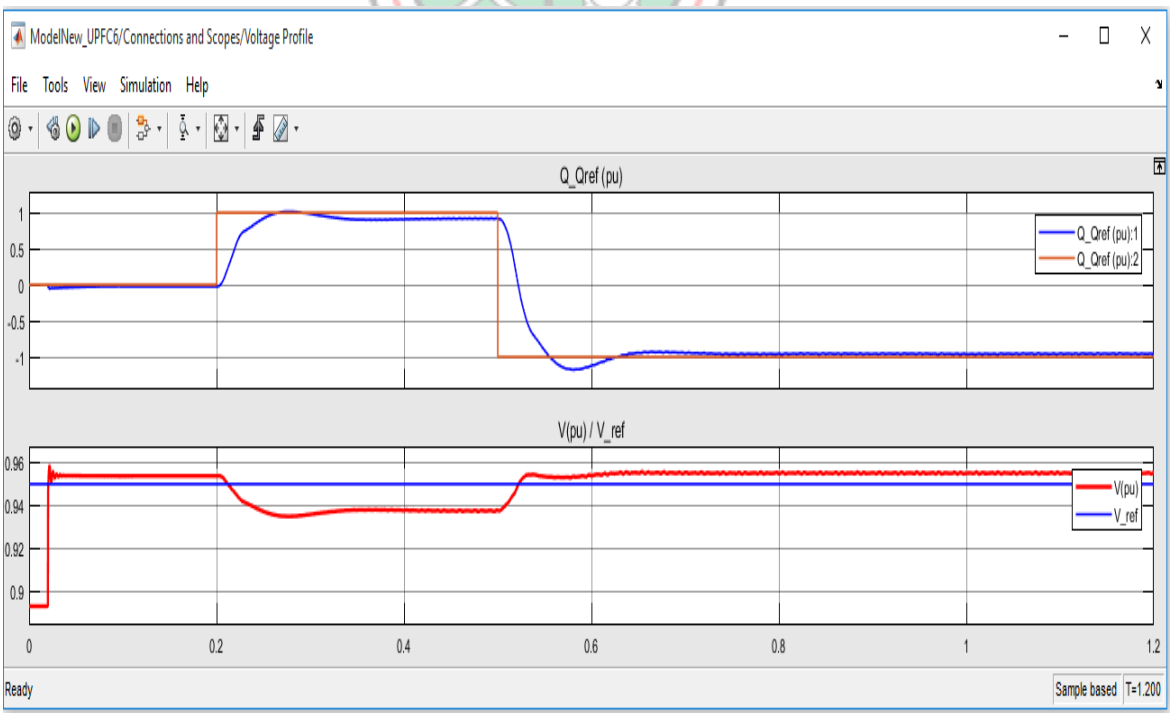

Figure 4.10 Simulation on the STATCOM in VAr Control Mode

At 0.2 s, a step change is introduced to the reference reactive power, which allowed the STATCOM controller to respond to the change by tracing its reference value. At this stage, the STATCOM is absorbing reactive power and the bus voltage went down to 0.938 p.u. At 0.5 s, the reference reactive power was reduced, the controllers' action enabled the device to generate reactive power, which increased the connecting bus voltage to a final value of 0.955 p.u.

4.7 Cost Analysis on Implementing the UPFC on the Transmission System

It has been realised that incorporating the UPFC into the network provides some amount of relief to the power system. The project will however not be feasible if no financial benefits are attained through the lifetime of the device. Hence, a cost analysis is made on installing the UPFC on the system. The analysis entails the cost of generating and transmitting electrical power on Ghana's grid network, which is compared to the cost of installing the device into the system. The time taken for the project to breakeven is also analysed.

According to the Public Utility Regulatory Commission (PURC), the average cost of generating power in the country now stands at GH¢ 1.08/kWh, considering 69.3% thermal, 30.4% hydro and 0.3% renewable generation (Anon., 2018c). From Table 4.6, the value of generation with and without UPFC on the Tumu Bus is 131.75 MW and 134.57 MW respectively. This is used to find the cost of generation for both cases.

The cost of generation without UPFC = 134.57 × 1000 × 1.08 = GH¢ 145,336.00

The cost of generation with UPFC = 131.75 × 1000 × 1.08 = GH¢ 142,290.00

Therefore gains of GH¢ 3,046 is made per hour. Hence annual gains made on installing the UPFC is computed as 3046 ×(24×365), which yeilds GH¢ 26,682,960.00 annually.

Equation (4.1) (Mireku-Gyimah, 2017) is used to determine the future value on the gains made when the UPFC project is carried out.

$$F_G = \frac{A\left[(1+i)^n - 1\right]}{i} \tag{4.1}$$

where, F_G = future gains made after installing UPFC (GH¢)

A = annual gains after installing UPFC (GH¢)

n = number of years

i = prevailing interest rate, which is 16% per annum (Anon., 2019a)

The installation and operational costs of the UPFC are determined using Equation (4.2) (Alamelu *et al.*, 2015). Equation (4.2) has been used by Karthikeyan (2018) and Alamelu *et al.* (2015) on the costing of UPFC projects.

$$C_{UPFC} = 0.0003S^2 - 0.261S + 188.22 \quad (4.2)$$

where, C_{UPFC} = cost of installing and operating UPFC ($/h)

S = maximum operating real power of the UPFC (MW)

The power factor of Ghana's grid is kept at 0.9 (Anon., 2018c), indicating that the maximum operating real power of the UPFC is 90 MW since the device was modelled at 100 MVA. Hence,

$$C_{UPFC} = 0.0003(90)^2 - 0.261(90) + 188.22 = 167.16 \text{ \$/h}$$

The dollar price of the UPFC can be converted to Ghana Cedi (GH₵) at an exchange rate of $ 1 = GH₵ 5.2285 (Anon., 2019b). C_{UPFC} becomes $167.16 \times 5.2285 = 874$ GH₵/h

Annual cost for the installation and operation of the UPFC is

$$874 \times 24 \times 365 = 7{,}656{,}240 \text{ GH₵/yr}$$

The future value on the investment cost can be calculated using Equation (4.3) (Mireku-Gyimah, 2017).

$$F_C = P(1 + i)^n \quad (4.3)$$

where, F_C = future cost of installing UPFC (GH₵)

P = present cost of installing UPFC

Using Equation (4.1), the annual gains made in the first year is calculated as:

$$F_G = \frac{26{,}682{,}960\left[(1 + 0.16)^1 - 1\right]}{0.16} = \text{GH₵ } 26{,}682{,}960$$

The cost incurred on installation and operation of the UPFC in the first year is calculated with Equation (4.3) as:

$$F_C = 7{,}656{,}240\,(1 + 0.16)^1 = \text{GH₵ } 8{,}881{,}238$$

Annual profits made on the UPFC is determined by:

Annual gains on UPFC installation – Cost of UPFC installation

Hence the profits made in the fist year is determined as follows:

GH¢ 26,682,960 - GH¢ 8,881,238 = GH¢ 17,801,722

The cost analysis on the UPFC installation and gains made after its installation for the next ten (10) years is calculated using Equation (4.1) and Equation (4.3).

Table 4.7 Cost Analysis on UPFC Installation and Gains Made in 10 Years

Year	Cost of UPFC Installation (GH¢)	Annual Gains on UPFC Installation (GH¢)	Annual Profits on UPFC Installation (GH¢)
1.	8,881,238	26,682,960	17,801,722
2.	10,302,237	57,635,194	47,332,957
3.	11,950,594	93,539,785	81,589,190
4.	13,862,689	135,189,110	121,326,421
5.	16,080,720	183,502,328	167,421,608
6.	18,653,635	239,545,660	220,892,025
7.	21,638,217	304,555,926	282,917,709
8.	25,100,331	379,967,834	354,867,503
9.	29,116,384	467,445,647	438,329,263
10.	33,775,006	568,919,911	535,144,905

From Table 4.7, the project will break even in the first year after its installation and start making profits in excess of 17,000,000.00 GH¢ per annum.

4.8 Summary of Findings

The findings made during this research are as follows:

i. The weakest bus in the network was determined as the Tumu bus with a stability index of 0.58. Its corresponding connecting bus to Wa was identified as the line with the least loadability, and is overloaded with a reactive power of 86 MVAr, capable of causing voltage collapse;
ii. The maiden load flow performed on the system without the FACTS devices confirmed Tumu as the weakest bus, with a voltage of 0.8843 p.u., which is way below the stability limit value of 0.95 p.u. A voltage in this range is termed by the grid code to be in the critical state and is capable of collapsing at any time;
iii. The power and voltage control capabilities of the UPFC brought relief when connected to the system. The Tumu voltage increased from 0.8843 p.u. to 0.9756 p.u. The power losses experienced in the network reduced by 3.01 MW and stood at 10.39 MW when the UPFC was connected;

iv. A comparison made on the UPFC and the STATCOM showed that the UPFC provides more functionalities and hence, better system improvements as compared to the STATCOM's capabilities. The UPFC controlled both active power and reactive power whereas the STATCOM controlled only the reactive power on the network;
v. Significant savings are made on the introduction of the UPFC. The installation and operation of the device cost GH¢ 7,656,240.00 annually. The 3.01 MW power loss recovered by installing the UPFC is able to make an annual financial gain of GH¢ 26,682,960.00. Hence, a profit of about GH¢ 17,801,722.00 is made every year; and
vi. Locating the UPFC at Wa was not too different from placing the UPFC at Tumu. The Yendi bus however had a low voltage when the UPFC was placed at Wa since the Yendi bus is a radial network and it is also far from the UPFC location. When the UPFC was sent to the Bolga and Tamale buses, the voltage improvement was less due to the radial lines connected to these buses.

CHAPTER 5

CONCLUSIONS AND RECOMMENDATIONS

5.1 Conclusions

In this research, a computer model of the northern part of Ghana's transmission system is presented. The software chosen for modelling was MATLAB Simpower Systems, which was used to incorporate the UPFC into the system. The entire model was simulated to demonstrate the capability of the device in controlling power flow and regulating voltage on the network. The control and regulation were achieved by the combined efforts of the series and shunt converters as well as the DC link capacitor. To prove the effectiveness of the UPFC on the system, the study was first conducted without the UPFC and later with the UPFC and STATCOM, noting the changes in system parameters for all cases.

The following conclusions are drawn based on the findings.

i. The introduction of the UPFC into the system improved the bus voltage to levels within the stability margin. The device achieved this by controlling the active power, reactive power and the phase angle of the network. This, in turn, increased the power transfer capability of the network with the system losses reducing significantly across the entire power system;
ii. Installation of an UPFC not only provides stability of a power network but also yields a cost effective means of generating and transmitting electric power;
iii. The simulations confirmed that Ghana's power system was prone to voltage instability, which results in higher power losses. These losses cause a generation deficit that can account for a portion of the recent power outages experienced in the country;
iv. The combined effect of the FVSI and the MLA provides a great solution on the optimum location of the FACTS devices; and
v. Simscape Power Systems software is capable of modelling a complete electric power system. Interconnecting the system blocks makes it easier and simpler to design the power network as compared to writing an entire code for the same purpose.

5.2 Recommendations

The following recommendations are made in respect to the thesis:

i. UPFC should be installed on the Tumu bus to improve the total stability of the power network, as well as reduce electric power transmission losses;
ii. In order to implement the UPFC at any voltage level, its components must be modelled to conform to the desired voltage and power rating of the system under study; and
iii. A more dynamic and sustainable approach should be considered when dealing with voltage stability on Ghana's transmission system.

5.3 Further Work

Further studies to be considered in relation to this research are as follows:

i. The work focused on developing a computer model of only the northern part of the countries' transmission system due to the nature of instability in the area. Moving forward, the entire transmission system together with its interconnecting neighbouring lines can be modelled to determine the performance of the device on the entire system; and
ii. A hybrid system that is made up of several current generation FACTS devices like a number of UPFCs or a combination of UPFC and IPFC can be considered to be placed at vantage locations in the network to ascertain further effectiveness.

REFERENCES

Adebayo, I. G., Aborisade, D. O. and Oyesina, K. A. (2013), "Steady State Voltage Stability Enhancement Using Static Synchronous Series Compensator, A Case Study of Nigerian 330 kV Grid System", *Research Journal in Engineering and Applied Sciences*, Vol. 2, No. 1, pp. 54 - 61.

Alamelu, S., Baskar, S., Babulal, C. K. and Jeyadevi, S. (2015), "Optimal Siting and Sizing of UPFC Using Evolutionary Algorithms", *International Journal of Electrical Power and Energy Systems*, Vol. 69, No. 1, pp. 222 – 231.

Albatsh, F. M., Ahmad, S., Mekhilef, S., Mokhlis, H. and Hassan, M. A. (2015), "Optimal Placement of Unified Power Flow Controllers to Improve Dynamic Voltage Stability Using Power System Variable based Voltage Stability Indices", *PLOS ONE*, Vol. 10, No. 4, pp. 1 – 32.

Al Shamli, Y., Hosseinzadeh, N., Yousef, H. and Al Hinai, A. (2015), "A Review of Concepts in Power System Stability", *Proceedings of the 8th IEEE GCC Conference and Exhibition*, Muscat, Oman, pp. 1 - 6.

Ametani, A., Nagaoka, N., Baba, Y., Ohno, T. and Yamabuki, K. (2016), *Power System Transients: Theory and Applications*, CRC Press, Florida, USA, 1st edition, 600 pp.

Anon. (2012a), "Electricity Supply Plan", *www.gridcogh.com/.../supplyplan/2012_Electricity_Supply_Plan.pdf.* Accessed: August 1, 2016.

Anon. (2012b), "Investigation into the Causes of the Three Total System Collapses in the Ghana Power System", *www.purc.com.gh/purc/sites/default/files/ffcreport_0.pdf.* Accessed: August 4, 2016.

Anon. (2013), "Electricity Supply Plan", *www.gridcogh.com/.../supplyplan/2013_Electricity_Supply_Plan.pdf.* Accessed: August 1, 2016.

Anon. (2014), "Electricity Supply Plan", *www.gridcogh.com/.../supplyplan/2014_Electricity_Supply_Plan.pdf.* Accessed: August 1, 2016.

Anon. (2015), "KEMET Electronic Component Capacitor Selection Guide", *http://www.kemet.com/Lists/FileStore/Capacitor%20Selection%20Guide.pdf* Accessed: June 6, 2019.

Anon. (2016a), "Electricity Supply Plan", *www.gridcogh.com/.../supplyplan/2016_ Electricity_Supply_Plan.pdf.* Accessed: July 17, 2017.

Anon. (2016b), "Power Outages in Ghana" *www.myjoyonline.com/news.* Accessed: December 2, 2018.

Anon. (2016c), *Simscape Power Systems User's Guide,* The Mathworks Publishers, 32nd edition, Natick, Massachusetts, USA, 374 pp.

Anon. (2017), "Electricity Supply Plan", *http://energycom.gov.gh/files/2017%20 Electricity%20Supply%20Plan%20-%20Final%20Report.pdf.* Accessed: June 8, 2018.

Anon. (2018a), "Electricity Supply Plan", *www.gridcogh.com/.../supplyplan/2018_ Electricity_Supply_Plan.pdf* Accessed: January 20, 2019.

Anon. (2018b), "Power Outage", *http://citifmonline.com/tag/power-outage.* Accessed: December 2, 2018.

Anon. (2018c), "Energy Supply and Demand Outlook for Ghana", *www.energycom.gov.gh /data-center/energy-outlook-for-ghana.pdf.* Accessed: October 7, 2018.

Anon. (2019a), "Ghana Interest Rate", *https://tradingeconomics.com/ghana/interest-rate.* Accessed: June 6, 2019.

Anon. (2019b), "Daily Interbank FX Rates", *https://www.bog.gov.gh/markets/daily-interbank-fx-rates*. Accessed: June 6, 2019.

Aung, T. N., Lin, K. M. and Oo, K. Z. (2017), "Line Stability Index Based Optimal Placement of Unified Power Flow Controller", *International Journal of Energy and Power Engineering*, Vol. 6, No. 4, pp. 1 – 47.

Barot, H., Varma, R. K. and Lake, S. (2014), "Operational Experience with Static VAr Compensators" *IEEE PES General Meeting, Conference and Exposition*, Ontario, Canada, pp. 1 - 5.

Benaissa, M., Hadjeri, S. and Zidi, S. A. (2017), "Impact of PSS and SVC on the Power System Transient Stability," *Advances in Science, Technology and Engineering Systems Journal*, Vol. 2, No. 3, pp. 562 - 568.

Bhattacharyya, B., Gupta, V. K. and Kumar, S. (2014), "UPFC with Series and Shunt FACTS Controllers for the Economic Operation of a Power System", *Ain Shams Engineering Journal*, Vol. 5, No. 3, pp. 775 - 787.

Bhesdadiya, R. H., Patel, C. R. and Patel, R. M. (2014), "Transmission Line Loadability Improvement Using FACTS Device*", International Journal of Research in Engineering and Technology*, Vol. 3, No. 5, pp. 626 - 630.

Bhowmick, S. (2016), *Flexible AC Transmission Systems, Newton Power-Flow Modelling of Voltage-Sourced Converter based Controllers*, Taylor and Francis Group, Boca Raton, Florida, USA, 1st edition, 314 pp.

Bruno, S., De-Carne, G. and La Scala, M. (2016), "Transmission Grid Control through TCSC Dynamic Series Compensation", *IEEE Transactions on Power Systems*, Vol. 31, No. 4, pp. 3202 - 3211.

Cano, J. M., Norniella, J. G., Rojas, C. H., Orcajo, G. A. and Jatskevich, J. (2015), "Application of Loop Power Flow Controllers for Power Demand Optimization at Industrial Customer Sites", *IEEE Power and Energy Society General Meeting*, Denver, Colorado, USA, pp. 1 - 5.

Danish, M. S. S. (2015), *Voltage Stability in Electric Power System: A Practical Introduction*, Logos Verlag Publishers, Berlin, Germany, 2nd edition, 219 pp.

Eremia, M., Liu, C. C. and Edris, A. A. (2016), *Advanced Solutions in Power Systems HVDC, FACTS, and Artificial Intelligence,* John Wiley and Sons, Inc., Hoboken, New Jersey, USA, 1st edition, 405 pp.

Essilfie, J. E., Tlusty, J. and Santarius, P. (2013), "Using SVC to Improve Voltage Stability of the Ghana Power Network", *Przegląd Elektrotechniczny*, Vol. 89, No. 5, pp. 47 - 53.

Essilfie, E. J., Muller, Z., Svec, J. and Tlusty, J. (2014), "STATCOM Effect on Voltage Stability in Ghanaian Electrical Grid", *Proceedings of the 15th IEEE International Scientific Conference*, Brno, Czech Republic, pp. 235 - 240.

Farooq, A. (2018), "Influence of Unified Power Flow Controller on Flexible Alternating Current Transmission System Devices in 500 kV Transmission Line", *Journal of Electrical and Electronic Engineering*, Vol. 6, No. 1, pp. 12 - 22.

Gawande, A. V. and Jadhao, C. W. (2018), "Placement of FACTS Device Using Reduction of Total System Reactive Power Loss Sensitivity Indices Analysis Method", *International Journal of Engineering Technology Science and Research*, Vol. 5, Issue 3, pp. 925 – 931.

Ghahremani, E. and Kamwa, I. (2013), "Optimal Placement of Multiple-type FACTS Devices to Maximise Power System Loadability Using a Generic Graphical User Interface.", *IEEE Transactions on Power Systems*, Vol. 28, No. 2, pp. 764 - 778.

Ghosh, A. and Ledwich, G. (2012), *Power Quality Enhancement using Custom Power Devices,* Springer Science and Business Media Publishers, New York, USA, 2nd edition, 457 pp.

Gibbard, M. J., Pourbeik, P. and Vowles, D. J. (2015), *Small-Signal Stability, Control and Dynamic Performance of Power Systems*, University of Adelaide Press, Adelaide, South Australia, 1st edition, 650 pp.

Gomez-Exposito, A., Conejo, A. J. and Canizares, C. (2018), *Electric Energy Systems: Analysis and Operation*. CRC Press, Boca Raton, Florida, USA, 2nd edition, 749 pp.

Grigsby, L. L. (2016), *Power System Stability and Control*, CRC Press, Boca Raton, Florida, USA, 4th edition, 438 pp.

Gupta, A. and Sharma, P. R. (2013), "Static and Transient Stability Enhancement of Power System by Optimally Placing UPFC, *Proceedings of the IEEE 3rd International Conference on Advanced Computing and Communication Technologies*, Rohtak, Haryana, India, pp. 121 - 125.

Hongmei, L., Haobo, S., Qi, W. and Yunfan, Z. (2017), "Research on the Installation Location and Parameter Configuration Method of UPFC in Energy Internet, *Proceedings of the IEEE Conference on Energy Internet and Energy System Integration*, Beijing, China, pp. 1 - 6.

Hossain, J. and Pota, H. R. (2014) *Power Systems,* Springer Science and Business Media Publishers, Gateway East, Singapore, 1st edition, 311 pp.

Ismail, B., Naain, M. M., Wahab, N. I. A., Awalin, L. J., Alhamrouni, I. and Rahim, M. F. A. (2017), "Optimal Placement of DSTATCOM in Distribution Network, based on Load Flow and Voltage Stability Indices Studies, *Proceedings of the IEEE International Conference on Engineering Technology and Technopreneurship,* Kuala Lampur, Malaysia, pp. 1 - 6.

Kannan, S. and Miah, S. J. (2019), "Integration of Knowledge Management and Business Intelligence for Lean Organisational Learning by the Digital Worker", In: *Applying Business Intelligence Initiatives in Healthcare and Organisational Settings,* IGI Global Publishers, Glasgow, Scotland, 1st edition, pp. 130 - 140.

Karthikeyan, M. (2018), "A Solution to Optimal Power Flow Problem on IEEE 57 Bus System, *International Journal of Engineering, Science and Mathematics*, Vol. 7, Issue 5, pp. 138 – 150.

Kwon, J., Wang, X., Blaabjerg, F., Bak, C. L., Sularea, V. S. and Busca, C. (2017), "Harmonic Interaction Analysis in a Grid-connected Converter Using Harmonic State-space Modelling", *IEEE Transactions on Power Electronics*, Vol. 32, No. 9, pp. 6823 – 6835.

Krishna, A. D. and Sindhu, M. R. (2016), "Application of Static Synchronous Series Compensator to Enhance Power Transfer Capability in IEEE Standard Transmission System", *International Conference on Soft Computing System*, Chennai, India, pp. 1 - 8.

Larruskain, D. M., Zamora, I., Abarrategui, O., Iraolagoitia, A., Gutiérrez, M. D., Loroño, E. and de la Bodega, F. (2016), Power Transmission Capacity Upgrade of Overhead Lines, *www.icrepq.com/icrepq06/296_Larruskain.pdf*. Accessed: July 27, 2016.

Lavanya, K. S. L. and Rani, P. S. (2016), "A Review on Optimal Location and Parameter Settings of FACTS Devices in Power Systems", *International Journal for Modern Trends in Science and Technology*, Vol. 2, No. 11, pp. 112 - 117.

Mensah, K. S. (2009), *Improving Stability of Ghana's Power System Using Power System Stabiliser*, Master's Thesis, Institutt for elkraftteknikk, Stockholm, Sweden, 190 pp.

Mireku-Gyimah, D. (2017), "Mine Economic and Financial Evaluation", *Unpublished MSc Lecture Notes*, University of Mines and Technology, Tarkwa, 92 pp.

Modarresi, J., Gholipour, E. and Khodabakhshian, A. (2016), "A Comprehensive Review of the Voltage Stability Indices", *Renewable and Sustainable Energy Reviews*, Vol. 63, No. 1, pp. 1 – 12.

Morval, B., Evins, R. and Carmeliet, J. (2016), "Optimisation Framework for Distributed Energy Systems with Intergrated Electrical Grid Constraints", *Applied Energy*, Vol. 171, Issue C, pp. 296 – 313.

Narain, A. and Srivastava, S. K. (2015), "An Overview of FACTS Devices used for Reactive Power Compensation Techniques", *International Journal of Engineering Research and Technology*, Vol. 4, No. 12, pp. 81 - 85.

Padiyar, K. R. and Kulkarni, A. M. (2019), *Dynamics and Control of Electric Transmission and Microgrids*, Wiley Publishers, West Sussex, UK, 2nd edition, 485 pp.

Paul, S., Datta, M. and Nandi, C. (2016), "Controlling SSSC by Full Order State Feedback Controller", *International Journal of Computer Applications*, Vol. 151, No. 9, pp. 1 - 3.

Perelmuter, V. M. (2013), *Electrotechnical Systems: Simulation with Simulink and SimPowerSystem*, CRC Press, Florida, USA, 1st edition, 441 pp.

Patel, H. and Paliwal, R. (2015) "Congestion Management in Deregulated Power System Using FACTS Devices", *International Journal of Advances in Engineering and Technology*, Vol. 8, No. 2, pp. 175 - 184.

Qatamin, A., Etawi, A., Safasfeh, G., Ajarmah, N., Al-Jufout, S., Drous, I., Wang, C. and Soliman, A. H. (2017), "SVC versus STATCOM for Improving Power System Loadability: A Case Study", *Proceedings of the 8th International Renewable Energy Congress*, Amman, Jordan, pp. 1 – 4.

Ray, A. and Chandle, J. O. (2015), "Voltage Stability Enhancement during Excess Load Increments through Optimal Location of UPFC Devices", *Proceedings of the IEEE International Conference on Technological Advancements in Power and Energy*, Kollam, Kerala, India, pp. 443 – 448.

Saadati, E. and Mirzaei, A. (2016), "Voltage Stability Indices", *International Journal of Science, Engineering and Innovative Research*, Vol. 8, Issue 1, pp. 1 – 7.

Sarker, J. and Goswami, S. K. (2014), "Solution of Multiple UPFC Placement Problems Using Gravitational Search Algorithm, *International Journal of Electrical Power and Energy Systems*, Vol. 55, Issue 1, pp. 531 – 541.

Sauer, P. W., Pai, M. A. and Chow, J. H. (2018), *Power System Dynamics and Stability: with Synchrophasor Measurement and Power System Toolbox*, John Wiley and Sons, New Jersey, USA, 2nd edition, 353 pp.

Savulescu, S. C. (2014), *Real-time Stability in Power Systems: Techniques for Early Detection of the Risk of Blackout*, Springer International Publishing, Basel, Switzerland, 2nd edition, 429 pp.

Sharma, S. and Vadhera, S. (2016), "Enhancement of Power Transfer Capability of Interconnected Power Systems Using Unified Power Flow Controller", *International Journal on Electronics and Electrical Engineering*, Vol. 4, No. 3, pp. 199 - 202.

Singh, B., Tiwari, P. and Singh, S. N. (2018), "Enhancement of Power System Performances by Optimally Placed FACTS Controllers by Using Different Optimization Techniques in Distribution Systems, *5th IEEE Uttar Pradesh Section International Conference on Electrical, Electronics and Computer Engineering*, Gorakhpur, Pradesh, India, pp. 1 - 7.

Sode-Yome, A., Mithulananthan, N. and Lee, K. Y. (2013), "Comprehensive Comparison of FACTS Devices for Exclusive Loadability Enhancement", *IEEJ Transactions on Electrical and Electronics Engineering*, Vol. 8, Issue 1, pp. 7 – 18.

Songkin, M., Barsoum, N. N., Wong, F. and Lim, P. Y. (2017), "A Study on Sabah Grid System Stability, *IEEE 2nd International Conference on Automatic Control and Intelligent Systems*, Kota Kinabalu, Sabah, Malaysia, pp. 207 – 212.

Sundaram, N. M., Udhayashankar, C. and Thottungal, R. (2018), "An Investigation of Small-signal Stability of IEEE 14 Bus System with AVR, PSS and Performance Comparison with FACTS Devices", *Intelligent and Efficient Electrical Systems,* Vol. 446, Issue 1, pp. 175 - 185.

Taleb, M., Salem, A., Ayman, A., Azma, M. A. and Abido, M. A. (2017), "Advanced Technique for Optimal Allocation of Static Var Compensators in Large-scale Interconnected Networks", *Annual Conference of the IEEE Industrial Electronics Society*, Beijing, China, pp. 73 – 78.

Verma, R. K., Sahu, A. K. and Patil, P. A. (2017), "Optimization Technique Based for Optimal Location of FACTS Devices", *International Journal of Interdisciplinary Innovative Research and Development,* Vol. 1, No. 2 pp. 71 – 76.

Verma, S. N. and Vandana (2014), "Comparative Study of Different FACTS Devices", *International Journal of Engineering Research and Technology*, Vol. 3, No. 6, pp. 1821 – 1822.

Zhang, X. P., Pal, B. and Rehtanz, C. (2012), *Flexible AC Transmission Systems: Modelling and Control*, Springer Publishers, Berlin, Germany, 2nd edition, 568 pp.

APPENDICES

APPENDIX A

FIELD DATA

Table A1 GRIDCo Transmission Line Data

Identifier	From	To	Length km	Year const.	Voltage (kV)	Conductor		Electrical Characteristics					
						Type	Bundled	Positive Impedance (ohms/km)			Zeros Impedance (ohms/km)		
								R/km	X/km	B/km	R	X	B
SN3MM	Mim	Sunyani	60.0	2016	161	ACSR	Yes	0.0687	0.2894	3.9032E-06	0.3766	1.1444	1.8203E-06
-	Sunyani	Berekum	45.0	2015	161	ACSR	Yes	0.0687	0.2894	3.9032E-06	0.3071	1.0074	1.8800E-06
KY6SN	Kenyasi	Sunyani	40.0	-	161	ACSR	Yes	0.0687	0.2894	3.9032E-06	0.3167	1.0215	1.8652E-06
K3TH	Kumasi	Techiman	115.0	1989	161	ACSR	Yes	0.0663	0.2894	3.9015E-06	0.3167	1.0215	1.8652E-06
TH2SN	Techiman	Sunyani	54.9	1989	161	ACSR	No	0.0850	0.3947	2.8952E-06	0.3121	1.0638	1.5460E-06
TH1KP	Techiman	Kintampo	52.0	2012	161	ACSR	Yes	0.0651	0.2868	3.9185E-06	0.3071	1.0074	1.8800E-06
KP3BP	Kintampo	Buipe	85.0	2011	161	ACSR	Yes	0.0651	0.2868	3.9185E-06	0.3071	1.0074	1.8800E-06
-	Buipe	Tamale	98.0	2011	161	ACSR	Yes	0.0651	0.2868	3.9185E-06	0.3071	1.0074	1.8800E-06
TM2BG	Tamale	Bolga	158.1	1990	161	ACSR	No	0.0458	0.2874	1.9797E-06	0.3082	1.0582	1.5495E-06
BU2KP	Bui	Kintampo	67.5	2012	161	ACSR	Yes	0.0651	0.2868	1.8696E-05	0.3071	1.0074	1.8800E-06
BU4TH	Bui	Techiman	98.5	2013	161	ACSR	Yes	0.0651	0.2868	3.9185E-06	0.3071	1.0074	1.8800E-06
BU5SN	Bui	Sunyani	137.6	2014	161	ACSR	Yes	0.0651	0.2868	3.9185E-06	0.3071	1.0074	1.8800E-06
BU1SA	Bui	Sawla	67.2	2014	161	ACSR	Yes	0.0651	0.2868	3.9185E-06	0.3071	1.0074	1.8800E-06
TM3YD	Tamale	Yendi	100.0	1992	161	ACSR	No	0.1374	0.4098	2.7725E-06	0.3749	1.1423	1.7643E-06
BG3ZB	Bolga	Zebilla	45.0	1991	161	ACSR	No	0.1376	0.4100	2.8355E-06	0.3733	1.1400	1.7639E-06
ZB2BK	Zebilla	Bawku	35.0	2015	161	ACSR	No	0.1371	0.4093	2.8092E-06	0.3733	1.1400	1.7639E-06
TM5BG	Bolga	Tumu	109.6	2015	161	ACSR	Yes	0.0687	0.2894	3.9034E-06	0.3759	1.1435	1.7853E-06
SA2WA	Sawla	Wa	95.0	1995	161	ACSR	No	0.1374	0.4099	2.8300E-06	0.3752	1.1426	1.7688E-06
WA1TM	Wa	Tumu	150.0	2014	161	ACSR	No	0.1374	0.4099	2.8300E-06	0.3759	1.1435	1.7853E-06

Table A2 GRIDCo Load and Shunt Data

BSP	Code	Area Name	2017 Load Data				Shunt Capacitor		Shunt Reactor	
			MW	MVAr	Peak (MW)	Peak (MVAr)	Size (MVAr)	Status	Size (MVAr)	Status
Kintampo	1	GRIDCo	11.30	4.90	12.30	4.92	43.20	Offline	-	-
Buipe	1	GRIDCo	6.80	3.40	7.28	3.64	10.80	Offline	-	-
Tamale	1	GRIDCo	39.70	12.00	42.50	12.80	83.20	Offline	34	Online
Bui	1	GRIDCo			0.00	0.00	-	-	-	-
Bolga	1	GRIDCo	10.00	6.20	10.70	6.64	-	-	17	Online
Sawla	1	GRIDCo	9.50	3.80	10.17	4.07	-	-	17	Online
Wa	1	GRIDCo	13.30	3.10	14.23	3.317	-	-	-	-
Yendi	1	GRIDCo	11.70	6.80	9.52	5.28	-	-	-	-
Zebilla	1	GRIDCo	3.10	1.70	3.30	1.80	6.60	Online	-	-
Bawku	1	GRIDCo	1.30	0.60	1.40	0.64	-	-	-	-
Tumu	1	GRIDCo	8.10	10.90	8.70	11.64	-	-	-	-
Bui GS	1	GRIDCo	2.00	2.00	2.14	2.14	-	-	-	-
Total			**116.80**	**55.40**	**122.20**	**56.90**		**-**	-	-

APPENDIX B

COMPLETE LOAD FLOW RESULTS FOR THE MODELLED POWER SYSTEM

Summary for Model_without_FACTS: The Load Flow Converged in 2 Iterations !

	P (MW)	Q (MVAr)
Total Generation	134.5656	32.45384
Total PQ Load	121.1698	52.51
Total Z Shunt	-5.10E-11	-6.40E-11
Total ASM	0	0
Total Losses	13.39576	-20.0562

1 : BAWKU V = 0.8945 pu/161 kV 0.77 deg

	P (MW)	Q (MVAr)
Generation	0	0
PQ Load	1.399996	0.639993
Z Shunt	5.93E-13	-2.20E-11
Zebilla	-1.4	-0.63999

2 : BOLGA V = 0.8989 pu/161 kV 1.11 deg

	P (MW)	Q (MVAr)
Generation	0	0
PQ Load	10.69994	6.640047
Z Shunt	-9.30E-11	-4.90E-11
Tamale	-26.5333	-15.3742
Tumu	11.10777	7.536418
Zebilla	4.725613	1.197691

3 : BUI V = 1 pu/169 kV 0 deg

	P (MW)	Q(MVAr)
Generation	0	0
PQ Load	-5.00E-10	-8.70E-11
Z Shunt	1.46E-11	-4.80E-11
2	-66.3608	-7.01885
Kintampo	42.15925	4.446238
Sawla	24.20159	2.572611

4 : BUIPE V = 0.981 pu/161 kV 0.17 deg

	P (MW)	Q (MVAr)
Generation	0	0
PQ Load	7.279995	3.64004
Z Shunt	1.32E-11	4.70E-11
Kintampo	-93.6133	-29.9555
Tamale	86.33333	26.31551

5 : KINTAMPO V = 0.996 pu/161 kV 0.00 deg; Swing bus

	P (MW)	Q (MVAr)
Generation	68.1541	24.92883
PQ Load	12.3	4.9
Z Shunt	-6.40E-11	1.30E-11
Bui	-40.1554	-8.33424
Buipe	96.00953	28.36308

6 : SAWLA V = 1.013 pu/161 kV -0.3 deg

	P (MW)	Q (MVAr)
Generation	0	0
PQ Load	10.17	4.07
Z Shunt	7.45E-13	-2.50E-11
Bui	-23.5879	-4.70355
Wa	13.4179	0.633549

7 : TAMALE V = 0.9248 pu/161 kV 0.85 deg

	P (MW)	Q (MVAr)
Generation	0	0
PQ Load	42.49995	12.8001
Z Shunt	2.75E-11	9.86E-11
Bolga	28.01591	12.74432
Buipe	-80.2047	-28.4945
Yendi	9.688814	2.950126

8 : TUMU V = 0.8843 pu/161 kV 1.84 deg

	P(MW)	Q(MVAr)
Generation	0	0
PQ Load	10.69994	9.639855
Z Shunt	5.74E-12	-1.30E-11
Bolga	-10.6999	-9.63985

9 : WA V = 1.001 pu/161 kV -0.31 deg

	P(MW)	Q(MVAr)
Generation	0	0
PQ Load	13.3	3.1
Z Shunt	9.43E-12	1.80E-12
1	0.000202	-1.1818
Sawla	-13.3002	-1.9182

10 : YENDI V = 0.9122 pu/161 kV 1.15 deg

	P(MW)	Q(MVAr)
Generation	0	0
PQ Load	9.519991	5.279985
Z Shunt	-9.80E-12	-5.80E-12

Tamale	-9.51999	-5.27998

11 : ZEBILLA V = 0.8953 pu/161 kV 0.77 deg

	P(MW)	Q(MVAr)
Generation	0	0
PQ Load	3.29999	1.799981
Z Shunt	2.56E-11	-3.00E-11
Bawku	1.401619	-0.60207
Bolga	-4.70161	-1.19791

12 : *2* V = 1.000 pu/169.102 kV 0.00 deg; Swing bus

	P(MW)	Q(MVAr)
Generation	66.41145	7.52501
PQ Load	0	0
Z Shunt	1.72E-11	-3.30E-11
Bui	66.41145	7.52501

Summary for Model_with_UPFC at TUMU: The Load Flow Converged in 2 iterations !

	P(MW)	Q(MVAr)
Total Generation	131.9524	32.32948
Total PQ Load	121.17	52.51
Total Z Shunt	0.192966	0.182078
Total ASM	0	0
Total Losses	10.58942	-20.3626

1 : BAWKU V = 0.9554 pu/161 kV 0.1 deg

	P(MW)	Q(MVAr)
Generation	0	0
PQ Load	1.4	0.64
Z Shunt	1.48E-12	4.12E-12
Zebilla	-1.4	-0.64

2 : BOLGA V = 0.9594 pu/161 kV 0.44 deg

	P(MW)	Q(MVAr)
Generation	0	0
PQ Load	10.7	6.64
Z Shunt	5.70E-07	3.17E-07
Tamale	-4.26447	-4.899
Tumu	-11.1576	-2.76313
Zebilla	4.722109	1.022131

3 : BUI V = 1.039 pu/161 kV -0.54 deg

	P(MW)	Q(MVAr)
Generation	0	0
PQ Load	-1.70E-09	5.78E-09

Z Shunt	-1.10E-11	-3.40E-11
2	-90.46	-19.6273
Kintampo	40.53095	6.696231
Sawla	49.92902	12.93103

4 : BUIPE V = 1.006 pu/161 kV 0.12 deg

	P(MW)	Q(MVAr)
Generation	0	0
PQ Load	7.28	3.64
Z Shunt	-6.70E-11	-1.20E-11
Kintampo	-66.5554	-19.0054
Tamale	59.27543	15.36544

5 : KINTAMPO V = 1.017 pu/161 kV 0.00 deg; Swing bus

	P(MW)	Q(MVAr)
Generation	41.39469	11.72491
PQ Load	12.3	4.9
Z Shunt	1.21E-11	-1.40E-11
Bui	-38.6313	-10.5772
Buipe	67.72595	17.40216

6 : SAWLA V = 0.9886 pu/161 kV -0.05 deg

	P(MW)	Q(MVAr)
Generation	0	0
PQ Load	10.17	4.07
Z Shunt	-3.90E-11	4.11E-12
Bui	-47.1647	-14.9984
Wa	36.99469	10.92842

7 : TAMALE V = 0.9635 pu/161 kV 0.56 deg

	P(MW)	Q(MVAr)
Generation	0	0
PQ Load	42.5	12.8
Z Shunt	1.26E-10	-2.40E-11
Bolga	4.307934	2.011114
Buipe	-56.4862	-17.6216
Yendi	9.678294	2.810487

8 : TUMU V = 0.9756 pu/161 kV 0.62 deg

	P(MW)	Q(MVAr)
Generation	0	0
PQ Load	10.7	9.64
Z Shunt	-3.60E-08	-4.40E-06
1	-22.0874	-9.90005
Bolga	11.38739	0.260052

9 : WA V = 0.9557 pu/161 kV 0.28 deg

	P(MW)	Q(MVAr)
Generation	0	0
PQ Load	13.3	3.1
Z Shunt	-2.30E-07	-4.20E-06
1	22.6633	9.019982
Sawla	-35.9633	-12.12

10 : YENDI V = 0.9504 pu/161 kV 0.86 deg

	P(MW)	Q(MVAr)
Generation	0	0
PQ Load	9.52	5.28
Z Shunt	-1.10E-11	1.84E-11
Tamale	-9.52	-5.28

11 : ZEBILLA V = 0.9562 pu/161 kV 0.11 deg

	P(MW)	Q(MVAr)
Generation	0	0
PQ Load	3.3	1.8
Z Shunt	2.25E-11	1.21E-11
Bawku	1.401425	-0.77762
Bolga	-4.70143	-1.02238

12 : *1* V = 0.960 pu/161 kV 1.11 deg

	P(MW)	Q(MVAr)
Generation	0	0
PQ Load	-1.00E-09	5.17E-08
Z Shunt	0.192965	0.182086
Tumu	22.08739	9.900047
Wa	-22.2804	-10.0821

13 : *2* V = 1.000 pu/169.102 kV 0.00 deg; Swing bus

	P(MW)	Q(MVAr)
Generation	90.55769	20.60457
PQ Load	0	0
Z Shunt	-7.70E-11	1.42E-11
Bui	90.55769	20.60457

Summary for Model_with_STATCOM at Tumu: The Load Flow Converged in 2 Iterations!

	P(MW)	Q(MVAr)
Total Generation	133.5458	32.72113
Total PQ Load	121.1698	52.51
Total Z Shunt	0.217335	0.205082
Total ASM	0	0

Total Losses	13.35863	-19.994

1 : BAWKU V = 0.9383 pu/161 kV 0.73 deg

	P(MW)	Q(MVAr)
Generation	0	0
PQ Load	1.399996	0.639993
Z shunt	-5.20E-14	7.57E-12
Zebilla	-1.4	-0.63999

2 : BOLGA V = 0.9431 pu/161 kV 1.07 deg

	P(MW)	Q(MVAr)
Generation	0	0
PQ Load	10.69994	6.640042
Z Shunt	1.12E-10	-7.50E-13
Tamale	-26.3473	-14.9658
Tumu	10.92177	7.129744
Zebilla	4.725575	1.196043

3 : BUI V = 1.039 pu/161 kV -0.43 deg

	P(MW)	Q(MVAr)
Generation	0	0
PQ Load	-3.20E-09	7.53E-09
Z Shunt	-1.80E-11	-6.40E-12
2	-66.7616	-7.7243
Kintampo	42.07856	4.478974
Sawla	24.68305	3.245323

4 : BUIPE V = 1.0 pu/161 kV 0.17 deg

	P(MW)	Q(MVAr)
Generation	0	0
PQ Load	7.279996	3.640038
Z Shunt	-2.00E-11	4.15E-11
Kintampo	-93.3372	-29.5426
Tamale	86.05719	25.90252

5 : KINTAMPO V = 1.013 pu/161 kV 0.00 deg; Swing bus

	P(MW)	Q(MVAr)
Generation	63.73281	24.48334
PQ Load	12.3	4.9
Z Shunt	-1.60E-11	1.31E-10
Bui	-40.0814	-8.36664
Buipe	95.71423	27.94997

6 : SAWLA V = 0.9967 pu/161 kV -0.27 deg

	P(MW)	Q(MVAr)

Generation	0	0
PQ Load	10.17	4.07
Z Shunt	6.40E-12	1.38E-11
Bui	-24.0396	-5.37483
Wa	13.86963	1.304833

7 : TAMALE V = 0.9539 pu/161 kV 0.83 deg

	P(MW)	Q(MVAr)
Generation	0	0
PQ Load	42.49995	12.8001
Z shunt	-1.30E-12	1.44E-10
Bolga	27.79311	12.3335
Buipe	-79.9818	-28.0823
Yendi	9.688703	2.948735

8 : TUMU V = 0.9514 pu/161 kV 1.77 deg

	P(MW)	Q(MVAr)
Generation	0	0
PQ Load	10.69994	9.639864
Z Shunt	-3.90E-12	1.72E-11
1	-0.16297	-0.40306
Bolga	-10.537	-9.2368

9 : WA V = 0.9695 pu/161 kV -0.26 deg

	P(MW)	Q(MVAr)
Generation	0	0
PQ Load	13.3	3.1
Z Shunt	-1.00E-12	-2.40E-11
1	0.442396	-0.51243
Sawla	-13.7424	-2.58757

10 : YENDI V = 0.941 pu/161 kV 1.14 deg

	P(MW)	Q(MVAr)
Generation	0	0
PQ Load	9.519992	5.279985
Z Shunt	-7.90E-13	7.25E-13
Tamale	-9.51999	-5.27999

11 : ZEBILLA V = 0.9392 pu/161 kV 0.73 deg

	P(MW)	Q(MVAr)
Generation	0	0
PQ Load	3.299991	1.799981
Z Shunt	1.28E-11	1.25E-11
Bawku	1.401617	-0.60372
Bolga	-4.70161	-1.19626

12 : *2* V = 1.000 pu/169.102 kV 0.00 deg; Swing bus

	P(MW)	Q(MVAr)
Generation	66.81296	8.237791
PQ Load	0	0
Z Shunt	-3.70E-11	-5.70E-12
Bui	66.81296	8.237791

Summary for Model_with_UPFC at Wa: The load flow converged in 2 iterations!

	P(MW)	Q(MVAr)
Total Generation	131.9521	32.33463
Total PQ Load	121.17	52.51
Total Z Shunt	0.198555	0.187444
Total ASM	0	0
Total Losses	10.58355	-20.3628

1 : BAWKU V = 0.95 pu/161 kV 0.1 deg

	P(MW)	Q(MVAr)
Generation	0	0
PQ Load	1.4	0.64
Z Shunt	4.74E-12	9.55E-12
Zebilla	-1.4	-0.64

2 : BOLGA V = 0.9592 pu/161 kV 0.44 deg

	P(MW)	Q(MVAr)
Generation	0	0
PQ Load	10.7	6.64
Z Shunt	-3.10E-11	1.46E-11
Tamale	-4.24697	-4.88261
Tumu	-11.1751	-2.77939
Zebilla	4.722107	1.021998

3 : BUI V = 1.036 pu/161 kV -0.54 deg

	P(MW)	Q(MVAr)
Generation	0	0
PQ Load	-1.70E-09	5.73E-09
Z Shunt	-4.90E-11	-2.60E-11
2	-90.478	-19.6502
Kintampo	40.52826	6.697792
Sawla	49.94978	12.95245

4 : BUIPE V = 1.004 pu/161 kV 0.12 deg

	P(MW)	Q(MVAr)
Generation	0	0
PQ Load	7.28	3.64

Z Shunt	-6.60E-11	8.65E-11
Kintampo	-66.5354	-18.9887
Tamale	59.25536	15.34869

5 : KINTAMPO V = 1.015 pu/161 kV 0.00 deg; Swing bus

	P(MW)	Q(MVAr)
Generation	41.37629	11.7066
PQ Load	12.3	4.9
Z Shunt	5.26E-11	1.39E-10
Bui	-38.6288	-10.5788
Buipe	67.70506	17.38539

6 : SAWLA V = 0.9862 pu/161 kV -0.05 deg

	P(MW)	Q(MVAr)
Generation	0	0
PQ Load	10.17	4.07
Z Shunt	-4.00E-06	5.81E-07
Bui	-47.1827	-15.0198
Wa	37.01269	10.94978

7 : TAMALE V = 0.9625 pu/161 kV 0.56 deg

	P(MW)	Q(MVAr)
Generation	0	0
PQ Load	42.5	12.8
Z Shunt	1.13E-10	2.39E-10
Bolga	4.290057	1.994521
Buipe	-56.4683	-17.6049
Yendi	9.678287	2.810383

8 : TUMU V = 1.002 pu/161 kV 0.61 deg

	P(MW)	Q(MVAr)
Generation	0	0
PQ Load	10.7	9.64
Z Shunt	-1.80E-05	1.95E-05
1	-22.1056	-9.91603
Bolga	11.40566	0.276009

9 : WA V = 0.978 pu/161 kV 0.28 deg

	P(MW)	Q(MVAr)
Generation	0	0
PQ Load	13.3	3.1
Z Shunt	0.19858	0.187424
1	22.48142	8.853839
Sawla	-35.98	-12.1413

10 : YENDI V = 0.9494 pu/161 kV 0.86 deg

	P(MW)	Q(MVAr)
Generation	0	0
PQ Load	9.52	5.28
Z Shunt	-9.10E-12	-1.20E-11
Tamale	-9.52	-5.28

11 : ZEBILLA V = 0.9555 pu/161 kV 0.1 deg

	P(MW)	Q(MVAr)
Generation	0	0
PQ Load	3.3	1.8
Z Shunt	7.21E-11	1.98E-11
Bawku	1.401425	-0.77775
Bolga	-4.70143	-1.02225

12 : *1* V = 0.993 pu/161 kV 0.76 deg

	P(MW)	Q(MVAr)
Generation	0	0
PQ Load	-4.70E-08	4.45E-08
Z Shunt	-2.90E-06	-6.60E-07
Wa	-22.4814	-8.85384

13 : *2* V = 1.000 pu/169.102 kV 0.00 deg; Swing bus

	P(MW)	Q(MVAr)
Generation	90.57582	20.62803
PQ Load	0	0
Z Shunt	-5.80E-11	-5.10E-11
Bui	90.57582	20.62803

Summary for Model_with_STATCOM at Wa: The Load Flow Converged in 2 Iterations !

	P(MW)	Q(MVAr)
Total Generation	133.6127	33.05227
Total PQ Load	121.1698	52.51
Total Z Shunt	0.217372	0.205117
Total ASM	0	0
Total Losses	13.2255	-19.6628

1 : BAWKU V = 0.9384 pu/161 kV 0.49 deg

	P(MW)	Q(MVAr)
Generation	0	0
PQ Load	1.399996	0.639993
Z Shunt	-1.40E-12	-2.90E-13
Zebilla	-1.4	-0.63999

2 : BOLGA V = 0.9431 pu/161 kV 0.84 deg

	P(MW)	Q(MVAr)
Generation	0	0
PQ Load	10.69994	6.640041
Z Shunt	1.12E-10	2.57E-13
Tamale	-26.3069	-14.131
Tumu	10.8814	6.295499
Zebilla	4.725561	1.195433

3 : BUI V = 1.038 pu/161 kV -0.43 deg

	P(MW)	Q(MVAr)
Generation	0	0
PQ Load	-3.10E-09	7.40E-09
Z Shunt	5.11E-11	-1.10E-11
2	-66.6664	-8.87078
Kintampo	41.9556	4.458783
Sawla	24.71075	4.411994

4 : BUIPE V = 0.9995 pu/161 kV 0.15 deg

	P(MW)	Q(MVAr)
Generation	0	0
PQ Load	7.279996	3.640038
Z Shunt	1.73E-11	3.60E-11
Kintampo	-93.2056	-28.7057
Tamale	85.9256	25.06568

5 : KINTAMPO V = 1.012 pu/161 kV 0.00 deg; Swing bus

	P(MW)	Q(MVAr)
Generation	66.89489	23.66715
PQ Load	12.3	4.9
Z Shunt	6.39E-12	1.88E-10
Bui	-39.9696	-8.34593
Buipe	95.56453	27.11308

6 : SAWLA V = 0.9957 pu/161 kV -0.14 deg

	P(MW)	Q(MVAr)
Generation	0	0
PQ Load	10.17	4.07
Z Shunt	-2.00E-11	5.93E-11
Bui	-24.054	-6.54089
Wa	13.884	2.470886

7 : TAMALE V = 0.9534 pu/161 kV 0.73 deg

	P(MW)	Q(MVAr)
Generation	0	0
PQ Load	42.49995	12.80009

Z Shunt	4.88E-11	1.60E-10
Bolga	27.71217	11.49765
Buipe	-79.9008	-27.2459
Yendi	9.688654	2.948116

8 : TUMU V = 0.9687 pu/161 kV 1.35 deg

	P(MW)	Q(MVAr)
Generation	0	0
PQ Load	10.69994	9.639861
Z Shunt	-2.20E-12	8.21E-12
1	-0.17457	-1.23612
Bolga	-10.5254	-8.40374

9 : WA V = 0.9518 pu/161 kV 1.26 deg

	P(MW)	Q(MVAr)
Generation	0	0
PQ Load	13.3	3.100001
Z Shunt	0.217372	0.205117
1	0.235259	0.448081
Sawla	-13.7526	-3.7532

10 : YENDI V = 0.9405 pu/161 kV 1.03 deg

	P(MW)	Q(MVAr)
Generation	0	0
PQ Load	9.519992	5.279985
Z Shunt	-5.50E-12	1.74E-12
Tamale	-9.51999	-5.27999

11 : ZEBILLA V = 0.9393 pu/161 kV 0.5 deg

	P(MW)	Q(MVAr)
Generation	0	0
PQ Load	3.299991	1.799982
Z Shunt	9.07E-12	1.79E-11
Bawku	1.401617	-0.60433
Bolga	-4.70161	-1.19565

13 : *2* V= 1.000 pu/169.102kV 0.00 deg; Swing bus

	P(MW)	Q(MVAr)
Generation	66.71779	9.385123
PQ Load	0	0
Z Shunt	-5.20E-11	1.12E-10
Bui	66.71779	9.385123

Summary for Model_with_UPFC at Bolga: The load flow converged in 2 iterations!

	P(MW)	Q(MVAr)
Total Generation	131.9474	32.3215

Total PQ Load	121.17	52.51
Total Z Shunt	0.185362	0.174902
Total ASM	0	0
Total Losses	10.59202	-20.3634

1 : BAWKU V = 1.017 pu/161 kV 0.1 deg

	P(MW)	Q(MVAr)
Generation	0	0
PQ Load	1.4	0.64
Z Shunt	-4.10E-12	-2.70E-12
Zebilla	-1.4	-0.64

2 : BOLGA V = 0.9555 pu/161 kV 0.45 deg

	P(MW)	Q(MVAr)
Generation	0	0
PQ Load	10.7	6.64
Z Shunt	-1.60E-06	2.06E-08
2	-11.114	-2.7196
Tamale	-4.30808	-4.94286
Zebilla	4.722115	1.022463

3 : BUI V = 1.026 pu/161 kV -0.54 deg

	P(MW)	Q(MVAr)
Generation	0	0
PQ Load	-1.70E-09	5.75E-09
Z Shunt	-1.80E-11	4.54E-11
1	-90.409	-19.5714
Kintampo	40.53755	6.691747
Sawla	49.87143	12.87963

4 : BUIPE V = 0.9837 pu/161 kV 0.12 deg

	P(MW)	Q(MVAr)
Generation	0	0
PQ Load	7.28	3.64
Z Shunt	-3.30E-11	4.36E-11
Kintampo	-66.6056	-19.0502
Tamale	59.3256	15.41018

5 : KINTAMPO V = 0.9966 pu/161kV 0.00 deg; Swing bus

	P(MW)	Q(MVAr)
Generation	41.44081	11.77413
PQ Load	12.3	4.9
Z Shunt	1.42E-11	2.22E-11
Bui	-38.6374	-10.5728
Buipe	67.77819	17.44692

6 : SAWLA V = 0.9821 pu/161 kV -0.05 deg

	P(MW)	Q(MVAr)
Generation	0	0
PQ Load	10.17	4.07
Z Shunt	1.52E-11	2.79E-11
Bui	-47.1145	-14.9472
Wa	36.94452	10.87717

7 : TAMALE V = 0.9365 pu/161 kV 0.56 deg

	P(MW)	Q(MVAr)
Generation	0	0
PQ Load	42.5	12.8
Z Shunt	1.27E-07	2.78E-07
Bolga	4.352541	2.055455
Buipe	-56.5309	-17.6662
Yendi	9.678313	2.810747

8 : TUMU V = 1.022 pu/161 kV 0.61 deg

	P(MW)	Q(MVAr)
Generation	0	0
PQ Load	10.7	9.64
Z Shunt	2.08E-06	3.18E-07
2	11.53573	0.391359
Wa	-22.2357	-10.0314

9 : WA V = 0.9543 pu/161 kV 0.27 deg

	P(MW)	Q(MVAr)
Generation	0	0
PQ Load	13.3	3.1
Z Shunt	-1.80E-11	-2.70E-12
Sawla	-35.9166	-12.0689
Tumu	22.61664	8.968944

10 : YENDI V = 0.9235 pu/161 kV 0.86 deg

	P(MW)	Q(MVAr)
Generation	0	0
PQ Load	9.52	5.28
Z Shunt	-2.00E-12	6.63E-12
Tamale	-9.52	-5.28

11 : ZEBILLA V = 1.017 pu/161 kV 0.11 deg

	P(MW)	Q(MVAr)
Generation	0	0
PQ Load	3.3	1.8

Z Shunt	1.36E-07	-1.80E-07
Bawku	1.401426	-0.77729
Bolga	-4.70143	-1.02271

12 : *1* V = 1.000 pu/169.102 kV 0.00 deg; Swing bus

	P(MW)	Q(MVAr)
Generation	90.50658	20.54737
PQ Load	0	0
Z Shunt	-6.80E-12	4.26E-12
Bui	90.50658	20.54737

13 : *2* V = 0.959 pu/157 kV 1.27 deg

	P(MW)	Q(MVAr)
Generation	0	0
PQ Load	-4.60E-08	5.06E-08
Z Shunt	0.185361	0.174902
Bolga	11.11403	2.719603
Tumu	-11.2994	-2.89451

Summary for Model_with_STATCOM at Bolga: The Load Flow Converged in 2 Iterations!

	P(MW)	Q(MVAr)
Total Generation	133.8531	32.04982
Total PQ Load	121.17	52.51
Total Z Shunt	0.205358	0.19378
Total ASM	0	0
Total Losses	10.47779	-20.654

1 : BAWKU V = 0.9377 pu/161 kV 0.02 deg

	P(MW)	Q(MVAr)
Generation	0	0
PQ Load	1.4	0.639999
Z Shunt	-8.80E-13	8.12E-11
Zebilla	-1.4	-0.64

2 : BOLGA V = 0.9523 pu/161 kV 0.36 deg

	P(MW)	Q(MVAr)
Generation	0	0
PQ Load	10.7	6.639998
Z Shunt	-3.30E-10	9.93E-11
2	-0.11923	-0.18
Tamale	-15.3044	-7.56675
Zebilla	4.723679	1.106748

3 : BUI V = 1.039 pu/161 kV -0.49 deg

	P(MW)	Q(MVAr)
Generation	0	0
PQ Load	-7.50E-11	-2.70E-09
Z Shunt	4.67E-12	4.08E-13
1	-77.6938	-15.4974
Kintampo	41.11789	5.48025
Sawla	36.57589	10.01715

4 : BUIPE V = 1.0 pu/161 kV 0.11 deg

	P(MW)	Q(MVAr)
Generation	0	0
PQ Load	7.28	3.640003
Z Shunt	-1.80E-11	2.20E-11
Kintampo	-79.3107	-21.8994
Tamale	72.03073	18.25942

5 : KINTAMPO V = 1.013 pu/161 kV 0.00 deg; Swing bus

	P(MW)	Q(MVAr)
Generation	56.08787	15.83741
PQ Load	12.3	4.9
Z shunt	-7.30E-11	2.85E-11
Bui	-39.1895	-9.36381
Buipe	80.97732	20.30122

6 : SAWLA V = 0.9969 pu/161 kV 0.05 deg

	P(MW)	Q(MVAr)
Generation	0	0
PQ Load	10.17	4.07
Z Shunt	1.58E-14	-4.80E-12
Bui	-35.0759	-12.1162
Wa	24.90594	8.046229

7 : TAMALE V = 0.9536 pu/161 kV 0.52 deg

	P(MW)	Q(MVAr)
Generation	0	0
PQ Load	42.5	12.8
Z Shunt	3.68E-12	7.47E-11
Bolga	15.72208	4.802394
Buipe	-67.9052	-20.4791
Yendi	9.683132	2.876741

8 : TUMU V = 0.9424 pu/161 kV 0.81 deg

	P(MW)	Q(MVAr)
Generation	0	0
PQ Load	10.7	9.64

Z shunt	1.06E-11	8.52E-12
2	0.339957	-2.33211
Wa	-11.04	-7.30789

9 : WA V = 0.9701 pu/161 kV 0.42 deg

	P(MW)	Q(MVAr)
Generation	0	0
PQ Load	13.3	3.1
Z shunt	-2.60E-12	2.31E-11
SAWLA	-24.4424	-9.28501
TUMU	11.14235	6.185007

10 : YENDI V = 0.9407 pu/161 kV 0.82 deg

	P(MW)	Q(MVAr)
Generation	0	0
PQ Load	9.519999	5.279998
Z Shunt	-5.50E-12	-4.00E-12
Tamale	-9.52	-5.28

11 : ZEBILLA V = 0.9385 pu/161 kV 0.03 deg

	P(MW)	Q(MVAr)
Generation	0	0
PQ Load	3.299999	1.799999
Z Shunt	6.33E-11	3.53E-11
Bawku	1.401513	-0.69302
Bolga	-4.70151	-1.10698

13 : *2* V = 1.009 pu/161 kV 0.66 deg

	P(MW)	Q(MVAr)
Generation	0	0
PQ Load	-1.40E-08	9.53E-09
Z Shunt	0.205358	0.19378
Bolga	0.132868	0.192936
Tumu	-0.33823	-0.38672

Summary for Model_with_UPFC at Tamale: The load flow converged in 2 iterations !

	P(MW)	Q(MVAr)
Total Generation	131.9407	32.32078
Total PQ Load	121.17	52.51
Total Z Shunt	0.187665	0.177086
Total ASM	0	0
Total Losses	10.58302	-20.3663

1 : BAWKU V = 0.9728 pu/161 kV 0.1 deg

	P(MW)	Q(MVAr)
Generation	0	0
PQ Load	1.4	0.64
Z Shunt	4.40E-13	6.51E-12
Zebilla	-1.4	-0.64

2 : BOLGA V = 0.973 pu/161 kV 0.44 deg

	P(MW)	Q(MVAr)
Generation	0	0
PQ Load	10.7	6.64
Z Shunt	-1.10E-06	2.54E-06
1	-4.1569	-4.80459
Tumu	-11.2652	-2.85736
Zebilla	4.722106	1.021946

3 : BUI V = 1.03 pu/161 kV -0.54 deg

	P(MW)	Q(MVAr)
Generation	0	0
PQ Load	-1.70E-09	5.64E-09
Z Shunt	2.53E-11	1.31E-11
2	-90.3679	-19.5294
Kintampo	40.54255	6.688103
Sawla	49.82533	12.84125

4 : BUIPE V = 0.9747 pu/161 kV 0.12 deg

	P(MW)	Q(MVAr)
Generation	0	0
PQ Load	7.28	3.64
Z Shunt	7.85E-07	7.91E-06
Kintampo	-66.6431	-19.0889
Tamale	59.36315	15.44888

5 : KINTAMPO V = 0.9893 pu/161 kV 0.00 deg; Swing bus

	P(MW)	Q(MVAr)
Generation	41.47532	11.81647
PQ Load	12.3	4.9
Z Shunt	-1.40E-11	9.32E-11
Bui	-38.642	-10.5692
Buipe	67.81734	17.48564

6 : SAWLA V = 0.9981 pu/161 kV -0.06 deg

	P(MW)	Q(MVAr)
Generation	0	0
PQ Load	10.17	4.07
Z Shunt	-2.70E-11	-8.00E-12

Bui	-47.0743	-14.9089
Wa	36.90427	10.83891

7 : TAMALE V = 0.9507 pu/161 kV 0.56 deg

	P(MW)	Q(MVAr)
Generation	0	0
PQ Load	42.5	12.8
Z shunt	2.18E-05	1.15E-05
1	4.385771	2.093842
Buipe	-56.5641	-17.7048
Yendi	9.678327	2.81094

8 : TUMU V = 0.9991 pu/161 kV 0.6 deg

	P(MW)	Q(MVAr)
Generation	0	0
PQ Load	10.7	9.64
Z Shunt	-7.80E-13	7.25E-12
Bolga	11.49983	0.353481
Wa	-22.1998	-9.99348

9 : WA V = 0.9402 pu/161 kV 0.27 deg

	P(MW)	Q(MVAr)
Generation	0	0
PQ Load	13.3	3.1
Z Shunt	-1.70E-11	-1.40E-11
Sawla	-35.8791	-12.0309
Tumu	22.57915	8.930854

10 : YENDI V = 0.9075 pu/161 kV 0.87 deg

	P(MW)	Q(MVAr)
Generation	0	0
PQ Load	9.52	5.28
Z Shunt	3.15E-07	-2.20E-06
Tamale	-9.52	-5.28

11 : ZEBILLA V = 0.9737 pu/161 kV 0.1 deg

	P(MW)	Q(MVAr)
Generation	0	0
PQ Load	3.3	1.8
Z Shunt	6.72E-11	2.94E-11
Bawku	1.401425	-0.77781
Bolga	-4.70143	-1.02219

12 : *1* V = 0.965 pu/161 kV 0.99 deg

	P(MW)	Q(MVAr)

Generation	0	0
PQ Load	-5.60E-10	3.23E-08
Z Shunt	0.187643	0.177066
Bolga	4.198127	1.916775
Tamale	-4.38577	-2.09384

13 : *2* V = 1.000 pu/169.102 kV 0.00 deg; Swing bus

	P(MW)	Q(MVAr)
Generation	90.46537	20.50431
PQ Load	0	0
Z Shunt	-4.70E-11	-1.40E-11
Bui	90.46537	20.50431

Summary for Model_with_STATCOM at Tamale: The load flow converged in 2 iterations!

	P(MW)	Q(MVAr)
Total Generation	133.7409	32.76611
Total PQ Load	121.17	52.51
Total Z Shunt	0.177009	0.167029
Total ASM	0	0
Total Losses	11.39393	-19.9109

1 : BAWKU V = 0.9381 pu/161 kV 0.8 deg

	P(MW)	Q(MVAr)
Generation	0	0
PQ Load	1.4	0.639999
Z Shunt	-4.10E-13	2.65E-11
Zebilla	-1.4	-0.64

2 : BOLGA V = 0.9528 pu/161 kV -0.46 deg

	P(MW)	Q(MVAr)
Generation	0	0
PQ Load	10.7	6.639996
Z Shunt	9.25E-11	1.62E-10
1	0.142948	-2.66197
Tumu	-15.5662	-5.06431
Zebilla	4.723279	1.086284

3 : BUI V = 1.039 pu/161 kV -0.58 deg

	P(MW)	Q(MVAr)
Generation	0	0
PQ Load	-6.60E-08	3.58E-07
Z Shunt	2.11E-11	-4.60E-11
2	-95.7828	-22.3929
Kintampo	40.17327	7.193378

Sawla	55.60951	15.19947

4 : BUIPE V = 0.9998 pu/161 kV 0.15 deg

	P(MW)	Q(MVAr)
Generation	0	0
PQ Load	7.28	3.64
Z Shunt	6.40E-12	4.48E-12
Kintampo	-61.8392	-17.0468
Tamale	54.55924	13.40678

5 : KINTAMPO V = 1.039 pu/161 kV 0.00 deg; Swing bus

	P(MW)	Q(MVAr)
Generation	37.84771	9.268769
PQ Load	12.3	4.9
Z shunt	-5.40E-11	1.01E-10
BUI	-38.2942	-11.0729
BUIPE	62.84192	15.44162

6 : SAWLA V = 0.9968 pu/161 kV -0.28 deg

	P(MW)	Q(MVAr)
Generation	0	0
PQ Load	10.17	4.070003
Z Shunt	-1.60E-11	6.20E-11
Bui	-52.1557	-17.253
Wa	41.98569	13.18299

7 : TAMALE V = 0.9632 pu/161 kV 0.75 deg

	P(MW)	Q(MVAr)
Generation	0	0
PQ Load	42.5	12.8
Z Shunt	4.04E-11	1.18E-10
1	0.039227	0.090533
Buipe	-52.2158	-15.6764
Yendi	9.676566	2.785902

8 : TUMU V = 0.9532 pu/161 kV 0.01 deg

	P(MW)	Q(MVAr)
Generation	0	0
PQ Load	10.7	9.640001
Z Shunt	9.42E-12	7.99E-11
Bolga	16.0544	2.651213
Wa	-26.7544	-12.2912

9 : WA V = 0.9702 pu/161 kV -0.12 deg

	P(MW)	Q(MVAr)

Generation	0	0
PQ Load	13.3	3.100002
Z Shunt	3.21E-12	3.12E-11
Sawla	-40.6268	-14.3545
Tumu	27.32679	11.25451

10 : YENDI V = 0.9404 pu/161 kV 1.05 deg

	P(MW)	Q(MVAr)
Generation	0	0
PQ Load	9.52	5.28
Z Shunt	3.32E-12	3.67E-12
Tamale	-9.52	-5.28

11 : ZEBILLA V = 0.939 pu/161 kV -0.79 deg

	P(MW)	Q(MVAr)
Generation	0	0
PQ Load	3.299999	1.799998
Z Shunt	3.55E-11	3.68E-11
Bawku	1.40149	-0.71348
Bolga	-4.70149	-1.08652

13 : *2* V = 1.000 pu/169.102 kV 0.00 deg; Swing bus

	P (MW)	Q(MVAr)
Generation	95.89322	23.49734
PQ Load	0	0
Z Shunt	-4.40E-11	4.83E-11
Bui	95.89322	23.49734

Index